Title
Integrated Maneuvering Control Design And Experiments: Phase II

Authors
Hedrick, J. K.
Pantarotto, M.
Yoshioka, T.
et al.

Publication Date
1996

CALIFORNIA PATH PROGRAM
INSTITUTE OF TRANSPORTATION STUDIES
UNIVERSITY OF CALIFORNIA, BERKELEY

Integrated Maneuvering Control Design and Experiments: Phase II

J.K. Hedrick, M. Pantarotto, T. Yoshioka, Y. Chen, T. Connolly, V.K. Narendran

University of California, Berkeley
Mechanical Engineering

California PATH Research Report
UCB-ITS-PRR-96-2

This work was performed as part of the California PATH Program of the University of California, in cooperation with the State of California Business, Transportation, and Housing Agency, Department of Transportation; and the United States Department of Transportation, Federal Highway Administration.

January 1996

ISSN 10551425

REPORT FOR PHASE-II

Integrated Maneuvering Control
Design and Experiments
(M.O.U. #99)

Submitted By:

J. K. Hedrick (P.I.)
M. Pantarotto
T. Yoshioka
Y. Chen
T. Connolly
V. K. Narendran

University of California, Berkeley
1995

Abstract

The first chapter of this report examines autonomous lateral vehicle control. Most lateral control work done thus far in PATH has involved the use of magnetic markers embedded in the road. The autonomous vehicle control philosophy is aimed at using line-of-sight sensor information to effect vehicle control, without the benefit of communications with other vehicles or with the roadside. Since the sensors used in detecting magnetic road markers have a range of about one meter, lane changing maneuvers cannot rely on road markers, but must be performed using line-of-sight sensors, such as Qualimatrix's PATH Optical Ranging System.

For simulation purposes, the longitudinal dynamics of the vehicle were based on models developed for a Ford Lincoln Towncar [Cho and Hedrick, 1989; Hedrick, et.al., 1991], and the lateral dynamics were based on models developed by Peng [1992]. This model has twenty states, and is highly nonlinear. Therefore a simplified model was presented for controller design purposes.

A sliding controller was chosen since it is a nonlinear control method which is particularly adept at handling nonlinearities while remaining robust to unmodelled dynamics. In simulation, this controller demonstrated good tracking on curved sections of road. Simulations also demonstrated the effectiveness of using a nonzero desired azimuth angle in the control law to reduce the lateral tracking error. In simulations of lane change maneuvers, a major problem is the large required field of vision for the lateral sensor (45 degrees in simulation).

The controller was found to be robust to certain lateral sensor errors, but is sensitive to sensor noise, and errors in the orientation of the sensor, especially at large desired intervehicular

spacings. In testing the Qualimatrix sensor, it was found to be reasonably accurate during static tests, but very noisy in dynamic tests.

Chapter two examines Cooperative Intelligent Cruise Control (CICC), which can be viewed as an intermediate step to the Advanced Vehicle Control System (AVCS) program. It requires an automatic throttle and brake control, and simple infrastructure-vehicle communication. It is designed to operate as an intelligent cruise control, without the high level of integrated infrastructure support required for AVCS.

The general characteristics of constant spacing control, constant headway control, and the linear-optimal control model (human model) were examined. Since constant headway control does not require information from other vehicles in order to maintain string stability, it is the most appropriate method for vehicle-following control in a mixed traffic flow. However, the string stability conditions may be violated given large enough time delays in the sensors, actuators, or the plant. The maximum allowable delays tend to decrease as control gains increase and as headway times decrease. In addition, since human drivers provide the lateral control for a vehicle using CICC, the headway time must be at least 0.3 seconds.

The effects of several factors on the static flow rate of traffic were examined. It was verified that the percentage of automated vehicles present on the highway affected the total highway capacity. Inter-vehicle communication and automated vehicle only lanes could significantly increase the capacity of highways only when at least 30% of the vehicles on the road were automated.

Dynamic flows were considered where a lead vehicle would initiate a change in velocity. A constant headway control yielded delays in the following vehicle's response to such a velocity change, while a constant spacing control did not show any delay in its tracking response.

However, in comparison with the human model, headway control still provides superior distance tracking. It was also verified that constant headway control can be applied to a dynamic mixed traffic flow.

Two methods of infrastructure-vehicle communication were compared in terms of the transient response of the traffic flow to a change in the desired flow-rate (i.e. velocity) along a section of highway. How this information is relayed to each vehicle has a significant effect on the transient response of the traffic flow. To achieve a stable transition, a wide-range media, such as radio, is much better than a local media, such as beacons.

Collision avoidance was also examined for several cases. In the cases where collision could not be avoided, the constant headway control yielded better results than the human model. This implies that a controller which responds faster to a preceding vehicle's deceleration will provide better rear-end collision avoidance. Therefore, although the information of a preceding vehicle's acceleration is not necessary for constant headway control, estimating it is very helpful in collision avoidance.

Chapter three examines the effect of communication delays on the control performance of vehicle platoons. To safely implement a platoon of closely spaced vehicles, it is necessary to have a communications link within the platoon. Delays in transmitting information from one vehicle in the platoon to another can have a significant effect on longitudinal tracking performance. A radio based system using a token bus architecture was examined, since a token type architecture is especially suited for systems where the transfer of information is highly deterministic with respect to time. Time delays are incurred in transmission, and in processing data packets.

An acceptable delay occurs when the token cycle is three to four times the length of a control cycle. Since the discrete time control law is computed every 20 milliseconds, this

translates to a maximum token cycle length of 60 to 80 milliseconds. Of course, the token cycle should ideally be shorter or equal to the control cycle, but that is not always possible for large platoons.

Chapter four looks at the three basic transition maneuvers in an Automated Highway System: join, split, and lane change. The first two apply to platoons of vehicles, while the third can only be performed by an individual vehicle not associated with any platoon. Several trajectories for the join maneuver were examined. It was recommend that a transition maneuver module should be capable of determining initial errors, design trajectories, and contain the necessary control laws to ensure the vehicle follows the desired trajectory. Work also needs to be done with the system level commands and tasks to ensure that safe transition maneuvers occur when multiple platoons are present.

Table of Contents

Table of Figures

1. Introduction

The concept of automated highway systems was first introduced to the public in the 1939 World Fair at the GM Pavilion. The first research efforts can be traced to the Radio Corporation of America then working in association with GM. Since then, a considerable amount of time and money has been invested in this concept. The Personal Rapid Transit (PRT) and Automated Guideway Transit (AGT) studies of the 60's and 70's have addressed the feasibility, management, and operational concepts of the system. Similar studies have been carried out in Europe.

The automated highway system is primarily aimed at reducing congestion on highways through closer packing of vehicles per unit mile of the highway. The system will also result in improved safety on the highway, and an easier and more comfortable ride for the individual. The longitudinal and lateral control studies of automobiles on the highway thus far have established the theoretical and practical feasibility of the concept.

The PATH program in California has been on the forefront of research in the area of Intelligent Transportation Systems (ITS). The research is focused in the areas of system management issues, intervehicle communications, vehicle control, and actuator and sensor development for Intelligent Vehicle Highway Systems (IVHS) applications. The experimental work in PATH has resulted in the validation of the pure longitudinal and lateral vehicle control aspects of the program. Work in the area of transition maneuvers, fault detection, and fault tolerant vehicle control has also progressed. This report looks at some of the other aspects of vehicle control. Transition maneuvers address issues such as platoon formation and splitting, lane

changing, entry and exit of vehicles to and from the automated lanes. This must go hand-in-hand with system level decision making to allow for smooth transition maneuvers.

The first part of the report is devoted to examining autonomous vehicle control. Lateral control studies and experimental work thus far in PATH have concentrated on the use of magnetic markers imbedded in the roadway for effecting vehicle control. The autonomous vehicle control philosophy is aimed at using line-of-sight sensor information to effect vehicle control. The method addresses lateral control of vehicles without any roadside information or information communicated from other vehicles.

The AVCS program envisioned right now will require a high level of integrated infrastructure support to effect safe vehicle control. The Cooperative Intelligent Cruise Control (CICC) method proposed in Chapter 3 looks at an intermediate solution which can be introduced in a few years. It will require an automatic throttle and brake control, and simple infrastructure-vehicle communication. The method is designed to let a vehicle operate under a conventional cruise control system in the absence of traffic around the controlled vehicle, but will work as a distancing control system when other vehicles are within the range of its sensors. The chapter examines the organization of the CICC method, and the information necessary to make the system work. The work includes an analytical approach. Comparison is made with spacing and headway control approaches, and also the human approach to vehicle control. The report examines the flow characteristics under the various approaches.

The spacing control approach requires information from other vehicles to ensure non-propagation of errors down a platoon of vehicles. This part of the project addresses the analysis of the effect of an imperfect communications system on the performance of the control law. An

effort has been made to come up with requirements on the communications system in order to ensure the preservation of a “nice” behavior with respect to the spacing error and ride quality of the vehicles in the platoon,

In the longitudinal control group in PATH, a standardized "C" program was developed to allow several researchers the use of a standard vehicle model for control law development. The last part of the report deals with the extension of this program to include modules that will allow researchers to perform a variety of transition maneuvers. This lets one compare various maneuvering strategies in an effort to develop optimal transition maneuver strategies.

2. Autonomous Vehicle Control

Marc Pantarotto

2.1 Introduction

The problem of traffic congestion on highways today is compounded by space constraints and the limited ability to construct new roads. As a result, much recent research is focused on raising the traffic flow rates on highway lanes via intelligent vehicle systems such as intelligent cruise control. One possible solution, proposed by the Partners for Advanced Transit and Highways (PATH), is to create an automated highway lane for platoons of closely spaced, automatically controlled vehicles. Vehicles in a platoon would maintain a desired longitudinal spacing (on the order of one meter, bumper to bumper), while following a path of magnetic markers placed in the center of the lane.

The PATH plan presents many different problems, from the control of individual vehicles to the coordination of different platoons. The longitudinal control, lateral control, merge and lane changing aspects of this project have all been looked at previously by Hedrick, McMahon et. al. (1991), Peng (1992) and Pham (1993). One of the difficulties in lateral control is the dependence upon magnetic marker readings, since the lateral sensor can only read the markers within a distance of one meter. Lane changing schemes, therefore, must be done open loop. One way to overcome this problem is to have a sensor that can detect the lateral position of a preceding vehicle, allowing the vehicle to follow the car instead of the road. Such a lateral controller is the topic of this project.

This report discusses autonomous lateral vehicle control, or lateral control without any information from the road or communicated from other vehicles. A strategy for autonomous control is presented and a nonlinear controller is developed to implement it. The effectiveness of the controller in general lane following applications will also be examined. This report will look at problems such as the lateral errors on curved sections and the propagation of lateral errors in a platoon of vehicles.

First, a vehicle model is developed for simulation purposes. The model's lateral dynamics are derived from a Toyota lateral model while a Ford longitudinal model is the basis for the longitudinal dynamics. The model has twenty states and is highly nonlinear. Its inputs are the throttle angle, brake torque and steering angle, while its outputs are the relative longitudinal and lateral distances of the preceding vehicle. A simplified model is then presented for controller design purposes.

The strategies used for autonomous lateral control are then discussed and their effectiveness is examined. Basically, the goal of the controller is to drive the lateral offset to a desired lateral offset which depends upon vehicle velocity, yaw rate and desired longitudinal spacing. The controller also maintains a desired longitudinal spacing between the two vehicles. In order to handle the highly nonlinear vehicle system, a sliding mode controller is used to control both the lateral and longitudinal dynamics.

Simulation results are presented next. The controller is evaluated in terms of tracking performance and the resulting lateral errors. The effects of desired spacing, acceleration, road curvature and lateral sensor errors are all discussed. Lateral sensor specifications are developed.

One of the proposed sensors for use in the above scheme is Qualimatrix's PATH Optical Ranging System. This sensor uses two light detectors to detect an infrared light mounted on a previous car. It outputs the longitudinal distance of the light from the center of the two detectors and the lateral offset off of the centerline of the car. Some static and dynamic tests were performed on this sensor and the results are presented here.

2.2 Vehicle Model

2.2.1 Complex Vehicle Model

The complex vehicle model is developed for simulation purposes and is described using 20 states:

$$x\ ,\ V_x, y, V_y,\ z,\ V_z,\ \theta\ ,\ \theta\ ,\ \phi,\ \phi,\ \psi,\ \psi,\ m_{air},\ \omega_{eng},\ \omega_w, y_r,\ y_r,\ T_{br}\ ,\ \alpha, \delta,\ x_{rel}, \dot{x}_{rel}, y_{rel}, \dot{y}_{rel}$$

The inputs to this model are the commanded steering angle δ_{com}, the commanded throttle angle, a,,,, and the commanded brake torque, T_{brake}. The outputs of this model, x_{rel} and y_{rel}, are the x and y positions of the previous car's transmitter relative to the car's body-fixed coordinate system.

2.2.1.1 Engine Dynamics

The model of the engine dynamics is based on models developed by Cho and Hedrick (1989), and by McMahon and Hedrick (1991) for a Ford Lincoln Town Car V-8 engine. The engine model consists of two states, the engine speed, ω_e, and the mass of air in the manifold, m_a:

$$\begin{aligned} \dot{m}_a &= \dot{m}_{ai} - \dot{m}_{ao} \\ \dot{\omega}_e &= (T_{net} - T_{pump})/J_e \end{aligned} \tag{2.2.1}$$

where:

$\dot{m}_{ai}, \dot{m}_{ao}$	Mass rates of air into and out of the intake manifold, respectively.
T_{net}, T_{pump}	Net engine and the pump torques, respectively.
J_e	Effective engine inertia.

$\dot{m}_{ao}$ and T_{net} are determined from look-up tables developed from steady state engine maps. These tables are indexed by ω_e and the pressure in the manifold, p_m. $\dot{m}_{ai}$ is determined from the relationship

$$\dot{m}_{ai} = \beta_1 PRI(p_m / p_m) TC(\alpha) \tag{2.2.2}$$

PRI() is the manifold pressure influence function, and TC() is the throttle characteristic. p_a is the atmospheric pressure, β_1 is a constant, and a is the throttle angle.

2.2.1.2 Drive Train Dynamics

The drive train model is made up of the torque converter and the transmission. The torque converter output, T_{turb}, is determined from torque converter maps and is a function of the ratio, $\omega_{turbine}/\omega_e$. The gear shift dynamics have not been modeled, so gear changes are taken to occur instantaneously. In simulations, the vehicle remains in third gear. The shaft dynamics have been neglected, so the shaft torque, T_{shaft} is proportional to T_{turb}. The turbine speed is thus proportional to the wheel speed:

$$\omega_{wheel} = \left(r_{gear} r_{drive}\right)\omega_{turbine} \tag{2.2.3}$$

where r_{gear} and r_{drive} are the gear and drive ratios, respectively.

2.2.1.3 Vehicle Sprung Mass Dynamics

The vehicle sprung mass model is based on one developed by Peng (1992). The sprung mass model has 6 degrees of freedom, accounting for translational and rotational motions in the x, y, z directions. The road gradient and superelevation angles are neglected. The variables and parameters used to describe the sprung mass dynamics are illustrated in figure 2.2.1 and listed in the table below.

m	vehicle mass

X_s, Y_s, Z_s	vehicle sprung mass coordinate system
X, Y,Z	inertia coordinate system
I_x, I_y, I_z	moment of inertia of sprung mass in x,y,z directions resp.
$V_x,$, V_y, V_z	velocities in x,y,z directions respectively
M_x, M_y, M_z	external moments in the x,y,z directions respectively
F_{xi}	traction (braking) force on i^{th} tire
F_{yi}	side force on i^{th} tire
F_{Ai},(F_{Bi})	longitudinal (lateral) force on i^{th} tire
F_{Pi}	normal force on i^{th} tire
δ_i	steering angle of i^{th} tire
F_{roll}	rolling resistance
ψ	yaw angle
θ	pitch angle
ϕ	roll angle
β	side slip angle
χ	velocity angle ($\chi = \psi + \beta$)
l_1,(l_2)	length from c.g. to front (rear) axle
s_{b1},(s_{b2})	track of front (rear) axle
h_2	vertical distance from c.g. to roll center
h_4, (h_5)	vertical (longitudinal) distance from c.g. to pitch center

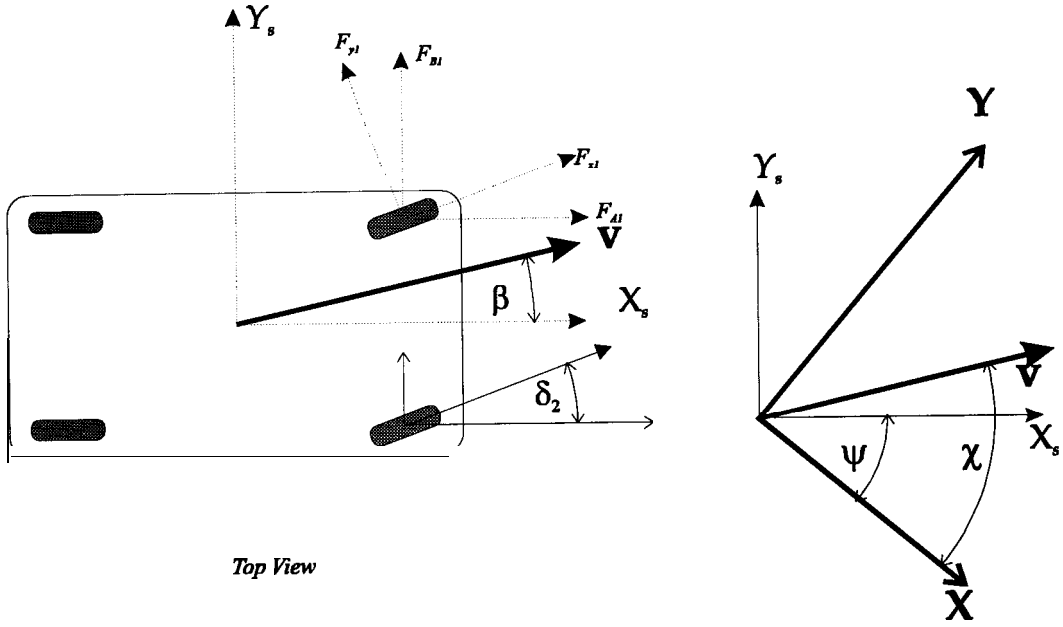

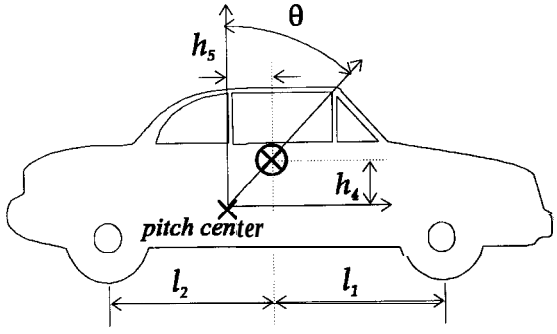

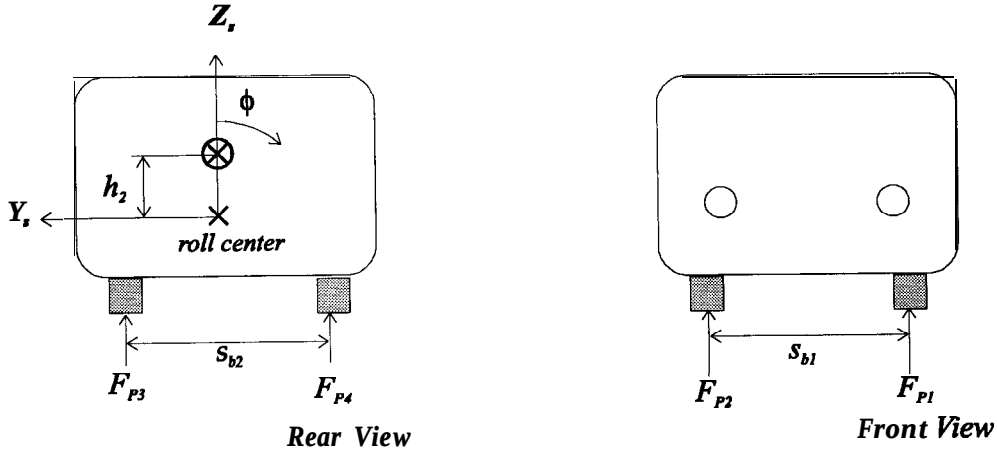

Figure 2.2.1: Parameters for Sprung Mass Dynamics

Assuming the pitch and roll angles to be small, the equations of motion of the vehicle sprung mass are:

$$m(\dot{V}_x - \dot{V}_y\dot{\psi} + h_4\ddot{\theta} + h_2\dot{\phi}\dot{\psi} + h_2\phi\ddot{\psi}) = \sum_{i=1}^{4} F_{Ai} - C_x V_x^2 - F_{roll}$$

$$m(\dot{V}_y + \dot{V}_x\dot{\psi} - h_2\ddot{\phi} + h_4\dot{\theta}\dot{\psi} + h_4\theta\ddot{\psi}) = \sum_{i=1}^{4} F_{Bi} - C_y V_y^2$$

$$m(\dot{V}_z + V_x\dot{\chi}\beta - h_5\ddot{\theta}) = \sum_{i=1}^{4} F_{Pi} - mg$$

$$I_x(\ddot{\phi} - \theta\ddot{\psi} - \dot{\theta}\dot{\psi}) - (I_y - I_z)\dot{\theta}\dot{\psi} = M_x - \theta M_z$$

$$I_y(\ddot{\theta} + \phi\ddot{\psi} + \dot{\theta}\dot{\psi}) - (I_z - I_x)\dot{\phi}\dot{\psi} = M_y + \phi M_z$$

$$I_z(\ddot{\psi} + \theta\ddot{\phi} - \ddot{\theta}\phi) - (I_x - I_y)\dot{\phi}\dot{\theta} = M_z + \theta M_x - \phi M_y$$

2.2.1.4 Tire Forces

The tire model is based on Peng's model (1992), which was developed from the Bakker-Pacjecka-Lidner model (1989). This model is based on curve-fits of experimental data from tests performed on Yokohama P205/60R1487H steel belted radial tires. Bakker determined nominal functional relationships between the longitudinal and lateral forces of the i^{th} tire, f_{xi0}, and f_{yi0}, and the normal force f_{zi}, the slip ratio, λ_i. and the slip angle, γ_i:

$$\begin{aligned} f_{xi} &= f_{x0i}(\lambda_i, f_{zi}) \\ f_{yi} &= f_{y0i}(\gamma_i, f_{zi}) \end{aligned} \qquad (2.2.4)$$

These relationships are valid for traction only or cornering only maneuvers. The slip ratio, γ, is defined separately for braking and traction:

$$\lambda_i = \frac{r_{wi}\omega_{wi} - V_x}{r_{wi}\omega_{wi}} \tag{2.2.5a}$$

$$\lambda_i = \frac{r_{wi}\omega_{wi} - V_x}{V_x} \tag{2.2.5b}$$

where ω_{wi} is the angular velocity of the i^{th} wheel and r_{wi} is the effective wheel radius of the i^{th} wheel. The slip angle is the difference between the steering angle, 6 , and the tire velocity angle, ζ:

$$\gamma_i = \delta_i - \zeta_i \tag{2.2.6}$$

The tire velocity angle of each tire is related to the yaw rate, $\dot{\psi}$, the longitudinal and lateral velocities, V_x and V_y, as well as the parameters l_i and s_{bi}:

$$\tan(\zeta_1) = \frac{V_y + l_1\dot{\psi}}{V_x - \frac{s_{b1}\dot{\psi}}{2}} \qquad \tan(\zeta_2) = \frac{V_y + l_1\dot{\psi}}{V_x + \frac{s_{b1}\dot{\psi}}{2}} \tag{2.2.7}$$

$$\tan(\zeta_3) = \frac{V_y + l_2\dot{\psi}}{V_x - \frac{s_{b2}\dot{\psi}}{2}} \qquad \tan(\zeta_4) = \frac{V_y - l_2\dot{\psi}}{V_x + \frac{s_{b2}\dot{\psi}}{2}}$$

In order to account for combined tractive and cornering maneuvers, Bakker defined normalized slip factors λ^*, and γ^*:

$$\lambda^* = \frac{\lambda}{\lambda_{max}} \qquad \gamma^* = \frac{\gamma}{\gamma_{max}} \tag{2.2.8}$$

where λ_m and γ_m are the values of λ and γ at which F_x and F_y are equal to their respective maximum values. A correction factor is then defined:

$$\sigma^* = \sqrt{(\lambda^*)^2 + (\gamma^*)^2} \tag{2.2.9}$$

F_{xi}, and F_{yi} are then found from

$$F_{xi} = \frac{\lambda^*}{\sigma^*} f_{x0i}(\sigma^*, f_{zi})$$
$$F_{yi} = \frac{\gamma^*}{\sigma^*} f_{y0i}(\sigma^*, f_{zi}) \tag{2.2.10}$$

2.2.1.5 Suspension Model

The suspension model is based on that of Peng (1989) and consists of a spring and a damper at each of the wheels. The suspension forces F_{pi}, are equal to the sum of the spring and the damper forces, $F_{spring} + F_{damper}$. The spring is modeled as a nonlinear hardening spring:

$$P_{spring} = C_1\left(e + C_2 e^5\right) \tag{2.2.11}$$

where C_1 and C_2 are the spring constants and e is the suspension joint deflection. The damping force is modeled as a piecewise linear function of the joint deflection velocity.

2.2.1.6 Wind Force Model

The modeled wind force is proportional to the square of the wind speed:

$$F_{wx} = -C_x V_x^2 \tag{2.2.12a}$$

$$F_{wy} = -C_y V_y^2 \tag{2.2.12b}$$

where F_{wx} and F_{wy} are forces due to the wind in the x and y directions, respectively. C_x and C_y are the wind resistance coefficients. The wind force is assumed to be caused by vehicle velocity only, i.e. no external wind disturbances.

2.2.1.7 Wheel Equations

The angular velocities of the wheels, ω_i, are also state variables. The equations are

$$J_{wi}\dot{\omega}_i = \frac{T_{shaft}}{2} - \frac{T_{brake}}{4} - r_{wi}F_{xi} \tag{2.2.13a}$$

$$J_{wi}\dot{\omega}_i = \frac{-T_{brake}}{4} - r_{wi}F_{xi} \tag{2.2.13b}$$

where $J_{\omega i}$ is the wheel moment of inertia, T_{brake} is the brake torque, T_{shaft} is the drive-shaft torque.

2.2.1.8 Unsprung Mass

The external moments about the unsprung mass are

$$
\begin{aligned}
M_x &= \left(\frac{s_{b1}}{2}+h_2\phi\right)F_{P_1}+\left(\frac{s_{b2}}{2}+h_2\phi\right)F_{P_3}-\left(\frac{s_{b1}}{2}-h_2\phi\right)F_{p_2}-\left(\frac{s_{b2}}{2}-h_2\phi\right)F_{P_4} \\
&\quad +(z-h_5\theta)\sum_{i=1}^{4}F_{B_i} \\
M_y &= (l_2+h_4\theta)(F_{P_3}+F_{P_4})-(l_1-h_4\theta)(F_{P_1}+F_{P_2})-(z-h_5\theta)\sum_{i=1}^{4}F_{A_i} \\
M_z &= (l_1-h_4\theta)(F_{B_1}+F_{B_2})-(l_2+h_4\theta)(F_{B_3}+F_{B_4}) \\
&\quad -\left(\frac{s_{b+1}}{2}+h_2\phi\right)F_{A_1}+\left(\frac{s_{b1}}{2}-h_2\phi\right)F_{A_2}-\left(\frac{s_{b2}}{2}+h_2\phi\right)F_{A_3}+\left(\frac{s_{b2}}{2}-h_2\phi\right)F_{A_4}
\end{aligned}
\tag{2.2.14}
$$

where M_x, M_y and M_z are the moments in the x, y and z directions respectively.

2.2.1.9 Lateral Displacement

The lateral displacement from the center of the lane, y_r, and its derivative are also states. They are determined from the expression

$$
\ddot{y}_r \approx \dot{V}_y + \dot{V}_x(\psi-\psi_d)+V_x(\dot{\psi}-\dot{\psi}_d) \tag{2.2.15}
$$

where ρ is the road radius of curvature and ψ_d is the desired heading angle of the vehicle, i.e. the heading angle of the road.

2.2.1.10 Sensor Setup and Outputs

Each car has a sensor which can measure the longitudinal and lateral position of a transmitter on the previous vehicle. The sensor is positioned so that the centerline of the sensor is the same as that of the car. The longitudinal output of the sensor, x_{rel}, is distance of the transmitter to the sensor along this centerline. The lateral offset, y_{rel}, is the distance of the transmitter from this centerline. The sensor and transmitter can be placed at the front and back of the cars, respectively, or can be mounted somewhere on the roofs of the cars. The sensor setup is shown in figure 2.2.2. The sensor and transmitter positions shown here are similar to those of the Qualimatrix Optical Ranging System.

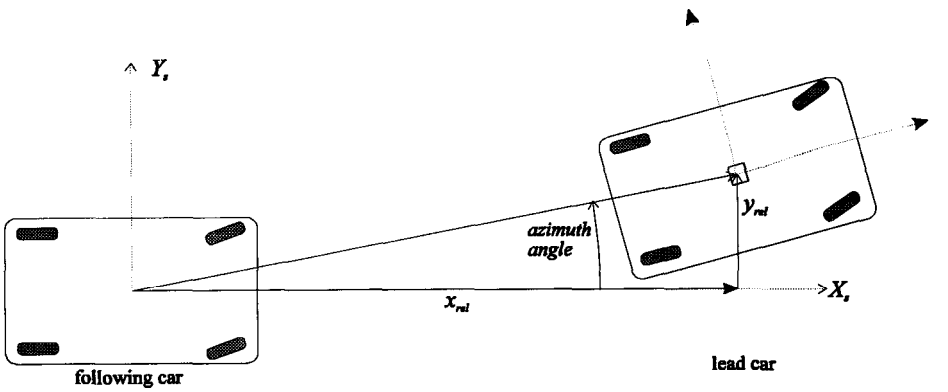

Figure 2.2.2: Definition of Azimuth Angle

The outputs of the system are then x_{rel}, and y_{rel}, the position of the center of mass of the preceding car relative to the car's body fixed coordinate system. Four states, $x_{rel}, v_{xrel}, y_{rel}$, and v_{yrel} can be used to describe the relative motions of the two cars.

$$\begin{aligned}
\dot{x}_{rel} &= v_{xrel} \\
\dot{v}_{xrel} &= \ddot{x}_l - \left(\dot{V}_x - \dot{\psi} V_y\right) + \dot{\psi}^2 x_{rel} + \ddot{\psi} y_{rel} + 2\dot{\psi}\dot{y}_{rel} \\
\dot{y}_{rel} &= v_{yrel} \\
\dot{v}_{yrel} &= \ddot{y}_l - \left(\dot{V}_y - \dot{\psi} V_y\right) + \dot{\psi}^2 y_{rel} - \ddot{\psi} x_{rel} - 2\dot{\psi}\dot{x}_{rel}
\end{aligned} \tag{2.2.16}$$

where $\ddot{x}_l$ and $\ddot{y}_l$ are the accelerations of the previous car relative to the inertial coordinate system with the same orientation as the following car's body fixed coordinate system. $\dot{V}_x$ and $\dot{V}_y$ are the longitudinal and lateral accelerations, respectively, which can be expressed in terms of the system states and inputs.

2.2.1 .11 Actuators

The steering, brake, and throttle actuator dynamics are complex and have not been fully modeled. For this project, the actuators are modeled as first order systems:

$$\begin{aligned}
\dot{\alpha} &= \frac{(\alpha_{com} - \alpha)}{\tau_{throt}} \\
\dot{T}_{brake} &= \frac{\left(T_{brake_com} - T_{brake}\right)}{\tau_{brake}} \\
\delta &= \frac{(\delta_{com} - \delta)}{\tau_{\delta}}
\end{aligned} \tag{2.2.17}$$

where α_{com}, $T_{brake\ corn}$ and δ_{corn} are the commanded throttle, brake torque and steering inputs. τ_{throt}, τ_{brake} and τ_{δ} are the time constants of the actuators with values of 11, 75 and 125 ms respectively. The throttle and steering actuators also have rate limits of 450 degs/sec and 7.5 degs/sec respectively.

2.2.2 Simple Model

The vehicle model above is too complex to use to design a controller. Several assumptions were made about the dynamics of the system to simplify the model.

1. Vertical, roll and pitch dynamics are negligible.
2. There is no wheel slip. The vehicle velocity is then

$$V_x = \omega_w r_w \tag{2.2.18}$$

3. There is no slip across the torque converter. This assumption is valid under high speed, high gear conditions. The engine and brake torques are then related to the engine speed:

$$\dot{\omega}_e = \frac{T_{net} - r^* T_{shaft}}{J_e} = \frac{T_{net} - r^*\left(T_{brake} + r_w \sum_{i=1}^{4} F_{xi}\right)}{J_e} \tag{2.2.19}$$

4. The lateral tire force, F_{yi}, is proportional to the vehicle slip angle, v. The cornering stiffness is defined as

$$C_s = \frac{\partial}{\partial \nu} F_y(\nu)\Big|_{\nu=0} \tag{2.2.20}$$

For small velocity angles, the cornering force can be approximated as

$$F_y = C_s(\delta - \zeta) \tag{2.2.21}$$

5. $C_s >> F_x$

6. Manifold dynamics are negligible.

7. Actuator dynamics are negligible.

8. Assume the steering angles of the front wheels are small and equal, while those of the rear wheels are zero:

$$\delta_1 = \delta_2 = \delta_f \tag{2.2.22}$$

$$\delta_3 = 64 = 0$$

The complex model can then be reduced to three state equations.

$$\dot{V}_x = -\frac{(r_w r^*)^2}{J^*}\left(C_x V_x^2 + F_{roll} - mV_y\dot{\psi}\right) + \frac{(r_w r^*)^2}{J^*}\left[\frac{1}{r_w r^*}T_{tot} - 2C_{sf}\delta^2 + 2C_{sf}\left(\frac{V_y + l_1\dot{\psi}}{V_x}\right)\delta\right] \quad (2.2.23)$$

$$\dot{V}_y = -\frac{1}{m}\left[C_y V_y^2 + mV_x\dot{\psi} + 2C_{sf}\left(\frac{V_y + l_1\dot{\psi}}{V_x}\right) + 2C_{sr}\left(\frac{V_y - l_2\dot{\psi}}{V_x}\right)\right] + \frac{2C_{sf}}{m}\delta$$

$$\ddot{\psi} = \frac{2}{I_z}\left[l_2\left(\frac{V_y - l_2\dot{\psi}}{V_x}\right) - l_1\left(\frac{V_y + l_1\dot{\psi}}{V_x}\right)\right] + \frac{2l_1 C_{sf}}{I_z}\delta$$

where

$C_{sf}(C_{sr})$	front (rear) cornering stiffness
$C_x(C_y)$	front (side) wind drag coefficients
$r^*=r_{drive}r_{gear}$	effective gear ratio
$J^* = (mr^2+4J_w)(r^*)^2+J_{eng}$	effective inertia

These equations can be represented in a simplified form:

$$\begin{aligned}\dot{V}_x &= f_1(\mathbf{x}) + c_{11}T_{tot} - c_{12}\delta^2 + b_1(\mathbf{x})\delta \\ \dot{V}_y &= f_2(\mathbf{x}) + c_{21}\delta \\ \ddot{\psi}_z &= f_3(\mathbf{x}) + c_{31}\delta\end{aligned} \quad \textbf{(2.2.24)}$$

where

$$
\begin{aligned}
f_1(\mathbf{x}) &= -\frac{\left(r_w r^*\right)^2}{J^*}\left(C_x V_x^2 + F_{roll} - mV_y\dot{\psi}\right) \\
f_2(\mathbf{x}) &= -\frac{1}{m}\left[C_y V_y^2 + mV_x\dot{\psi} + 2C_{sf}\left(\frac{V_y + l_1\dot{\psi}}{V_x}\right) + 2C_{sr}\left(\frac{V_y - l_2\dot{\psi}}{V_x}\right)\right] \\
f_3(\mathbf{x}) &= \frac{2}{I_z}\left[l_2\left(\frac{V_y - l_2\dot{\psi}}{V_x}\right) - l_1\left(\frac{V_y + l_1\dot{\psi}}{V_x}\right)\right]
\end{aligned}
\qquad \textbf{(2.2.25)}
$$

and

$$
c_{11} = \frac{\left(r_w r^*\right)}{J^*} \qquad c_{12} = \frac{2C_{sf}\left(r_w r^*\right)^2}{J^*} \qquad b(\mathbf{x}) = \frac{2C_{sf}\left(r_w r^*\right)^2}{J^*}\left(\frac{V_y + l_1\dot{\psi}}{V_x}\right) \qquad \textbf{(2.2.26)}
$$

$$
c_{21} = \frac{2C_{sf}}{m} \qquad c_{31} = \frac{2l_1 C_{sf}}{I_z}
$$

The inputs to this system are $\delta_{f\,com}$ and T_{tot}. T_{tot} is a synthetic input and is used to determine the inputs α_{com} and $T_{br\,com}$. The four states describing the relative positions of the following and lead cars from section 2.2.1, can now be written as

$$
\begin{aligned}
\dot{x}_{rel} &= v_{xrel} \\
\dot{v}_{xrel} &= f_5(\mathbf{x}) - c_{51} T_{tot} + c_{52}\delta^2 - b_5(\mathbf{x})\delta \\
\mathbf{Y}_{rel} &= v_{yrel} \\
\dot{v}_{yrel} &= f_7(\mathbf{x}) - c_{71}(\mathbf{x})\delta
\end{aligned}
\qquad \textbf{(2.2.27)}
$$

Depending upon the sensor used, the terms $\ddot{x}_l$ and $\ddot{y}_l$ may or may not be measurable. If they are not known, they are assumed to be zero.

2.3 Controller Design

Lateral vehicle control has been approached using both linear and nonlinear techniques. (Peng, 1992 and Pham, 1993). Autonomous lateral control differs from these works in that no information about the car's position relative to the road is directly available. Also, road curvature information is unknown. The only information the vehicle can use is the relative position and velocity (and possibly acceleration) of the previous car's transmitter. The object of the controller, then, is to use this information to reduce the lateral error, y_r.

One approach is to track the transmitter. The goal of such a procedure is to drive the azimuth angle, the angle the car's centerline makes with the line from the sensor to the transmitter, to zero. This approach causes steady state lateral errors on curved sections, since the car will tend to cut across the curve. Narendran proposed driving the azimuth angle to a desired azimuth angle (1993). If the radius of curvature is known, a desired azimuth angle can be defined which should drive the lateral error to zero. In general, however, road curvature is not known.

Because of the highly nonlinear nature of the vehicle dynamics, nonlinear control techniques are applied. Feedback is used to cancel the nonlinearities of the system and create an equivalent linear system. More specifically, a sliding mode controller is designed to control the two input, two output simple model. This section first discusses different approaches used to track the previous car, along with their limitations. A bit of theory behind sliding mode control is presented, followed by the development of a sliding mode controller. The use of secondary surfaces to account for the actuator dynamics is briefly described.

2.3.1 Approaches to Autonomous Control

The first and most intuitive approach to lateral control is to track the transmitter by driving the azimuth angle to zero. On straight roads, when the azimuth angle is driven to zero, the following car will fall behind the lead car and onto the center of the road. On a curved section of constant radius (all curves are assumed to have constant radius), steady state lateral error exists since the following car tries to cut across the arc while tracking the lead car. If the lead car is traveling a curve of constant radius, at steady state the following car travels an arc concentric to that traveled by the lead car but with smaller radius as shown in figure 2.3.1.

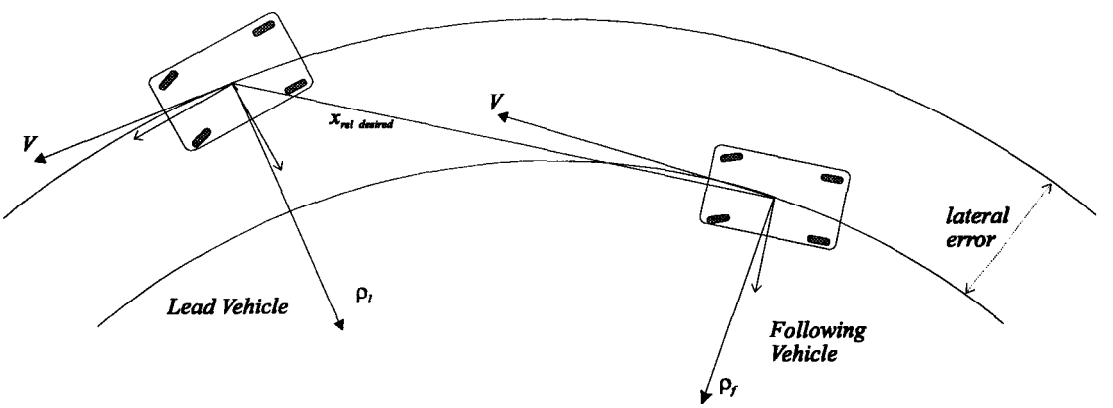

Figure 2.3.1: Vehicle Following on Curved Road

Consider the case in which the longitudinal velocity is constant and the lateral velocity is zero. Assuming constant curvature and perfect tracking, the lateral error dynamics for this simple system is:

$$\dot{y}_r = V_x(\psi - \psi_d) \tag{2.3.1}$$

Applying the law of cosines,

$$\left(\psi - \psi_d\right) \approx \left[\frac{\rho^2 - R^2 - \left(\rho - y_r\right)^2}{-2R\left(\rho - y_r\right)}\right] = \frac{y_r^2 - 2\rho y_r}{2R(\rho - y_r)} + \frac{R}{2(\rho - y_r)} \tag{2.3.2}$$

where ψ_d is the desired heading angle and R is the desired distance between the sensor and transmitter, which are assumed to be mounted over the center of the vehicles. At steady state y_r converges to

$$y_r = \rho - \sqrt{\rho^2 - R^2} \tag{2.3.3}$$

This lateral error is small for large radii and small R, but will propagate down a platoon of vehicles.

In order to keep the lateral error at zero along curved sections, one can drive the azimuth angle, φ, to φ_{des} (Narendran, 1993). This angle depends upon the radius of curvature and the inter-vehicular spacing as shown in figure 2.3.2.

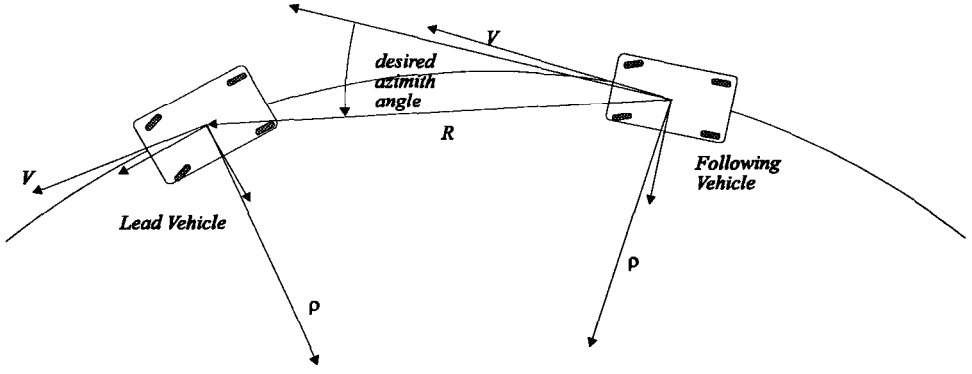

Figure 2.3.2: Desired Azimuth Angle

Making a couple of small angle assumptions, the desired azimuth angle at steady state on a curve of constant radius can be chosen as:

$$\varphi_{des} \approx \frac{R}{2\rho} \tag{2.3.4}$$

Now, substituting into the above expressions,

$$\dot{y}_r = V_x\left(\psi - \psi_d - \varphi_{des}\right) \approx V_x\left[\frac{y_r^2 - 2\rho y_r}{2R(\rho - y_r)} + \frac{R}{2(\rho - y_r)} - \frac{R}{2\rho}\right] \tag{2.3.5}$$

y_r has a stable equilibrium point at zero. This approach may not be practical since road curvature is generally not known. Instead of choosing the desired azimuth angle to be based on the road's radius of curvature, the expression, $\frac{V_x}{\dot{\Psi}}$, can be used. Note that this is approximately the radius of curvature of the path of the following vehicle. Intuitively this term will converge to p. Indeed, the lateral error dynamics are now

$$\dot{y}_r = V_x\left(\psi - \psi_d - \varphi_{des}\right) \approx V_x\left[\frac{y_r^2 - 2\rho y_r}{2R(\rho - y_r)} + \frac{R}{2(\rho - y_r)} - \frac{R\dot{\Psi}}{2V_x}\right] \tag{2.3.6}$$

where,

$$\dot{\psi} = -\dot{y}_r\left[\frac{(\rho - y_r)^2 + \rho^2 - R^2}{2R(\rho - y)^2}\right] + \frac{V_x}{\rho} \tag{2.3.7}$$

Substituting,

$$\dot{y}_r = \frac{2V_x y_r(\rho - y_r)(\rho y_r - 2\rho^2 + R^2)}{(2\rho^2 - 6\rho y_r + 3y_r^2 + R^2)(\rho R)} \tag{2.3.8}$$

y_r has a stable equilibrium point at zero. This can be shown be defining a Lyapanov function and calculating its time derivative:

$$V(y_r) = \frac{1}{2} y_r^2$$
$$\dot{V}(y_r) = y_r \dot{y}_r = \frac{2V_x y_r^2 (\rho - y_r)(\rho y_r - 2\rho^2 + R^2)}{(2\rho^2 - 6\rho y_r + 3y_r^2 + R^2)(\rho R)} \tag{2.3.9}$$

$\dot{V}$ is locally negative definite since $\rho > y_r$, so the system is asymptotically stable.

Note, that in reality, V_y is not zero, and the actual steady state lateral error when the desired azimuth angle is zero is:

$$y_r = \rho + \frac{RV_y}{V_x} - \sqrt{\rho^2 - R^2 + \left(\frac{RV_y}{V_x}\right)^2} \tag{2.3.10}$$

One can use this expression to estimate a maximum platoon size based on velocity, desired spacing and the radius of curvature. Assuming $R \approx x_{desired}$, the variation of lateral error with vehicle spacing and desired velocity can be determined. For the case of V_x **= 24.5 m/s** and p = 700 m, V_y is found in simulation to be -0.06 *m/s.* The plot of lateral error vs. desired spacing for these conditions is shown in figure 2.3.3. Also shown is the lateral error for the case in which the lateral velocity is zero.

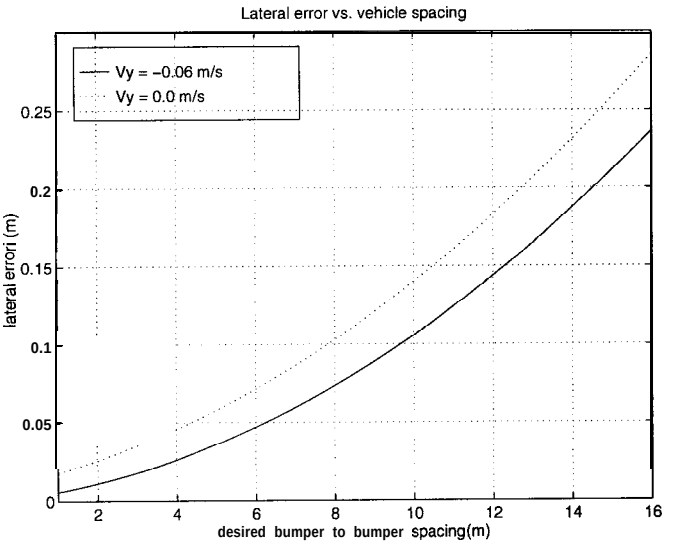

Figure 2.3.3: Lateral Error vs. Desired Spacing

The lateral error of each vehicle in a platoon relative to the path of the preceding vehicle is virtually the same, so one can determine the maximum number of vehicles in a platoon such that the last vehicle has an acceptable lateral error. For example, from the chart below, at a desired spacing of 4 meters, and for a maximum allowable steady state lateral error of 10 cm, one could have a 5 car platoon (including the lead vehicle, which is assumed to follow the road perfectly).

2.3.2 Nonlinear Controller Design

Sliding control is a nonlinear control method particularly adept at handling nonlinearities while remaining robust to unmodeled dynamics. It seems a good choice to control the highly nonlinear vehicle model, and is the controller used in this project. A brief description of sliding control follows (Slotine and Li, 1991).

Given an n^{th} order SISO nonlinear system in companion form, the goal of the controller is to make the output, y, track a desired output y_{des}. Let $\tilde{y}$ be the tracking error, y - y_{des}.

Define a surface $s(\mathbf{x};t)$ with a relative degree of one:

$$s(\mathbf{x};t) = \left(\frac{d}{dt} + \lambda\right)^{n-1} \tilde{y} \tag{2.3.11}$$

where λ is a positive constant. Note that as long as $s = 0$, the system has stable error dynamics. The n^{th} order tracking problem is now a first order problem of stabilizing s. If one chooses u to ensure that

$$s\dot{s} \leq -\frac{\eta}{\Phi} s^2 \tag{2.3.12}$$

where η is some positive constant and Φ is a boundary layer on either side of the surface s, then s is guaranteed to enter Φ. The bounds on the tracking error are related to those of the s:

$$|\tilde{y}| \leq \frac{|s|}{\lambda^{n-1}} \leq \frac{\Phi}{\lambda^{n-1}} \tag{2.3.13}$$

One variation on the above method is to introduce an integral term in the surface definition:

$$s(\mathbf{x};t) = \left(\frac{d}{dt}+\lambda\right)^{n-1}\int_0^t \tilde{y}\,dt \tag{2.3.14}$$

With modeling errors present, the surface converges to the boundary layer and the integral term. tends toward a constant value. This ensures the tracking error terms converge to zero.

One can extend this method to MIMO systems by defining a separate surface for each output. The control inputs are then chosen to satisfy the sliding condition for both surfaces.

2.3.3 Vehicle Controller

Consider the two input, two output simple vehicle model from section 2.2.2

$$\begin{aligned}\dot{V}_x &= f_1(\mathbf{x}) + c_{11}T_{tot} - c_{12}\delta^2 + b_1(\mathbf{x})\delta \\ \dot{V}_y &= f_2(\mathbf{x}) + c_{21}\delta \\ \ddot{\psi}_z &= f_3(\mathbf{x}) + c_{31}\delta\end{aligned} \tag{2.3.15}$$

The inputs are T_{tot} and δ, and the outputs are x_{rel} and y_{rel}. The goal of the controller is to drive x_{rel} and y_{rel} to their respective desired values. The input T_{tot} is actually a combination of the throttle and brake inputs, and a protocol has been created to select one of these inputs based upon the value of T_{tot}. The actuator dynamics are neglected in the development of the control law.

The inputs are treated using secondary surfaces (Green and Hedrick (1990), Hedrick, McMahon et. al. (1991) and Pham (1992)).

The surfaces are defined as:

$$S_1 = \dot{\tilde{x}}_{rel} + \lambda_{x1}\tilde{x}_{rel} + \lambda_{x2}\int_0^t \tilde{x}_{rel}d\tau$$
$$S_2 = \dot{\tilde{y}}_{rel} + \lambda_{y1}\tilde{y}_{rel} + \lambda_{y2}\int_0^t \tilde{y}_{rel}d\tau \qquad (2.3.16)$$

Differentiating the surfaces one obtains

$$\dot{S}_1 = \ddot{\tilde{x}}_{rel} + \lambda_{x1}\dot{\tilde{x}}_{rel} + \lambda_{x2}\tilde{x}_{rel}$$
$$\dot{S}_2 = \ddot{\tilde{y}}_{rel} + \lambda_{y1}\dot{\tilde{y}}_{rel} + \lambda_{y2}\tilde{y}_{rel} \qquad (2.3.17)$$

Substituting the state equations gives

$$\dot{S}_1 = f_5(\mathbf{x}) - c_{51}T_{tot} + c_{52}\delta^2 - b_5(\mathbf{x})\delta + \lambda_{x1}\dot{\tilde{x}}_{rel} + \lambda_{x2}\tilde{x}_{rel}$$
$$\dot{S}_2 = f_7(\mathbf{x}) - c_{71}(\mathbf{x})\delta - \ddot{y}_{rel\_desired} + \lambda_{y1}\dot{\tilde{y}}_{rel} + \lambda_{y2}\tilde{y}_{rel} \qquad (2.3.18)$$

The objective is to choose δ and T_{tot} such that the sliding condition

$$s\dot{s} \le -\frac{\eta}{\Phi}s^2 \qquad (2.3.19)$$

is satisfied. The inputs are chosen as:

$$T_{tot} = \frac{1}{c_{51}}\left(f_5(\mathbf{x}) + c_{52}\delta^2 - b_5(\mathbf{x})\delta + \lambda_{x1}\dot{\tilde{x}}_{rel} + \lambda_{x2}\tilde{x}_{rel} + k_1 S_1\right)$$
$$\delta = \frac{1}{c_{71}}\left(f_7(\mathbf{x}) - \ddot{y}_{rel\_desired} + \lambda_{y1}\dot{\tilde{y}}_{rel} + \lambda_{y2}\tilde{y}_{rel} + k_2 S_2\right) \qquad (2.3.20)$$

where k_i's are gains which can be adjusted to account for modeling error.

2.4 Simulations

Many simulations were run to test the controller under a wide variety of conditions. Its performance is evaluted on based its tracking ability and the resulting lateral errors. Vehicle ride quality and the propagation of lateral errors down a platoon of vehicles are also discussed. Some of the factors considered in this section are desired inter-vehicular spacing, lead vehicle acceleration and the use of a desired azimuth angle. A merge and lane changing scenerio is demonstrated, and noise and errors are added to the lateral position sensor readings to develop sensor specifications.

2.4.1 Lane Following

In the first set of simulations, the effects of lead car acceleration, vehicle spacing and road curvature on tracking performance are examined in a typical lane following situation, The platoon of vehicles travels on a straight road for 100 meters before entering a curved section with a constant radius of 700 m. The road is diagrammed in figure 2.4.1.

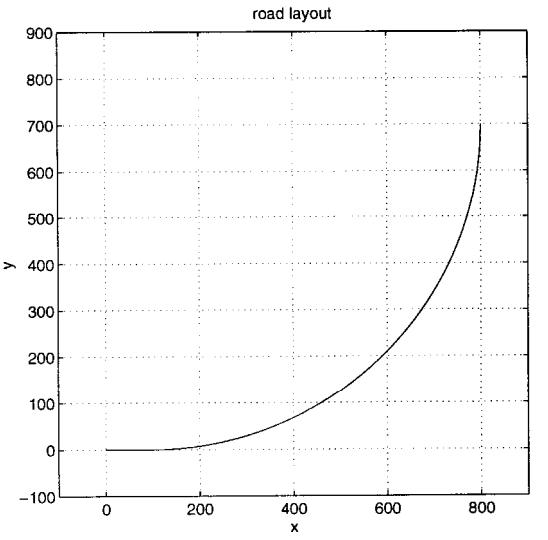

Figure 2.4.1: Road Layout for Lane Following Simulations

A nominal lane following case is presented first. The lead vehicle has a constant velocity of 24.5 m/s, and the following vehicles have initial conditions such that there is no error. The desired vehicle spacing is 2 meters. The sensor is mounted at the front of the vehicle, the transmitter is mounted on the rear of the preceding vehicle, and the desired azimuth angle is zero. The results of this simulation are shown in figure 2.4.2 and 2.4.3.

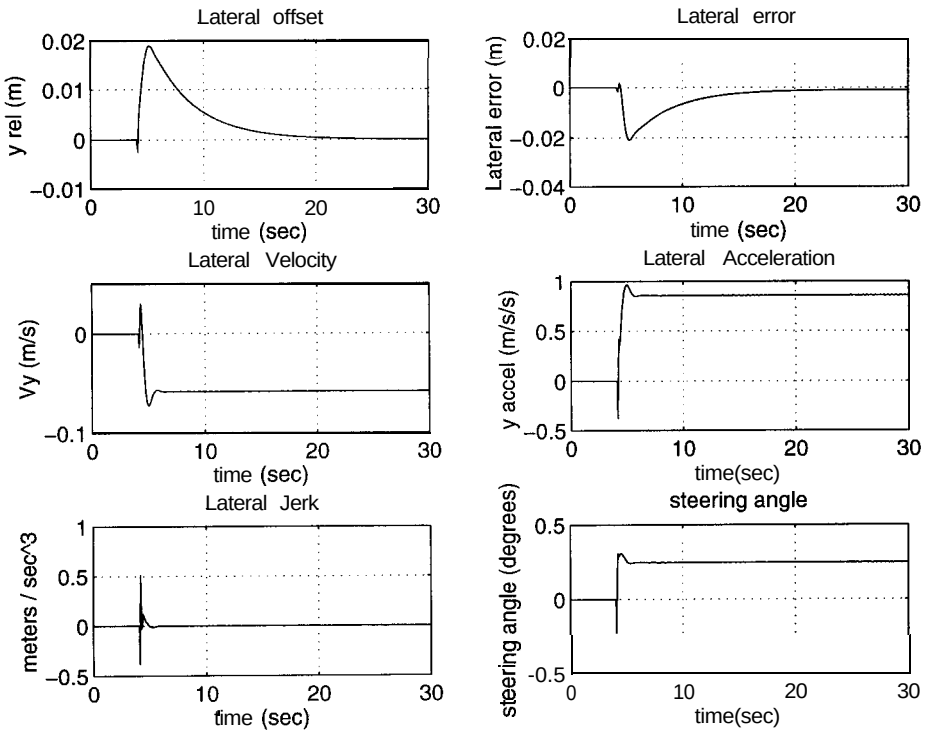

Figure 2.4.2: Lateral Results of Simulation

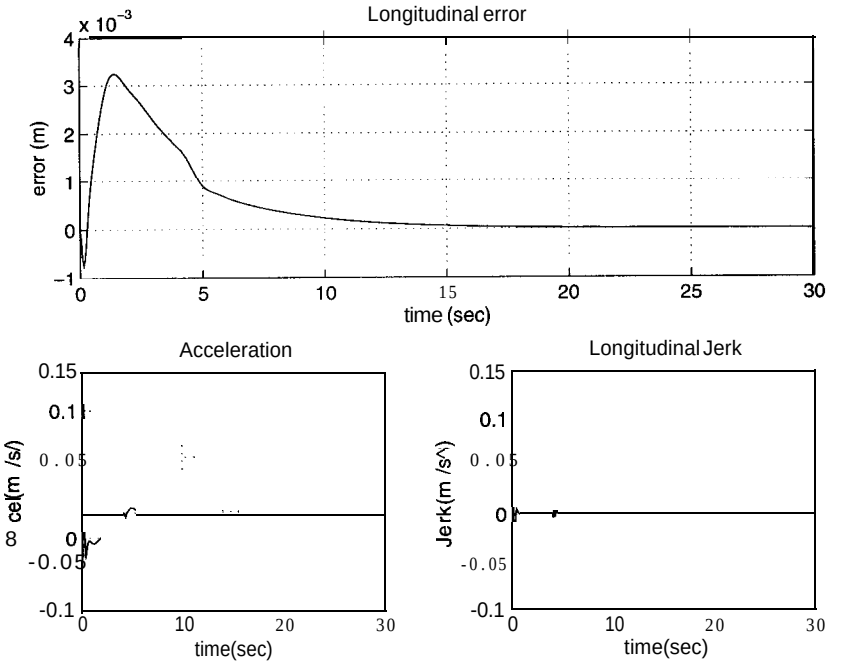

Figure 2.4.3: Longitudinal Results of Simulation

The controller tracks the lead car well while entering the curve. The lateral offset increases temporarily before going to zero. The lateral error term also increases and then settles at a steady state value near zero. The lateral acceleration, determined by speed and radius, is high but acceptable considering the small radius of curvature. The longitudinal tracking error is virtually unaffected by the entrance onto the curved section.

2.4.2 Vehicle Spacing

Desired vehicle spacing is considered next. Figure 2.4.4 shows the lateral error during the lane following situation above for different vehicle spacings. The velocity is still 24.5 m/s, and the sensor and light source are in the same positions as in the nominal case above. For a two car platoon, the following vehicle could maintain a large spacing and still remain near the center of the road. Even at a spacing of 12 meters, the lateral error is only 11 cm. At spacings less than two meters, the lateral error is actually negative, since the lateral velocity is negative and tends to push the vehicle toward the outside of the curve. In general, the change in desired spacing has only a small effect on lateral tracking performance.

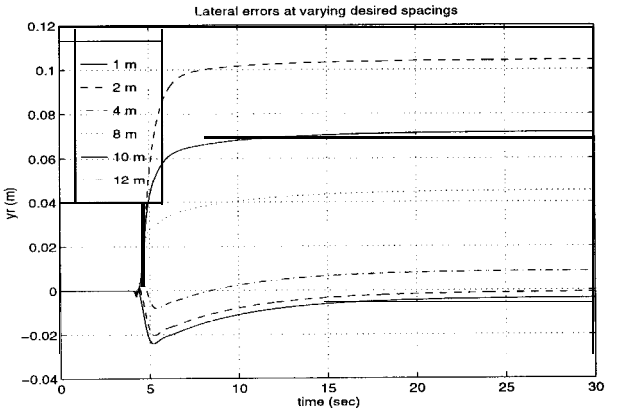

Figure 2.4.4: Lateral Error During Lane Following

2.4.3 Acceleration Profiles

The next set of simulations examines the effects of lead vehicle acceleration maneuvers. Since under normal conditions, relative longitudinal acceleration will be known and a longitudinal controller has already been developed, the focus of this study is on the lateral tracking performance. The desired spacing is 8 meters. After 18 seconds, the lead car either accelerates from 16.5 m/s to 24.5 m/s or decelerates from 24.5 m/s to 16.5 m/s. The deceleration and acceleration profiles, shown in figure 2.4.5, all have the same form. In the first 2 seconds, the lead car's acceleration increases or decreases to some maximum or minimum value (+/- 0.5, 1 .O, 1.5, or 2.0 m/s^2). The acceleration remains constant for a few seconds before returning to zero during the final 2 seconds.

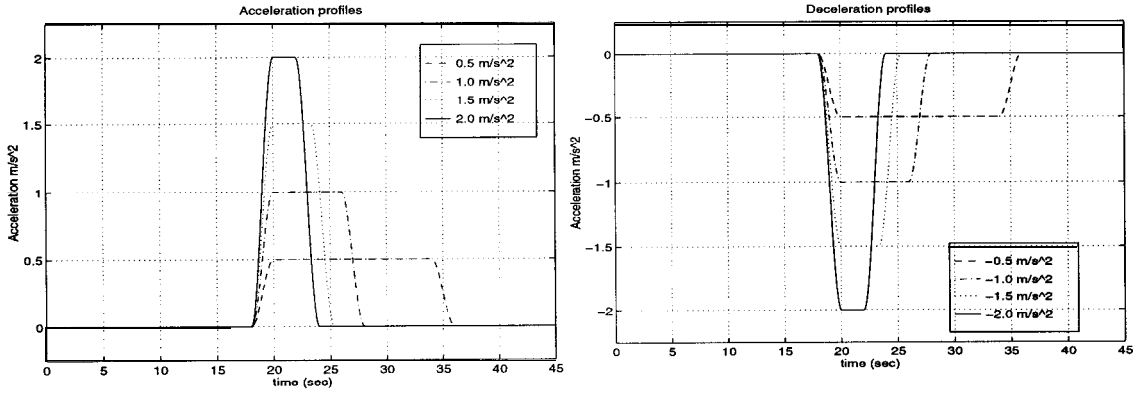

Figure 2.4.5: Acceleration and Deceleration Profile

2.4.3.1 Acceleration

The results of the acceleration tests are shown in figures 2.4.6-2.4.11. Figure 2.4.6-2.4.7 display the longitudinal error and throttle angle respectively. The longitudinal error increases while the acceleration is changing, at the beginning and end of the profiles. It decreases during the constant acceleration portion of the profile, when the maximum acceleration is less than 2.0 . m/s^2. In all cases, it remains within the acceptable limits for this desired spacing. The throttle angles for profiles with maximum accelerations below 2.0 m/s^2 display satisfactory responses. At 2.0 m/s^2, the throttle saturates, causing the sudden increase in the longitudinal error during the period of constant acceleration.

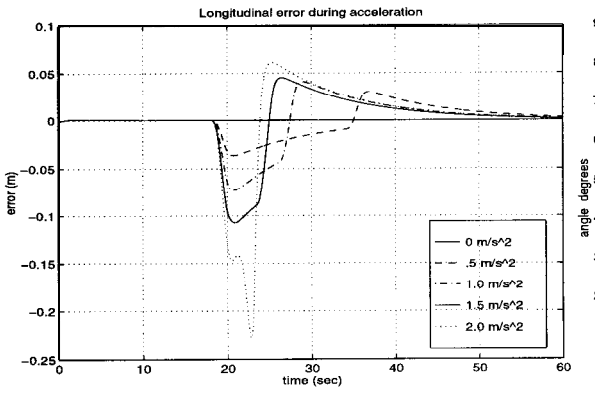

Figure 2.4.6: Longitudinal Error

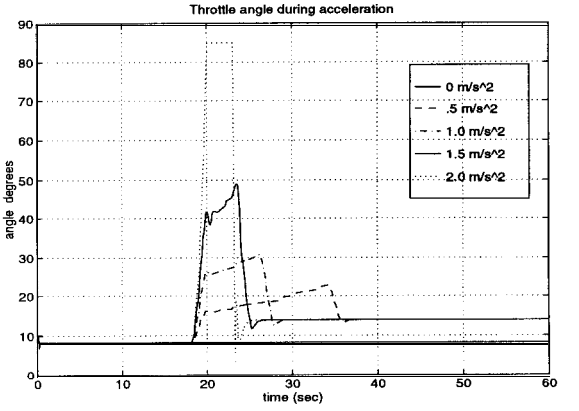

Figure 2.4.7: Throttle Angle

The plot of longitudinal jerk, figure 2.4.8, shows that the ride quality is satisfactory for profiles with low accelerations, (0.5 or 1.0 m/s^2). At 1.5 m/s^2, the maximum jerk nears its acceptable limit (approximately 2 m/s"). For the 2.0 m/s^2 profile, the jerk is unacceptable. Not completely shown on the plot, the maximum jerk in this case is nearly 8 m/s^3.

The lateral offset and lateral error plots are displayed in figures 2.4.9-2.4.10. The lateral offset increases when the vehicle enters a curved section, but eventually goes to zero as the lateral error reaches some constant value. During the acceleration profile, lateral offset increases, but is still well within an acceptable range, even with an acceleration of 2.0 m/s^2. The lateral errors change in an almost linear fashion to their new steady state values of about 4.5 cm, demonstrating that the small lateral tracking errors have little effect on the lateral error.

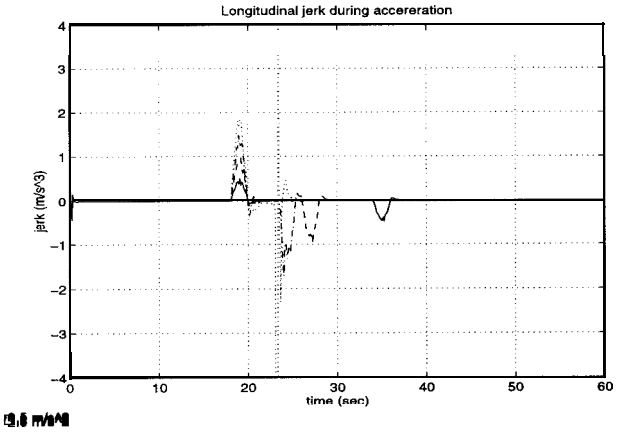

Figure 2.4.8: Longitudinal Jerk

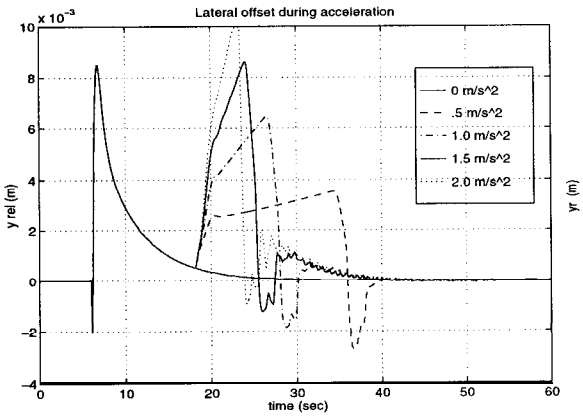

Figure 2.4.9 Lateral Offset

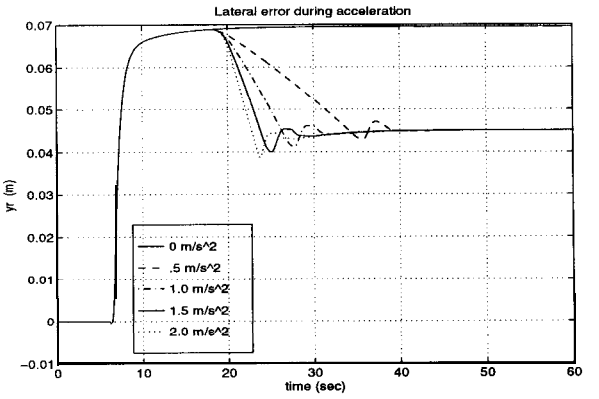

Figure 2.4.10: Lateral Error

The lateral jerk, shown in figure 2.4.11, is satifactory, even at high accelerations.

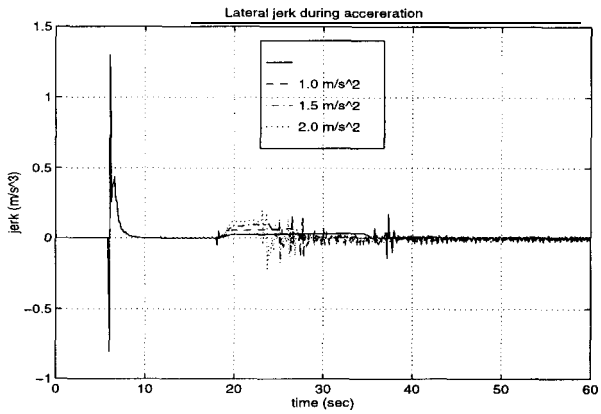

Figure 2.4.11: Lateral Jerk

2.4.3.2 Deceleration

The results of the deceleration tests, shown in figures 2.4.12-2.4.15 are comparable to those of the acceleration tests. The longitudinal and lateral tracking errors increase during periods of changing acceleration, but tend to level off when the acceleration is constant. In all cases, tracking errors are acceptable.

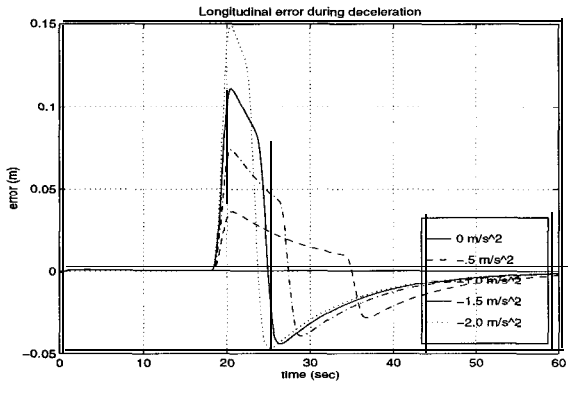

Figur 2.4.12: Longitudinal Error

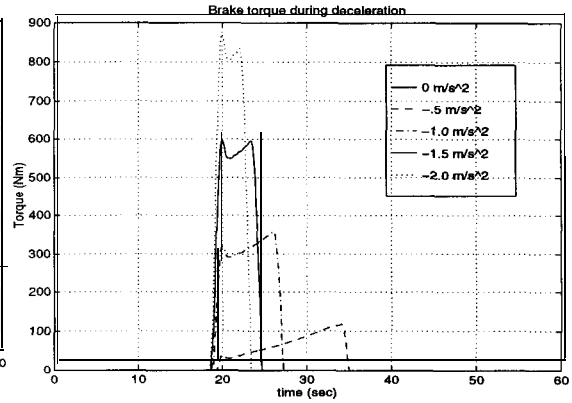

Figure 2.4.13: Brake Torque

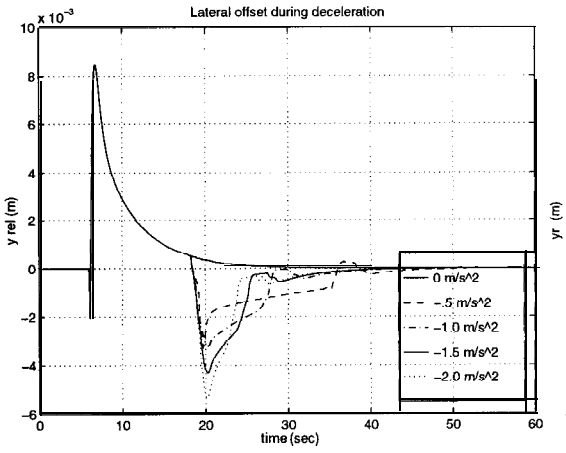

Figure 2.4.14: Lateral Offset

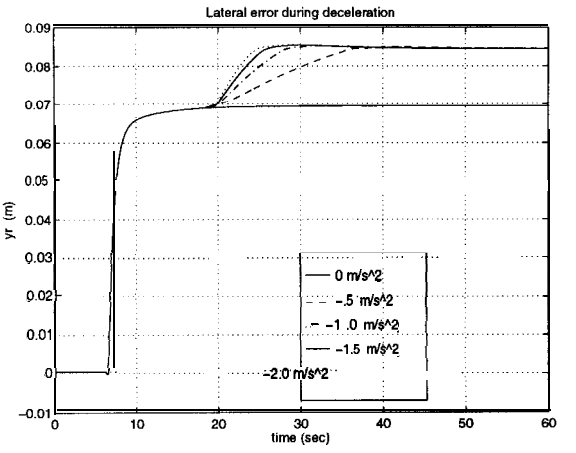

Figure 2.4.15: Lateral Error

Similarly to the acceleration case, the lateral tracking error has little effect on the lateral error, which increases linearly to its new steady state value.

2.5 Azimuth Angle

The next set of simulations demonstrates the effectiveness of using a desired azimuth angle to reduce the propagation of errors down a platoon of vehicles.

2.5.1 Zero Desired Azimuth Angle

It was shown above, that, for a two car platoon, a zero desired azimuth angle does not result in an excessively large lateral error, even for large vehicle spacings. In platoons of vehicles, however, the lateral errors propagate down the platoon and are not acceptable. Figures 2.5.1 and 2.5.2 display the results of simulations of a five car platoon (including the lead car) at 2 meter

spacing and 10 meter spacing with a zero desired azimuth angle. The sensor and transmitter are mounted over the centers of each of the vehicles in this and the following cases.

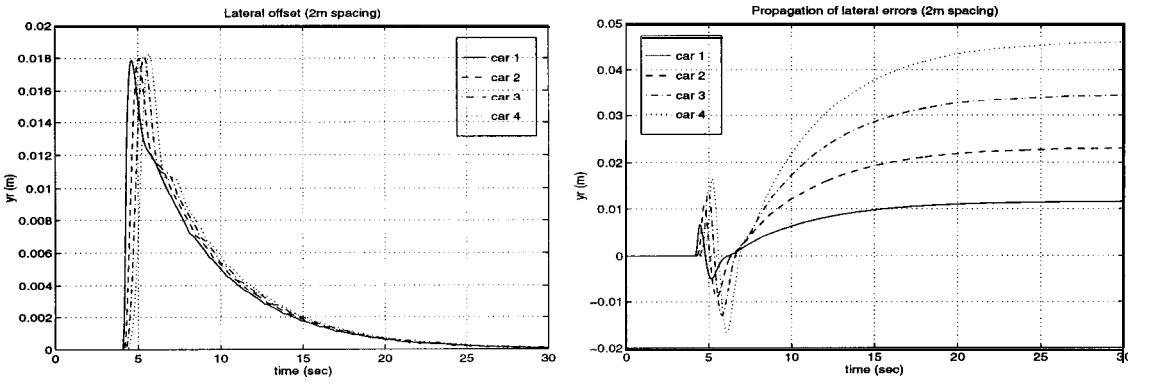

Figure 2.5.1: Simulation Results with 2 m Spacing and Zero Desired Azimuth Angle

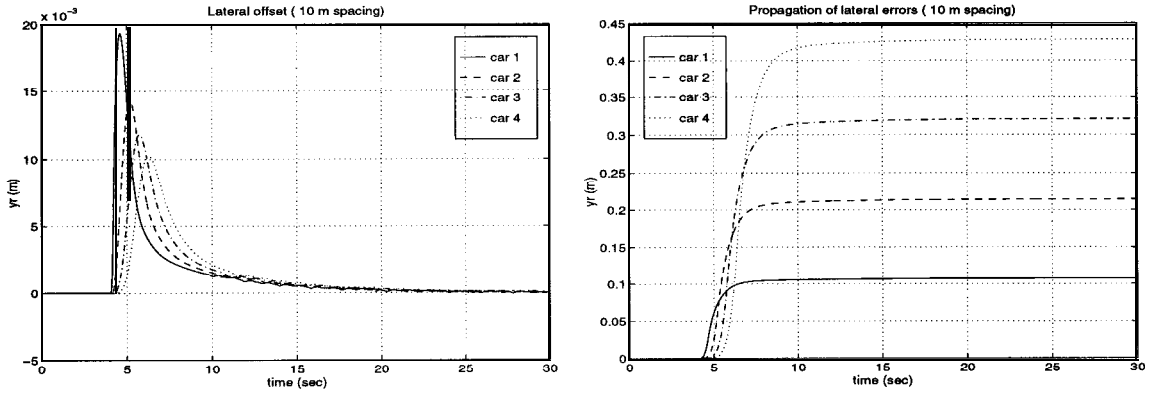

Figure 2.5.2: Simulation Results with 10 m spacing and Zero Desired Azimuth Angle

In both cases the lateral offsets of all the vehicles go to zero at steady state, while the steady lateral errors increase down the line of cars. The lateral errors of the fourth car behind the lead car in the 2 meter spacing test is a reasonable 5 cm. At 10 meter spacing, the lateral error of the same car is over 40 cm.

2.5.2 Non-Zero Desired Azimuth Angle

The same simulations as above were then run with a desired azimuth angle. The results are displayed in figure 2.5.3.

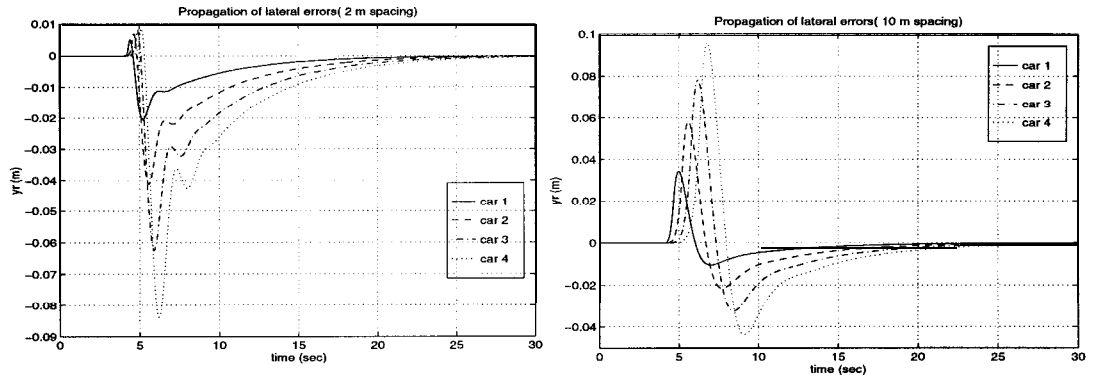

Figure 2.5.3: Simulation Results with Desired Azimuth Angle

In this case the lateral offsets tend to some desired value as the lateral errors, even of the fourth car in the platoon, go toward zero.

2.6 Merge / Lane Change

One of the motivations behind an autonomous lateral controller is its usefulness in lane change situations. A merge/ lane change simulation was run to demonstrate the controller's ability to perform such a manuever. Initially the following car is 5 meters behind and one lane (5 meters) to the side of the lead car, which is traveling at a constant speed of 24.5 m/s. The goal of the procedure is to guide the car to a position two meters directly behind the lead car. In order to

ensure acceleration and jerk constraints are met, the vehicle is made to track a smooth trajectory. The results of this manuever are shown in figure 2.6.1.

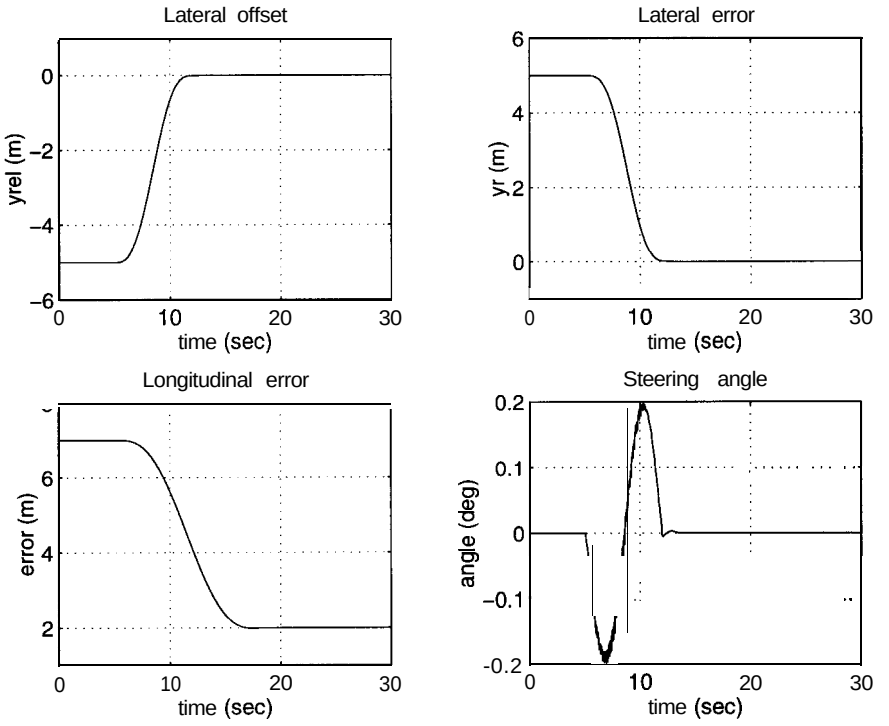

Figure 2.6.1: Simulation Results of Performing a Merge/Lane Change Maneuver

2.7 Sensor Specifications

In the final set of simulations, errors and noise are added to the lateral sensor readings to examine controller robustness to lateral sensor error and to develop sensor specifications. In these simulations, two vehicles travel at 24.5 m/s on the road with a curved section of radius 700 m. Desired spacings of 2 m and 10 m are considered.

Lateral measurement errors in the form of a percent of the actual lateral offset were first added. As one would expect, the controller is insensitive to such errors as long as the desired azimuth angle is zero. As seen in figures 2.7.1 and 2.7.2 , even with 50% error, the lateral tracking performance is still very good. The error does not have a large effect on the transient response of the system.

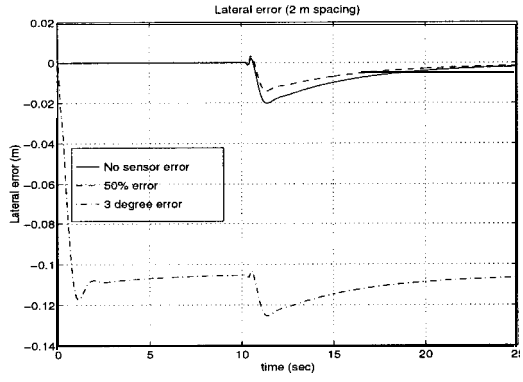

Figure 2.7.1: Lateral Error due to Sensor Error (2 m spacing)

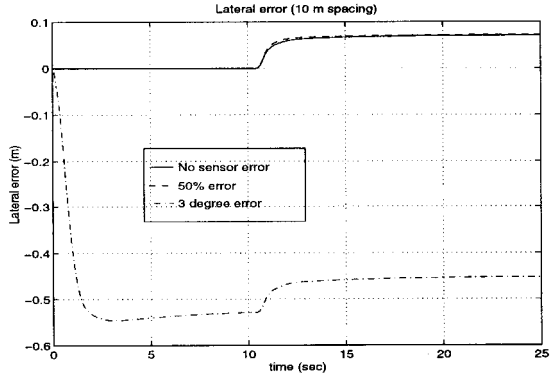

Figure 2.7.2: Lateral Error due to Sensor Error (10 m spacing)

In the next case, the centerline of the lateral sensor is offset by some angle from the centerline of the car. Such errors might occur if the sensor is not mounted properly. The controller is very sensitive to such errors, since small angle offsets causes large steady state lateral errors at large desired spacings. From the plots above, an error of 3 degrees results in barely acceptable lateral errors for 2 meter desired spacing, and leads to lateral errors of over 40 cm. if the desired spacing is 10 m.

Finally, the effect of noise is considered. Zero mean, white noise of a specified standard deviation is added to the lateral sensor readings, and the standard deviation of the lateral error is recorded. Figure 2.7.3 shows a plot of the lateral error standard deviation for several lateral offset standard deviations and desired vehicle spacings. One can use this to make estimates of the maximum amount of acceptable noise in the lateral offset readings.

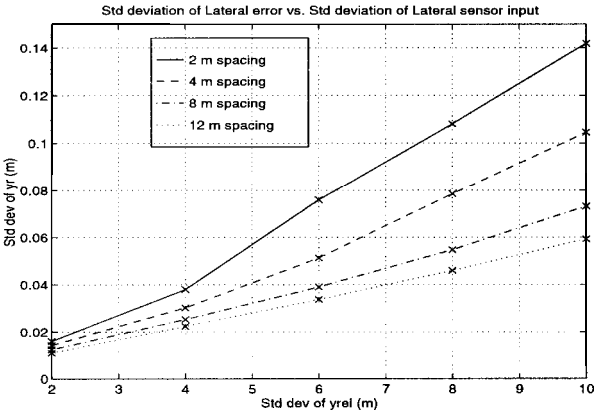

Figure 2.7.3: Standard Deviation of Lateral Error vs. Std. Deviation of Lateral Sensor Input

For example, in order to keep the standard deviation of the lateral error under 3 cm. at 4 meter spacing, one would require the standard deviation of the lateral offset readings to be less than 4 cm.

The angle about the centerline for which the sensor can get accurate measurements is an important parameter. In simulations, under worse case conditions, (1 m spacing, sensor and tranmitter at the front and rear of the car, respectively), the maximum azimuth angle is less than 1.5 degrees. It is recommended that the sensor be able to detect the transmitter at least 4 degrees on either side of the centerline.

2.8 Qualimatrix PATH Optical Ranging System

Qualimatrix, Inc. has developed an optical ranging system (ORS) for the PATH project which outputs the longitudinal position and lateral offset of an infrared light source. This system is being considered for use with an autonomous lateral control scheme. Some static and dynamics tests have been performed in order to judge its effectiveness. The systems and the tests are discussed below.

2.8.1 System Setup

The ORS consists of two light detectors, the infrared light source, and signal processing equipment (Qualimatrix, 1993). The detectors are mounted on the roof of the following vehicle while the light source is mounted over that of the lead vehicle. The light source consists of five rows of five LEDs which produce an infrared light modulated at a selected frequency. Each light detector focuses the light from the light source on a high resolution Position Sensitive Detector

(PSD). The outputs of each PSD are two currents whose ratio is proportional to the distance of this image from the origin of the PSD.

The outputs of the PSD's pass through a DSP chip and are sent to a 486 processor. Given these outputs and distance between the two detectors, one can determine the position of the light source relative to the midpoint between the two detectors. The longitudinal distance is given as the distance along perpendicular bisector of the line joining the two detectors. The detectors are mounted such that this line is the centerline of the car. The lateral offset is the distance off of this centerline.

2.8.2 Testing

2.8.2.1 Static Tests

Static tests were performed on the sensor to determine the accuracy of the longitudinal and lateral measurements over the sensor's viewing range. The standard deviation of these two measurements at these positions is also examined. The sensor was tested by taking sets of measurements at 9 longitudinal distances (20, 24, 25, 30, 40, 50, 60, 75, 100 m). At each longitudinal distance, measurements were taken at 30 cm intervals, 1.5 m on either side of the center line, for at total of 11 measurements. The longitudinal accuracy is then determined by comparing the actual longitudinal distance with the measured distance. Since it is very difficult to determine the actual centerline of the sensor, the accuracy of the lateral readings is found by assuming the measurement over the estimated centerline is correct and comparing the measured lateral distances from the estimated centerline with the actual distances. Because of problems

with saturation of the PSD's, readings at distances closer than 9.1 m were not able to taken. The results of the other tests are shown below.

Figure 2.8.1 displays longitudinal results of the static tests. The longitudinal readings are accurate to within 5% within 5 degrees on either side of the centerline at distances up to about 18.2 m. At 22.9 and 30.5 m, the longitudinal readings are accurate within 1.5 m, or about 3 degrees, of the centerline.

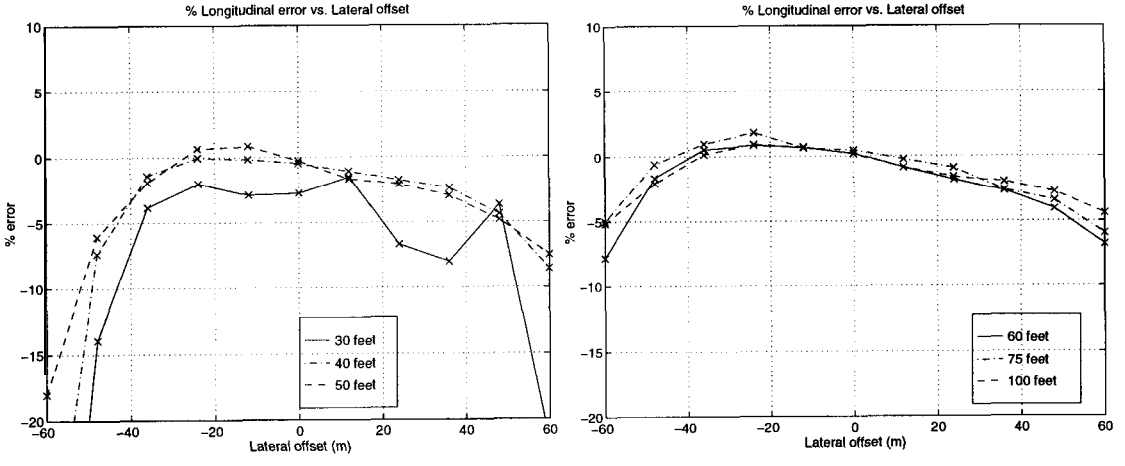

Figure 2.8.1: Longitudinal Results of Static Tests

Figure 2.8.2 shows the lateral test results. The lateral distance readings at longitudinal distances less than 18.3 m are accurate to within 5% about 5 degrees on either side of the centerline. Beyond 18.3 m, the accuracy declines somewhat.

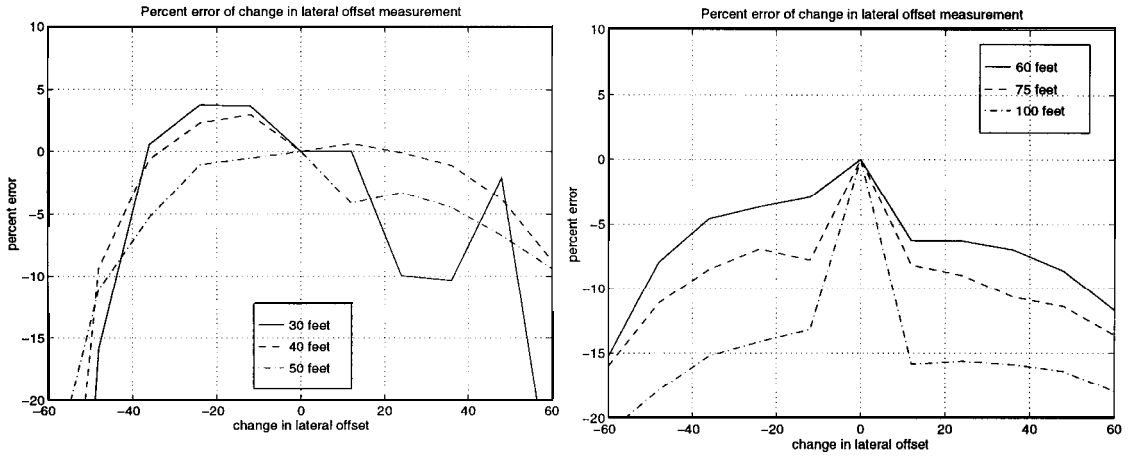

Figure 2.8.2: Lateral Test Results of Static Tests

Figures 2.8.3 and 2.8.4 are plots of the standard deviations of the longitudinal and lateral signals at each of the positions. For these static tests, the standard deviations are all well within the recommended bounds.

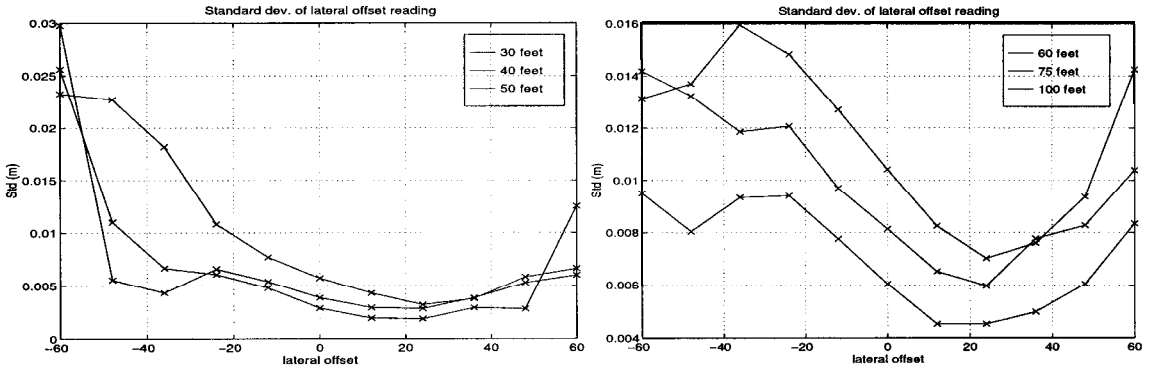

Figure 2.8.3: Standard Deviation of Lateral Offset Readings

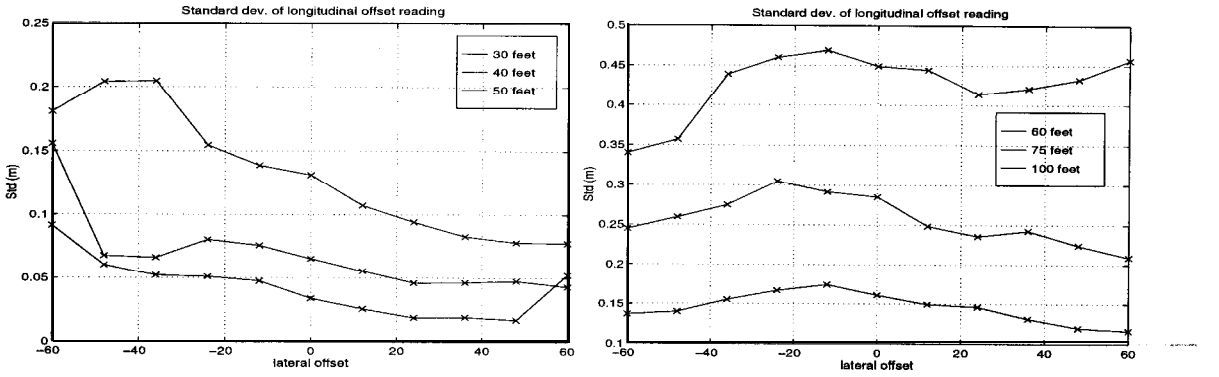

Figure 2.8.4: Standard Deviation of Longitudinal Offset Readings

In general, the static tests showed that sensor is accurate within a 4 or 5 degree angle of vision. Nothing can be said, however, about the sensor measurements for distances closer than 9.1 m. Qualimatrix currently is modifying the sensor to solve the saturation problem.

The data from the static tests was used to make a simple model of the sensor for purposes of simulation. The results of one such simulation, in which a two car platoon enters a curved section with a radius of 700 meters, is shown in figure 2.8.5. This plot suggests that, based on static tests, the Qualimatrix sensor is a feasible choice for a lateral sensor.

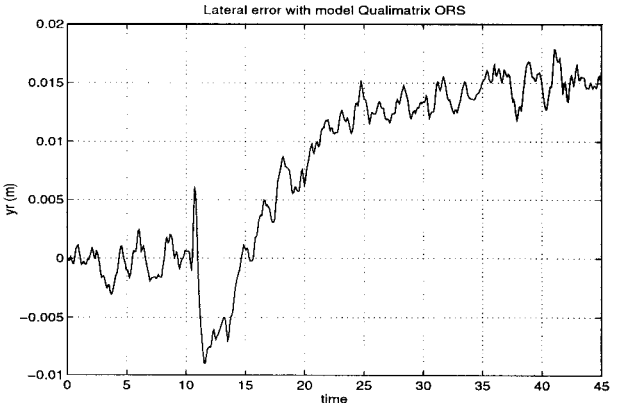

Figure 2.8.5: Simulation Results Using Sensor Model

2.8.2.2 Dynamic Tests

Several tests were performed by placing the light source on top of a fixed car and driving a car with light detectors back and forth behind it. Radar and sonar longitudinal sensor data were also taken for comparison. The results of the longitudinal sensor readings for these three sensors are shown in figures 2.8.6 and 2.8.7.

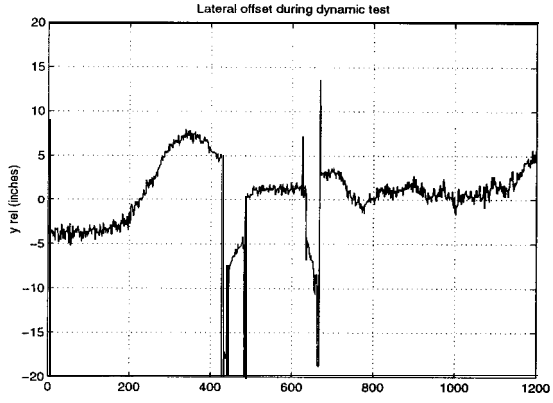

Figure 2.8.6: Lateral Offset During Dynamic Testing

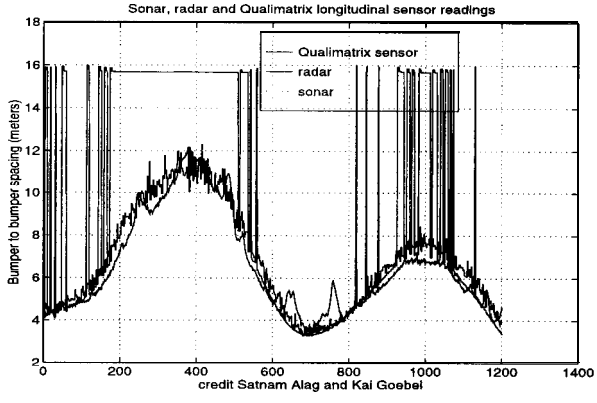

Figure 2.8.7: Longitudinal Sensor Readings

The longitudinal distance measurements of the Qualimatrix sensor are accurate relative to the other two sensors, but are also very noisy, especially while the vehicle is changing directions. Figure 2.8.10 illustrates the high standard deviation of lateral measurements during dynamic testing. It also shows the signal dropping out temporarily.

Based upon test data and on general observations made during testing, the Qualimatrix ORS works well under controlled circumstances but is very sensitive to disturbances. Slight changes in the angle of the detectors up or down, and changes in velocity during dynamic tests caused errors and unacceptable levels of noise. The system is in the process of being modified, so the results displayed here will hopefully be improved. In any case, more testing is recommended.

2.9 Conclusions

The proposed autonomous lateral control strategy is basically pointing the vehicle at a transmitter located on the previous vehicle. An analytic expression was developed to approximate the resulting steady state lateral error as a function of vehicle longitudinal and lateral velocity, longitudinal spacing and road curvature. Such an expression allows one to determine the maximum platoon size of a platoon of vehicles utilizing the above control scheme. If yaw rate and/or lateral velocity information are known, the method can be modified to include a desired azimuth angle which drives the error to zero, or at least reduces it significantly.

A sliding mode controller was developed to track the preceding vehicle's transmitter. The controller displayed good tracking performance in simulation. During acceleration, when tracking performance deteriorated somewhat, lateral errors did not increase significantly. Simulations also demonstrated the effectiveness of a using a non-zero desired azimuth angle. For a simulation in

which the intervehicular spacing was 10 meters, the lateral error is reduced from 10 cm to almost zero. Even if lateral velocity is not known, the lateral error is still reduced to 3 cm.

A merge/lane change maneuver was also simulated. The main problem with such a maneuver is that the angle of view required of the lateral sensor is very large (45 degrees in the simulation presented here). Obviously, this angle depends upon the initial relative positions of the two vehicles, but it remains a major limitation.

The controller is found to be robust to certain lateral sensor errors. The requirements on the lateral error as a percentage of the actual value are lax as long as the bias error is zero (for the case of zero desired azimuth angle). The controller is sensitive to errors in the orientation of the sensor, especially at large desired spacings. Noise also affects the lateral controller. Lateral offset reading noise with a standard deviation of greater than 3 or 4 cm is generally unacceptable.

The Qualimatrix sensor is found to be reasonably accurate during static tests but had a very noisy signal in dynamic testing.. In light of the fact that major modifications have been made to the system recently, more testing of the sensor is necessary.

The major drawback of this system is the propagation of lateral errors down a platoon of vehicles. This problem could be solved with communication of the relative positions of the vehicles down the platoon, giving the cars knowledge of the lead car position. This system would not be fully autonomous, however. For two to four car platoons, this proposal represents a feasible method for autonomous control.

3. AICC

Tohru Yoshioka

3.1 Introduction

In order to be feasible, a fully Automated Highway System will require a significant amount of infrastructure support. An intermediate step in the development of intelligent highways, which can be introduced in a few years, is an intelligent cruise control system called "Cooperative Intelligent Cruise Control System" (CICC System). It includes automatic throttle and brake (longitudinal) control, and simple infrastructure-vehicle communication. Through communication, infrastructures give certain kinds of information to each CICC vehicle so as to control the traffic flow on highways, and each CICC vehicle follows the instructions from infrastructures, CICC will be used in a mixed flow where both automated vehicles and manually operated vehicles exist on the highway at the same time. Then, CICC will be designed so that it works as a convenient cruise control system when there are no vehicles ahead or only some vehicles in the distance. It also works as a distancing control system when vehicles ahead are within a certain range. Moreover, CICC can achieve good riding comfort even if there exist vehicles that suddenly cut in front, while it can effectively avoid rear end collisions with braking vehicles

In this chapter, analytical work is done to investigate how CICC should be organized and what kinds of information is necessary to make CICC possible. The chapter is organized as follows. In section 3.2, the features of spacing control, headway control, and a human model are compared. Section 3.3 describes how static flow rates vary with respect to cruising speed and other factors. This is followed by comparisons of transient responses of flow rate due to the

change in a lead car's velocity in section 3.4. Section 3.5 deals with the transient responses of flow rate in headway control due to changes in headway time. In section 3.6, the capability of avoiding collisions is discussed under a few scenarios, such as collisions with stopping vehicles and those with vehicles that brake suddenly. Section 3.7 is a concluding section and describe the features of the CICC system.

3.2 Features of Distancing Control Strategies

There are two main distancing-control strategies for automated vehicle following: spacing control and headway control. Hedrick et. al., 1991, compare both strategies in terms of string stability, vehicle flow rate, and experiments on vehicle following. As for human driver models, several models are presented including vehicle following by Pipes, 1953, and Burnham, Seo and Bekey, 1974, and braking and steering control by Salman, 1990. The transient responses and vehicle flow rates among three human-driver models are compared by Shladover et. al., 1991.

3.2.1 Spacing Control

In constant spacing control, the spacing error ε_j is defined as

$$\varepsilon_j = x_{j-1} - x_j - L_v - L \tag{3.2.1}$$

where j, L_v, and L correspond to the jth car, the car length, and the constant, inter-vehicular distance, respectively. The transfer function of the spacing error $\hat{h}(s)$ can be described as

$$\hat{h}(s) \equiv \frac{\hat{\varepsilon}_j}{\hat{\varepsilon}_{j-1}} = \frac{k_a s^2 + k_v s + k_p}{s^2 + (k_v + c_v + k_1)s + (k_p + c_p)} \qquad \textit{(3.2.2)}$$

where k_a, k_v, k_p, c_v, and c_p represent control gains based on sliding-mode control theory. Then, by using these gains, the desired acceleration is defined as

$$u_1 = (k_p + C_p)\varepsilon_1 + (k_v + C_v)\dot{\varepsilon}_1 + (k_a + k,)a, - k_1(\dot{x}_1 - \dot{x}_1(0\_)) \qquad \textit{(3.2.3)}$$

and

$$\begin{aligned} u_j &= k_p \varepsilon_j + k_v \dot{\varepsilon}_j + k_a a_{j-1} + k_l a_l - k_1(\dot{x}_i - \dot{x}_i(0\_)) \\ &\quad - C_p\left(x_j - x_l + \sum_{i=1}^{j}(L_v + L)\right) - C_v(\dot{x}_j - \dot{x}_l) \qquad \textit{for } j > 1 \end{aligned} \qquad \textit{(3.2.4)}$$

For constant spacing control, the control gains should be chosen properly to avoid the slinky effects. Since information about velocity and acceleration of the lead car as well as acceleration of the preceding vehicle is necessary, which was shown by Hedrick et. al., 1991, inter-vehicular communication is essential for platooning. One advantage of constant spacing control is that with the information of the lead car and properly chosen gains, it can arbitrarily assign the poles of the system, so that it shows a desirable transient and steady state behavior.

3.2.2 Headway Control

Under constant headway control, the spacing error ε_j is defined as

$$\varepsilon_j = x_{j-1} - x_j - L_v - L_0 - h_w \dot{x}_j \tag{3.2.5}$$

where j, L_v, L_0, and h_w correspond to the jth car, the car length, the offset length, and the headway time, respectively. By applying the sliding-mode control theory, i.e. letting $S = \varepsilon_j$, and $\dot{S} = -\lambda S$, the desired acceleration can be expressed as

$$u = \frac{1}{h_w}\left(\lambda (x_{j-1} - x_j - L_v - L_0) + (\dot{x}_{j-1} - \dot{x}_j) - h_w \lambda \dot{x}_j\right) \tag{3.2.6}$$

and the transfer function of the spacing error $\hat{h}(s)$ is

$$\hat{h}(s) \equiv \frac{\hat{\varepsilon}_j}{\hat{\varepsilon}_{j-1}} = \frac{1}{h_w s + 1} \tag{3.2.7}$$

For constant headway control, string stability is assured whenever there is no delay time in the actuator. With this control, however, the gain λ can't change the system's dynamics: there will always exist a pole at $s = 1/h_w$. Since small headway time results in a large bandwidth, actuator saturation will occur, which means that headway control is not suitable for a very heavy vehicles.

Moreover, if the actuator's response is delayed, string stability is not always assured. Suppose that an actuator has a delay time of T , and the gain for sliding control is λ . The transfer function of the spacing error can then be expressed as

$$\hat{h}(s) \equiv \frac{\hat{\varepsilon}_j}{\hat{\varepsilon}_{j-1}} = \frac{(s+\lambda)e^{-sT}}{h_w s^2 + (I + h_w \lambda)e^{-sT} s + \lambda e^{-sT}} \qquad \textbf{(3.2.8)}$$

Then using the Pade approximation, the condition to satisfy string stability is

$$T \le \frac{4(1 + h_w \lambda) - 2\sqrt{4 + 4h_w \lambda + 3h_w{}^2 \lambda^2}}{\lambda (4 + h_w \lambda)} \qquad (3.2.9)$$

The maximum delay time is shown in figure 3.2.1, and as expected, it decreases as headway time decreases and control gain λ increases; actuator delay time should be less than 0.1 seconds with a control gain smaller than 1.2.

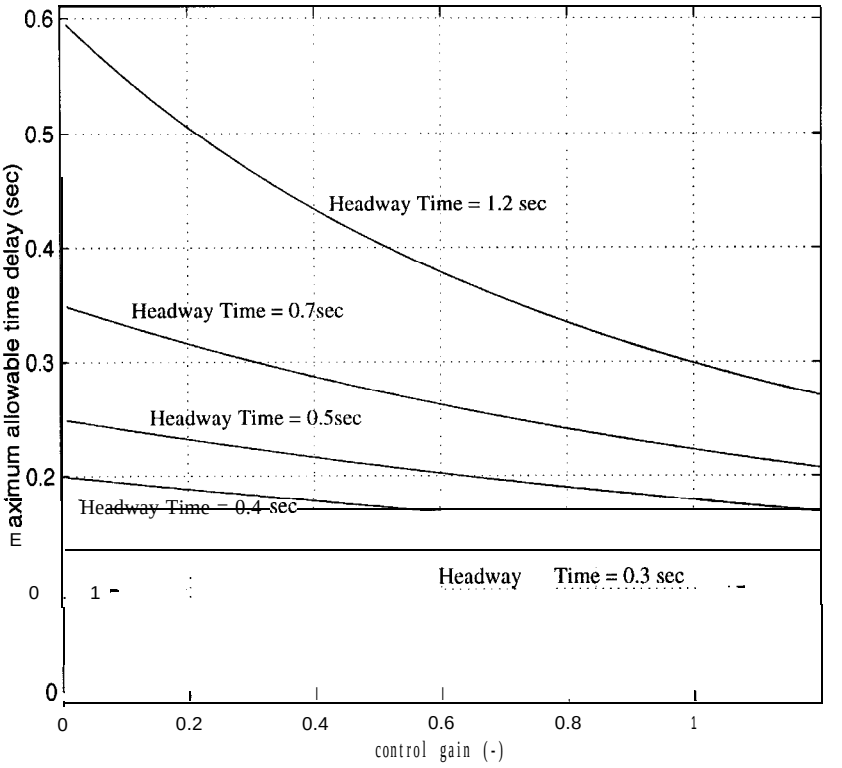

Fig. 3.2.1: Maximum Delay Time for String Stability

Similarly, if an actuator's response can be modeled as a first order delay, with a time constant τ , the transfer function of the spacing error is described as

$$\hat{h}(s) \equiv \frac{\hat{\varepsilon}_j}{\hat{\varepsilon}_{j-1}} = \frac{s+\lambda}{\tau h_w s^3 + h_w s^2 + (1+h_w\lambda)s + \lambda} \tag{3.2.10}$$

The condition to satisfy the string stability is now

$$\tau \le \frac{h_w}{2(1+h_w\lambda)} \tag{3.2.11}$$

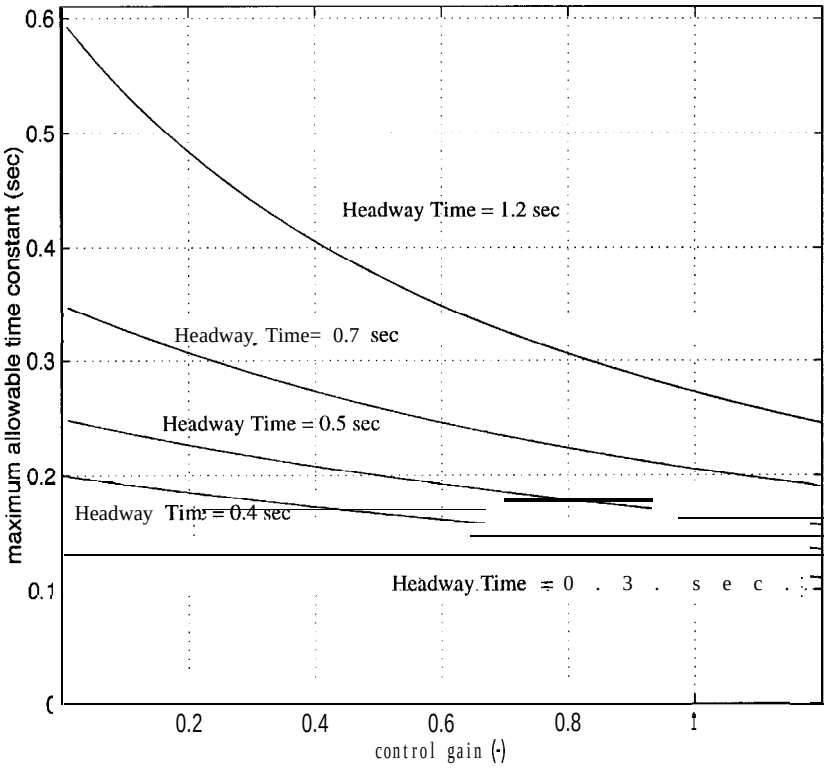

Fig. 3.2.2: Maximum Time Constant for String Stability

The maximum time constant is shown in figure 3.2.2, which is quite similar to the one in figure 3.2.1. It can be concluded that whatever small values the control gain takes, both the delay time and the time constant of an actuator must be less than $h_w / 2$ to maintain string stability.

3.2.3 Human Operation

Before evaluating the performance of automated vehicle following systems, it is first necessary to examine the performance of human drivers. Since the behaviors of human drivers are not always straightforward, many models are presented in various aspects that attempt to emulate these behaviors. In order to avoid excessive complexity, however, a simple human model for

vehicle following is presented, and one characteristic of human drivers regarding steering control is mentioned in the following sections.

3.2.3.1 Vehicle Following Control (Longitudinal Control)

Shladover et. al., 199 1, showed that the linear-optimal control model gives the best results for transient response and flow rate among three human models for vehicle following. The model can be described as

$$\begin{aligned} u = {} & C_s(x_{j-1}(t-\tau) - x_j(t-\tau) - L_v - L_0) \\ & + C_v(v_{j-1}(t-\tau) - v_j(t-\tau)) \\ & - C_s C_c v_j(t-\tau) \end{aligned} \tag{3.2.12}$$

where u and $\tau = 0.09$ sec are the acceleration output and delay time respectively, and gains are $C_s = 1.64\ \text{sec}^{-2}$, $C_v = 0.5\ \text{sec}^{-1}$, and $C_c = 1.14$ sec . This model is designed to keep headway time at a steady state, and its equivalent headway time is C_c.

3.2.3.2 Steering Control (Lateral Control)

To make clear how human drivers steer is also crucial to the design of an automated vehicle following system, because the system controls inter-vehicular distance, and the information about this distance is extremely important for human drivers to steer properly. Mitschke, 1990, performed simulations to evaluate human, steering-control behaviors in a cross wind. The simulations are evaluated from the standpoints of system stability, phase margin, and

magnitude slopes at crossover frequency. The results show; 1) human drivers need prediction time to control a vehicle properly, 2) the closed-loop system, which consists of a vehicle and human driver, becomes unstable if the prediction time, which is taken from the front axle of vehicle, is smaller than 0.3 seconds, and 3) the best results are achieved with the prediction time of 0.7 seconds.

Thus, if an automated vehicle-following system is not equipped with an effective lateral control, the headway time should be larger than 0.3 seconds, because a preceding vehicle disturbs a driver's line of sight if the headway is smaller than 0.3 seconds. Although a shorter headway time than this may not result in fatal instability directly, it can diminish the performance of human steering control and make it difficult for an automated vehicle following system to be implemented in real highways.

3.3 Analysis of Static Flow Rate

The major purpose of an automated highway system is to create greater carrying capacity by controlling traffic, and there are several factors which influence static flow rates on highways.

Then, static flow rates will be evaluated with respect to vehicle velocity, distancing control strategies, mixed flow, infrastructure-vehicle communication, and lanes for automated vehicle only.

3.3.1 Comparison of Static Flow Rates

Since static flow rates depend primarily on vehicle velocity, an evaluation should be first made on the relationship between steady state flow rate and vehicle velocity. Since the static flow

rates also depend on the distancing control strategies, the effects of some distancing controls on the static flow rates are evaluated.

3.3.1.1 Spacing Control (Platooning)

Hedrick et. al., 1991, show that the static flow rate, for platooning, can be expressed as

$$\phi = \frac{3600\ v}{L_v + L_c + \frac{L_p}{N}},\quad L_p = v\Delta t + \frac{v^2}{2}\left(\frac{1}{d_1} - \frac{1}{d_2}\right) \tag{3.3.1}$$

where $v, L_v, L_c, L_p, N, \Delta t, d_1$ and d_2 are the vehicle velocity, the car length, the intra-platoon spacing, the inter-platoon distance for collision safety, the number of vehicles in a platoon, the following platoon deceleration, and the lead platoon deceleration, respectively. From equ. 3.3.1, the static flow rates increase as Δt and d_2 decrease and as d_1 increases. Then, by changing these parameters, optimistic, practical, and pessimistic cases can be defined. To compare static flow rates, the following combinations of parameters will be simulated:

1) Optimistic Case

$L_v = 5\,m, L_c = 1m,\ N = 20,\ \Delta t = 0.1sec,\ d_1 = 0.4\,g, d_2 = 0.5\,g$

2) Practical Case

$L_v = 5\,m, L_c = 1m,\ N = 20, \Delta t = 0.3sec, d_1 = 0.4\,g, d_2 = 1g$

3) Pessimistic Case

$L_v = 5\,m, L_c = 1m,\ N = 20,\ \Delta t = 0.3sec, d_1 = 0.3\,g, d_2 = 2g$

3.3.1.2 Headway Control

For constant headway control, the static flow rate can be expressed as

$$\phi = \frac{3600\ v}{L_v + L_c + L_h}, L_h = h_w\ v \qquad (3.3.2)$$

where v, L_v, L_c, L_h, and h_w are the vehicle velocity, the car length, the distance offset, the inter-vehicular distance, and the headway time, respectively. The combinations of parameters used in the simulation are:

1) case 1: $L_v = 5$ m, $L_c = 1$m, $h_w = 0.3$ sec

2) case 2: $L_v = 5$ m, $L_c = 1$m, $h_w = 0.7$ sec

3) case 3: $L_v = 5$ m, $L_c = 1$m, $h_w = 1.2$ sec

3.3.1.3 Human Model (Linear-Optimal Control Model)

In the steady state, the linear-optimal control model works as a constant headway controller, and the headway time is $C_c = 1.14$ sec.

3.3.1.4 Comparison of Distancing Strategies on Static Flow Rates

Figure 3.3.1 shows the static flow rates for each case. For a baseline, a flow rate derived from the California Safety Rule is also shown.

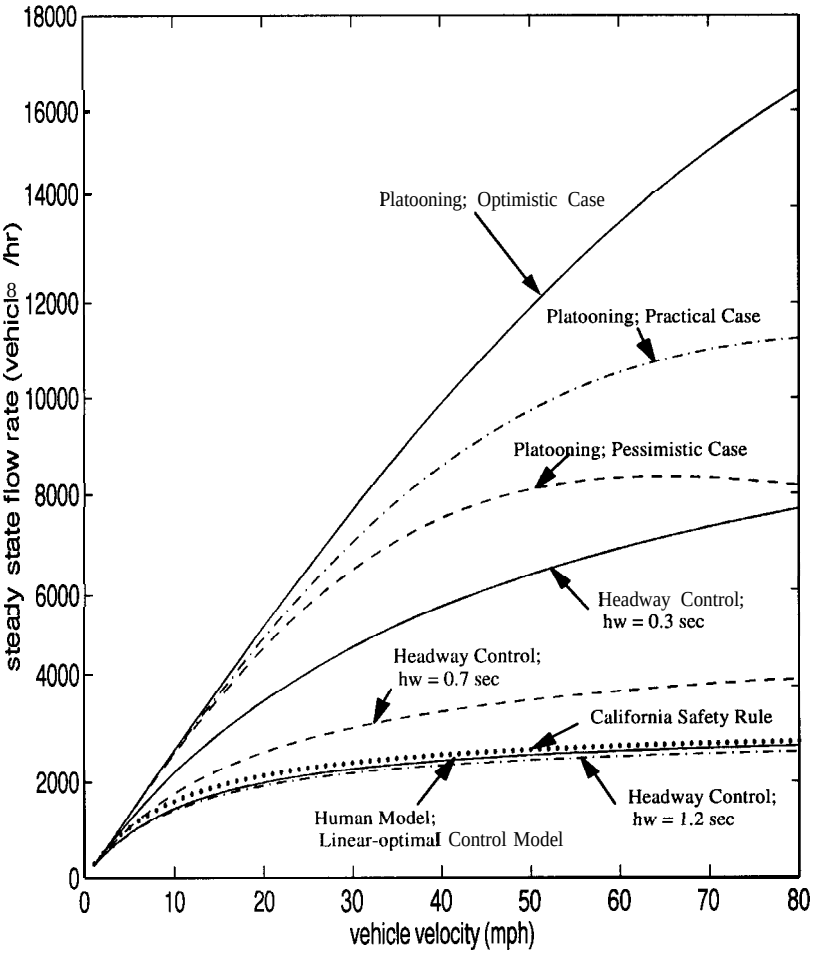

Fig. 3.3.1: Static Flow Rate Comparison

Under this rule, the desired distance is defined as one vehicle length for every 4.4 m/sec (10 mph) [Ioannou and Chien, 1992]. Assuming that a vehicle's length is 5 meters, the inter-vehicular distance is described as

$$d = 0.16\, L_v\, v \tag{3.3.3}$$

In figure 3.3.1, all flow rates for a platoon show the best results in comparison with constant headway control and human models. The results of the constant headway control with a 1.2 second headway time most nearly match California's safety rule and the linear-optimal control model. Thus, the constant headway control with headway time of less than 1.2 seconds can achieve a better static flow rate than can human control, though it cannot be comparable with rates for platooning. At 22.2 m/sec (50 mph), for instance, both a headway control with 0.3 seconds and with 0.7 seconds show 150% and 50% more flow rate respectively than does the human linear-optimal control model.

3.3.2 Static Flow Rate in Mixed Flow

The main advantages of headway control are that it does not need the information from lead car to achieve string stability, and it can be used in a mixed flow with manually operated vehicles. The static-flow rate in a mixed flow will be evaluated in terms of the percentage of the vehicles using headway control on highways .

The static-flow rate in a mixed flow can be calculated by a weighted means of the headway time under headway control and under human operation,

$$h_{mixed} = r\, h_{headway} + (1 - r)\, h_{locm} \tag{3.3.4}$$

where r, $h_{headway}$ and h_{locm} are the percentage of headway controlled vehicles, headway time under headway control, and headway time under linear-optimal control model, respectively.

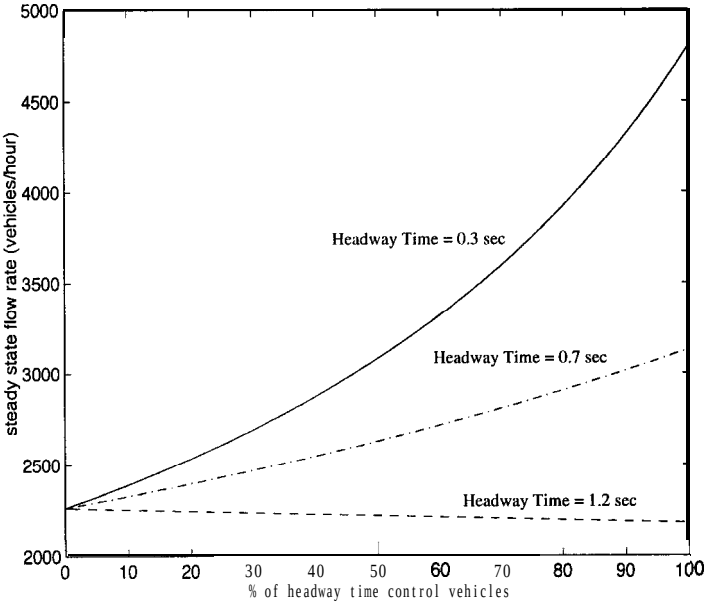

Fig. 3.3.2(a): Flow Rate in Mixed Flow at 13.3 m/sec

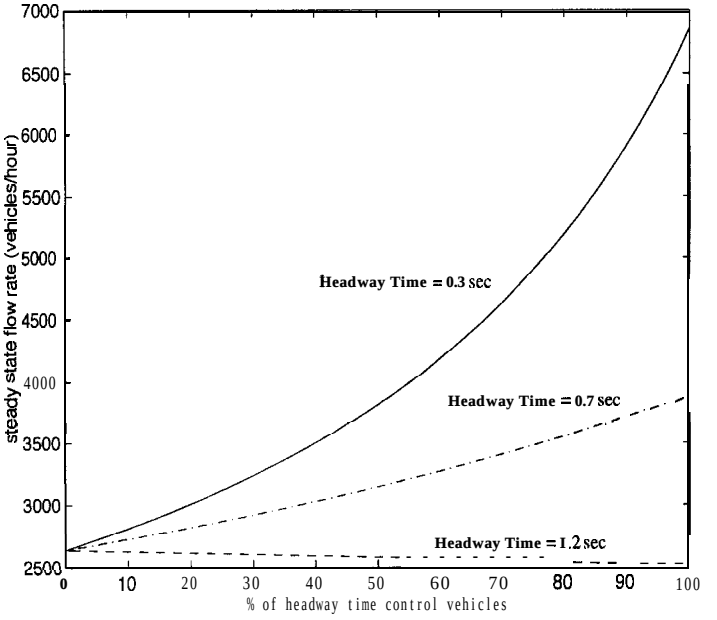

Fig. 3.3.2(b): Flow Rate in Mixed Flow at 26.7 m/sec

Figures 3.3.2(a) and 3.3.2(b) show the results of mixed flow rate at velocities of 13.3 and 26.7 m/sec (30 and 60 mph). Since the linear-optimal control model is equivalent to 1.14 seconds of headway control in the steady state, the net flow rate decreases as the percentage of headway controlled vehicles increases in a mixed flow of 1.2 seconds of headway control and human model. To increase the flow rate by 10% above that achieved under manual control, the percentage of headway controlled vehicles should be larger than about 15% for 0.3 seconds desired headway under control and 30% for 0.7 seconds desired headway under control at both velocities.

3.3.3 Effects of Intervehicular Communication on Mixed Flow

Inter-vehicular communication makes it possible for platooning to achieve string stability by supplying other vehicles with information about the lead car. Moreover, it is possible that inter-vehicular communication can also improve the performance of headway control.

For example, assume that a following vehicle knows that a preceding vehicle is controlled automatically. The headway time can then be considerably smaller than that for manually operated vehicles. This assumption is possible because automated vehicles that are controlled properly are less likely to brake suddenly and to collide with other vehicles than those driven by human drivers. Thus, the static flow rates that will be achieved with inter-vehicular communication can be larger than those without. Suppose that there are two headway-time policies as follows:

1) since headway controlled vehicles do not support inter-vehicular communication, their headway time should be 0.7 seconds, even if a preceding vehicle is headway controlled or human operated, or

2) every headway controlled vehicle is equipped with an inter-vehicular communication device so that it can tell whether the preceding vehicle is headway controlled or human operated through communication with other vehicles.

During inter-vehicular communication, it is assumed that each pair of adjacent vehicles communicates with each other. Note that communication is possible only between adjacent vehicles. In addition, if inter-vehicular communication is possible, the mean value of headway time can be expressed as

$$h_{mean} = h_{locm} + (h_{normal} - h_{locm})\, r + (h_{close} - h_{normal})\, r^2 \qquad (3.3.5)$$

where r, h_{locm}, h_{normal} and h_{close} are the percentage of headway controlled vehicles, headway time of human operated vehicles, headway time between a human operated vehicle and a headway controlled one, and headway time between two headway controlled vehicles when communication is available. If, however, inter-vehicular communication is not available, the quadratic term disappears because $h_{normal} = h_{close}$. Headway time values used in the simulation are as follows:

$$h_{locm} = 1.14 \text{ sec}$$

$$h_{normal} = 0.7 \text{ sec}$$

$$h_{close} = 0.3 \text{ sec}$$

The reasons why the minimum headway time is set to 0.3 seconds are because under headway control, human drivers steer their vehicles manually, which means that there should be enough distance for them to properly control their vehicles and, as equ. 3.2.6 shows, shorter headway time results in actuator saturation, which may degrade the system performance.

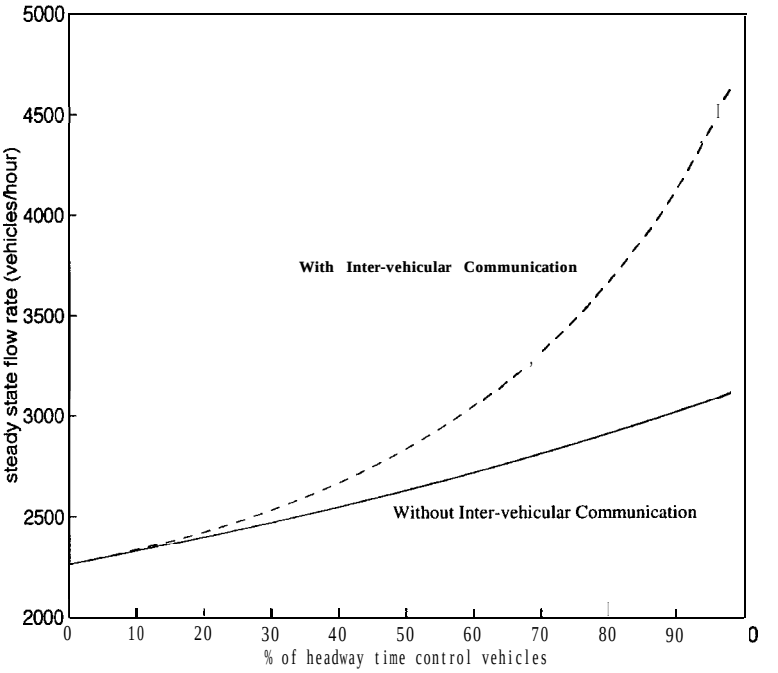

Fig. 3.3.3(a): Flow Rate at 13.3 m/sec with Intervehicular Communication

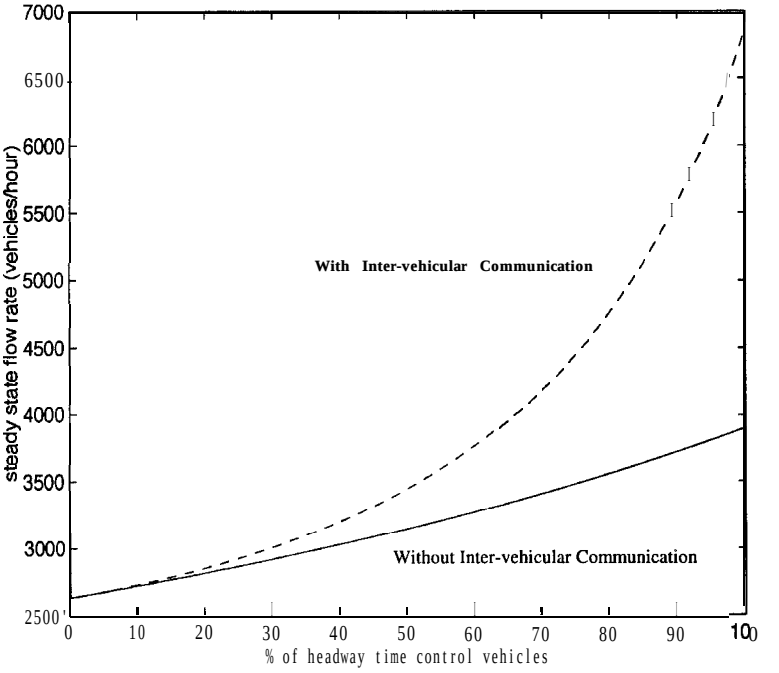

Fig. 3.3.3(b): Flow Rate at 26.7 m/sec with Intervehicular Communication

Figures 3.3.3(a) and 3.3.3(b) compare the two cases described above with static flow rates of 13.3 and 26.7 m/s (30 and 60 mph). Since a pair of adjacent vehicles tends to be headway controlled according to the increasing percentage of headway controlled vehicles, mean headway time decreases as this percentage approaches 100%. At any percentage, however, the static flow rate with inter-vehicular communication is superior to that without communication. Moreover, the difference becomes larger as the percentage of headway controlled vehicles increases.

The difference, however, is not as large when the percentage is smaller. For example, to get a 10% difference between the two cases, the percentage of headway controlled vehicles should be larger than 50% at either velocity; the inter-vehicular communication does not contribute to increasing static flow rate until the percentage of headway controlled vehicles is larger than 50%. A reasonable conclusion from this is that increasing the cost and complexity of inter-vehicular communication is unwarranted, especially when intelligent cruise control systems are first introduced.

3.3.4 Feasibility of Building Lanes for Headway Controlled Vehicles Only

In addition to inter-vehicular communication, another way to improve the flow rate with headway control is to design certain lanes for automated vehicles only. If the lanes for automated vehicles are not full of headway controlled ones, then all headway controlled vehicles can run in them exclusively, and manually operated vehicles can run in the conventional lanes. If headway time can be as small as 0.3 seconds in the automated lanes, a higher density flow will be achieved. If, however, the number of headway controlled vehicles exceeds a certain limit, some automated vehicles will run in conventional lanes where vehicle flow will be a mixed flow. For example,

suppose that there are four lanes in a particular highway. Then the relation between the flow rate and the percentage of headway controlled vehicles can be given as follows:

$$\text{For } 0 \le r \le r_0,$$
$$N = \frac{r\, i\, f_{close} + (1 + r)(4 - i)\, f_{locm}}{4}$$

$$\text{For } r_0 < r \le 1, \tag{3.3.6}$$
$$N = \frac{1}{4} \frac{3600\ (4 - i)}{h_{locm} + (h_{normal} - h_{locm})\, r' + (h_{close} - h_{normal})\, r'^2 + \frac{L_v + L_0}{v}} + \frac{i\, f_{close}}{4}$$

where N, r, i, f_{close} and f_{locm} are the mean flow rate per lane, the percentage of headway controlled vehicles, the number of lanes for automated lanes, the static flow rate with small headway time, and the static flow rate with the linear optimal control model. L_v, L_0 and v are as defined previously. r_0 is the percentage of headway controlled vehicles up to which there are only manually operated vehicles in conventional lanes, and r' is the percentage of headway controlled vehicles in the conventional lanes when r is larger than r_0. Thus, r_0 and r' are defined as

$$r_0 = \frac{i\ f,}{i\, f_{close} + (4 - i)\, f_{locm}}$$

$$r' = r - (1 - r) \frac{i\, f,}{4N - i\, f_{close}} \tag{3.3.7}$$

The results of the simulations are shown in figure 3.3.4. The simulations were conducted under each of the following scenarios: 1) no lanes are automated ones, 2) one of four lanes is used for automated vehicles, or 3) two of four lanes are for automated vehicles. It is also assumed that inter-vehicular communication is not available in the first scenario, while it is used in the other scenarios.

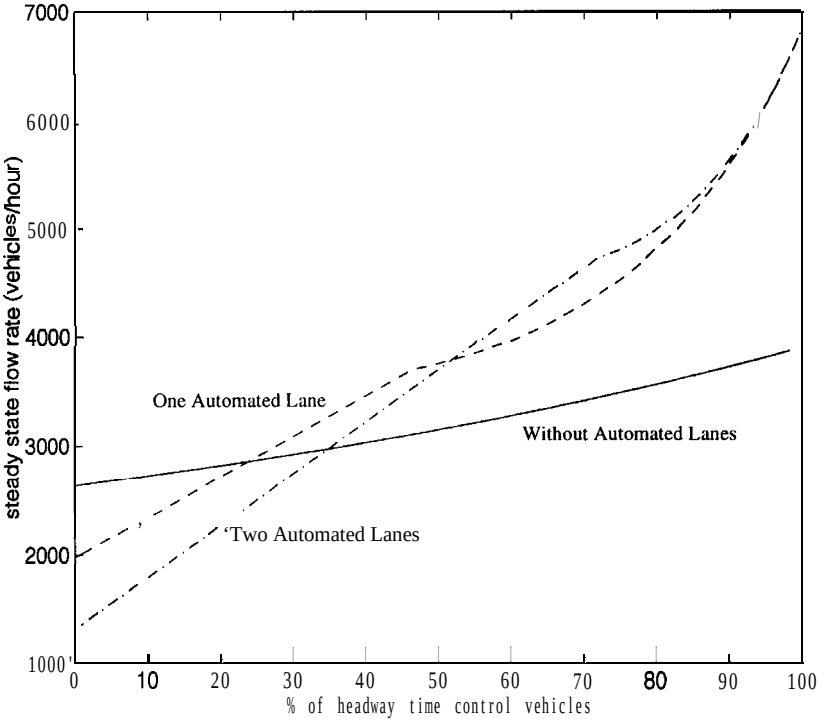

Fig. 3.3.4: Effects of Lanes for Automated Vehicles at 26.7 m/sec

It can be deduced from the figure that if the percentage of headway controlled vehicles is small, there are no benefits to increased static flow rate with lanes for automated vehicles. For one lane of automated vehicles, the percentage of headway controlled vehicles must be larger than 25% at 13.3 and 26.7 m/sec (30 and 60 mph) to get a higher flow rate than that of a normal mixed

flow, and the percentage must be larger than 40% at 13.3 m/sec (30 mph) and 35% at 26.7 m/sec (60 mph) for two lanes of automated vehicles. In the small percentage of headway controlled vehicles, the equivalent flow rates are smaller than those without lanes for automated vehicles. The reason for this is that the automated lanes are nearly empty for the case of small percentage of headway controlled vehicles. As a result of that, the small headway time in the automated lanes does not improve the total flow rates on highways. Thus, building lanes only for automated vehicles can not be justified to improve static flow rate when the population of automated vehicles using the roadway is small.

3.4 Analysis of Dynamic Flow Rate

To control the flow of traffic, the transient response of the flow rate due to the change in velocity is also crucial. Then, each control scheme will be evaluated for the transient responses due to the change in the velocity of the lead vehicle.

Suppose that once again the lead vehicle initially runs at 15 m/sec and accelerates at 1 m/sec^2 to 25 m/sec and that other vehicles follow the lead car under appropriate control schemes as shown in figure 3.4.1.

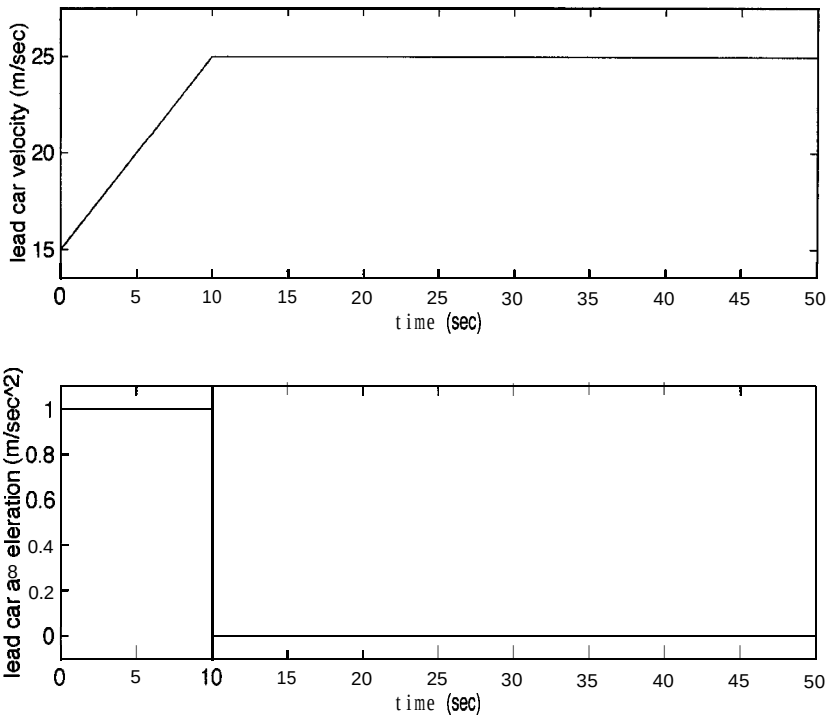

Figure 3.4.1: Velocity Profile of Lead Vehicle

Throughout the simulation, each vehicle is treated as a mass and the desired acceleration is used directly as a command input to each mass. To make the analysis simple and to grasp the general features of the human control model, it is assumed that all human drivers operate vehicles following the linear-optimal control model precisely.

3.4.1 Spacing Control (Platooning)

The simulation results of a twenty-vehicle platoon with delay times of 0.1 seconds and 0.3 seconds are shown in figure 3.4.2.

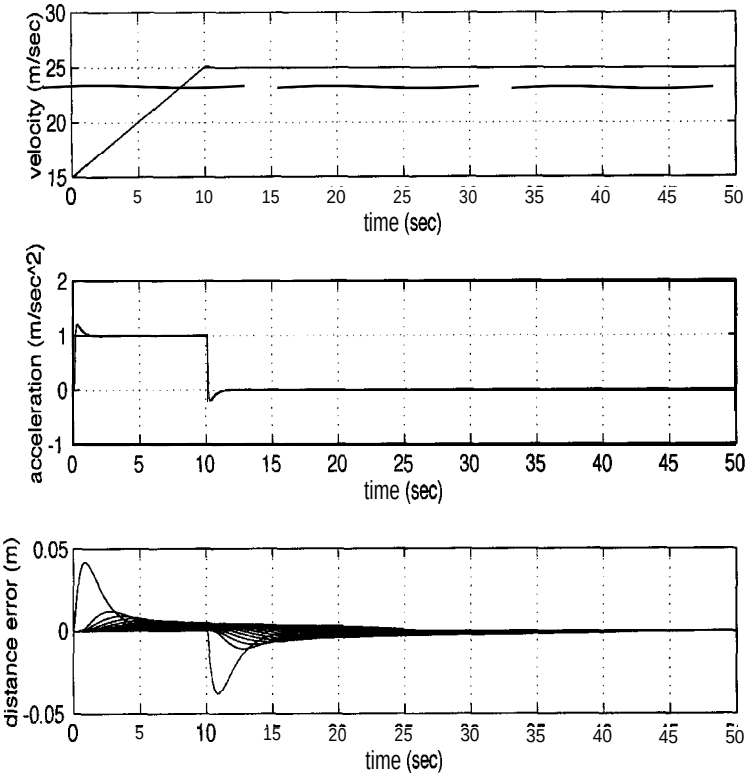

Figure 3.4.2: Transient Response of a Platoon

In this simulation, eqs. 3.1.1 and 3.1.2 are used for the inputs of each vehicle's acceleration, whereas the control gains are defined as follows:

$$k_a = 0.5,\ k_v = 1.0,\ k_l = 0.5,\ k_p = 1.0,\ c_v = 1.0,\ c_p = 0.0$$

Since the information from a lead car is supposed to be transmitted instantaneously to all vehicles, both the velocity and acceleration trajectories are excellent. Some overshoot observed in velocity and acceleration trajectories resulted from the sudden change in acceleration of the lead vehicle, but the oscillation disappeared within four seconds. The overshoot becomes larger

as the delay time increases. As for the spacing error, the first following vehicle shows the largest one at t = 10 seconds, but the magnitude is 18 cm at most. Other following vehicles, however, preserve the string stability of the system. Corresponding flow rates are shown in figure 3.4.3.

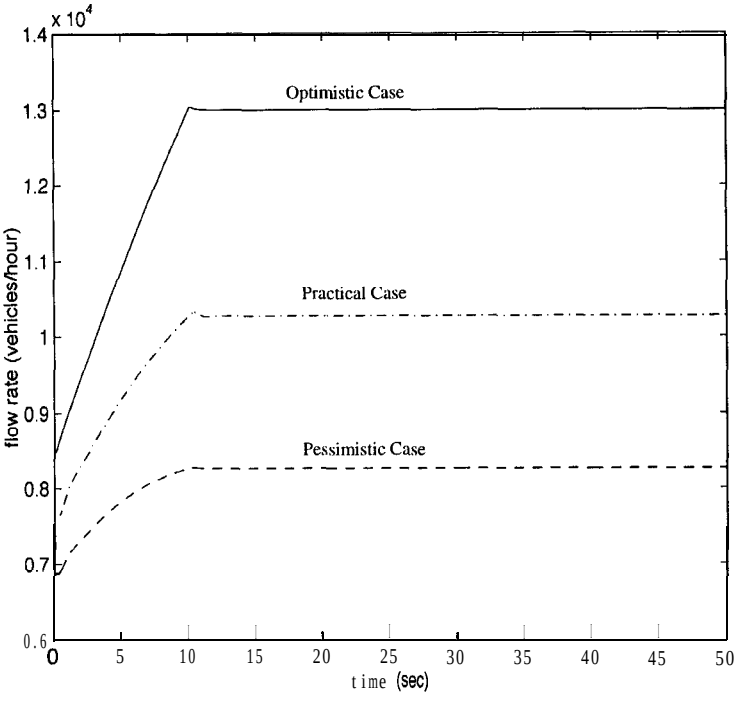

Figure 3.4.3: Flow Rate in a Platoon due to Change in Lead Car's Velocity

Each transient flow rate is calculated using equ. 3.3.1 by applying the mean value of the velocities of following vehicles for the platoon velocity in the equation. Since this simulation does not include intra-platoon dynamic responses, the transient flow rate defined above does not always represent the real dynamics of flow rates on highways. The flow rates, however, are nonetheless useful when platooning performance is compared with other control schemes. All of the transient flow rates are observed to converge at the steady state values within 10 seconds, which corresponds exactly to the duration of the lead car's acceleration.

3.4.2 Headway Control

The simulations of headway control with headway times of 0.3 seconds, 0.7 seconds and 1.2 seconds are done by applying equ. 3.2.6 for the input of each vehicle's acceleration. The transient responses of the first twenty following vehicles are shown in figure 3.4.4.

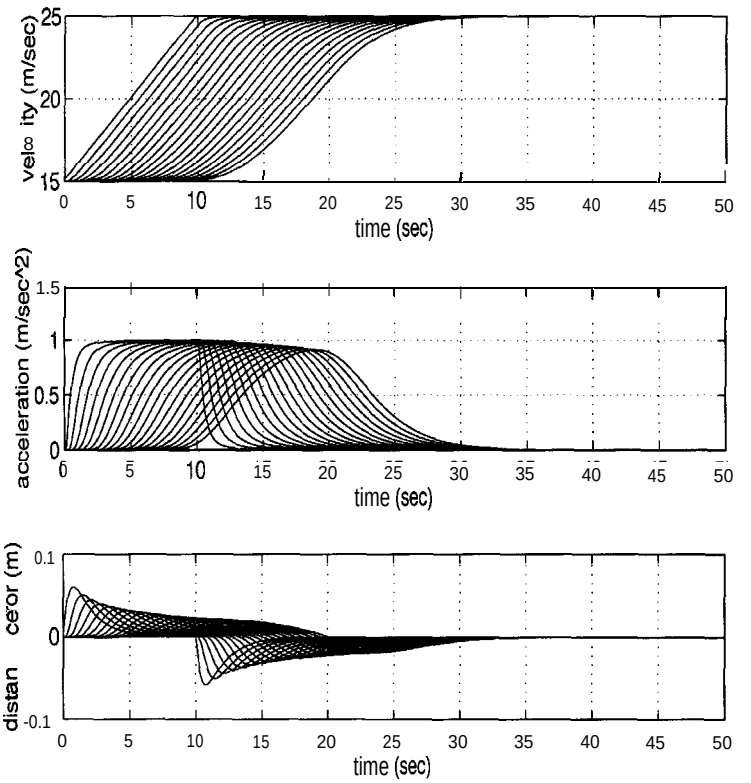

Figure 3.4.4: Transient Response of Headway Control with 0.7 Sec. Headway

In the simulations, the delay time of the system is set to 0.1 seconds in all cases. This delay time does not cause slinky effects like the ones shown in figure 3.2.1 because the maximum delay time is 0.15 seconds for $h_w = \lambda = 0.3$ sec, 0.25 seconds for $h_w = \lambda = 0.7$ sec, and 0.27 seconds for $h_w = \lambda = 1.2$ sec, respectively. As shown in simulation results, the responses of following

vehicles maintain string stability because the spacing error uniformly decreases as the vehicle index increases.

It was observed that the smaller headway time results in a faster convergence of the transient responses. For example, it takes about 17 seconds for twenty following vehicles to converge to the steady state acceleration, 0 m/sec^2, with 0.3 second headway time, 35 seconds with 0.7 second headway time, and 50 seconds with 1.2 second headway time. The reason for this difference in convergence time is that the pole of the system is defined by the headway time as shown in equ. 3.2.7, which means that the bandwidth becomes smaller as headway time increases.

Figure 3.4.5 shows the transient flow rate calculated from the transient responses of following vehicles, a rate which is calculated by the headway time of the vehicle that passes by the position where the lead car begins to accelerate. The convergence time of flow rates also depends on headway time. For example, when the headway time is 0.3 seconds, the flow rate converges to the steady state within 20 seconds, and it takes about 50 seconds for 0.7 seconds of headway time, and 80 seconds for 1.2 seconds of time. In other words, shorter headway time results in a better steady-state flow rate and a better transient flow rate response as predicted by equs. 3.2.7 and 3.3.2.

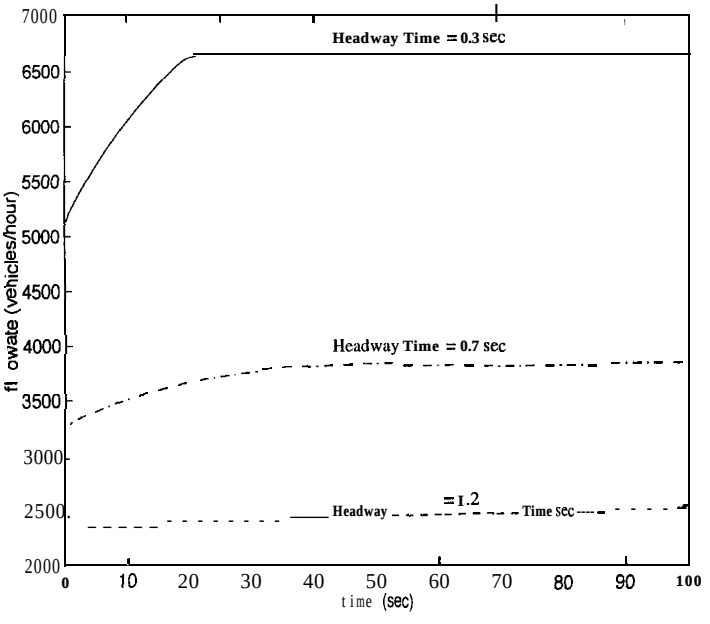

Figure 3.4.5: Flow Rate in Headway Control due to Change in Lead Car's Velocity

The smaller headway time, however, results in string instability as described in equ. 3.2.9. For instance, a simulation result with a relatively long delay time is shown in figure 3.4.6 where the headway time is 0.3 seconds and the delay time is 0.2 seconds while the maximum delay time for 0.3 second headway time is 0.15 seconds with $\lambda = 0.3$ in equ. 3.2.9. Because the string stability is violated, the oscillation on the transient responses is rapidly amplified as the vehicle index increases Thus, the actuator and the system's dynamics are key issues when a headway controller with a small headway time is designed.

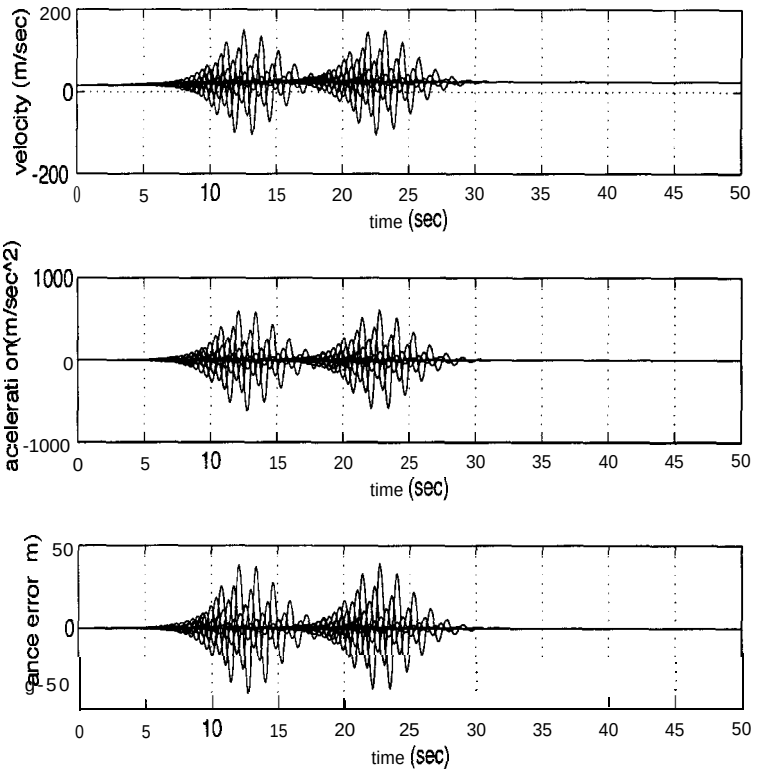

Figure 3.4.6: Headway Control with 0.3 Sec. Headway and 0.2 Sec. Delay Time

3.4.3 Human Model (Linear-Optimal Control Model)

The results of the linear-optimal control model are shown in figure 3.4.7, and apply to the first twenty following vehicles. It is assumed that every human driver follows the linear-optimal control model and that each vehicle's acceleration is defined by equ. 3.2.12.

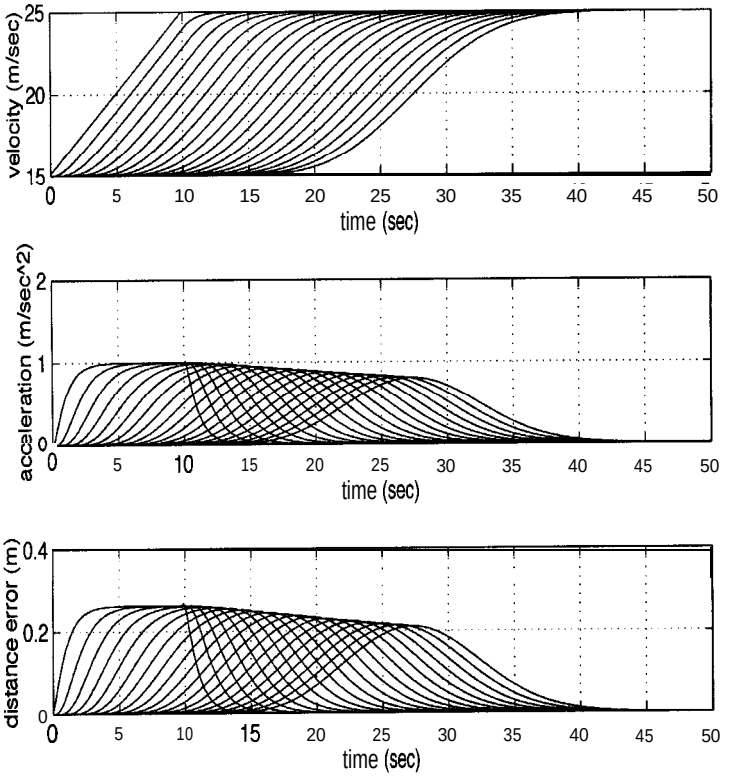

Figure 3.4.7: Transient Response of Linear-optimal Control Model

Throughout the simulation, there is no slinky effect observed in the transient responses; the responses converge within 45 seconds and the convergence is little faster than the headway control with 1.2 seconds of headway time. The maximum spacing error, however, is about 0.25 meters for the first following vehicle and is larger than that of the headway control, approximately 0.06 meters at most. This human model is very nearly equivalent to the headway control with 1.2 seconds of headway time in the static flow rate and the convergence time, but the headway control is still better than in the human model from the standpoint of spacing error.

In figure 3.4.8, the transient flow rate of the linear-optimal control model is shown, a flow rate that converges with the steady state within about 80-100 seconds.

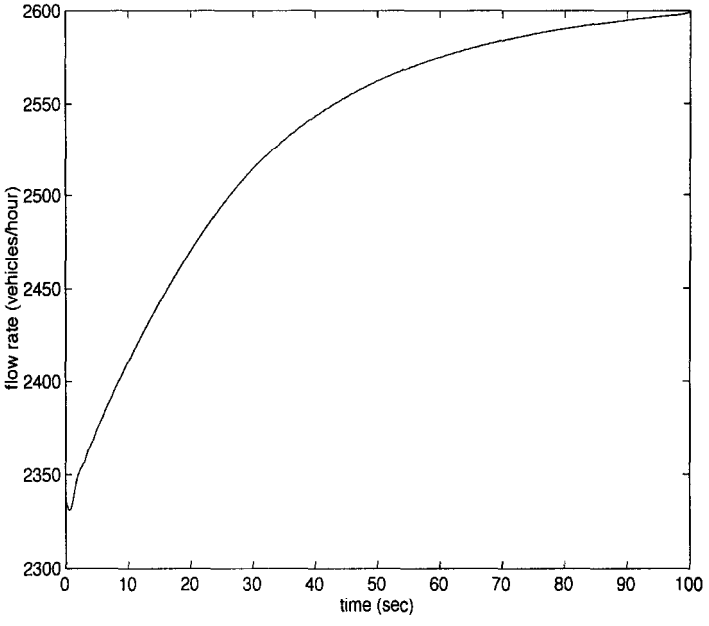

Figure 3.4.8: Flow Rate in a Linear-optimal Control Model due to Change in Lead Car's Velocity

3.4.4 Dynamic Flow Analysis in Mixed Flow

One result of the transient response of the mixed flow is shown in figure 3.4.9. Once again, it is assumed that all human drivers follow the linear-optimal control model. The headway time for control is 0.7 seconds, the percentage of headway controlled vehicles is about 50%, and the order of manual vehicles and headway controlled vehicles is assigned at random. The number of following vehicles is fifty.

As expected, the simulation results show intermediate dynamics between the human and headway control; string stability is also satisfied. The transient flow rate shown in figure 3.4.8 is not smooth since it is calculated by the headway time of vehicles when they pass by the origin. But it was observed that the mean value also takes an intermediate one between the human model and the headway control.

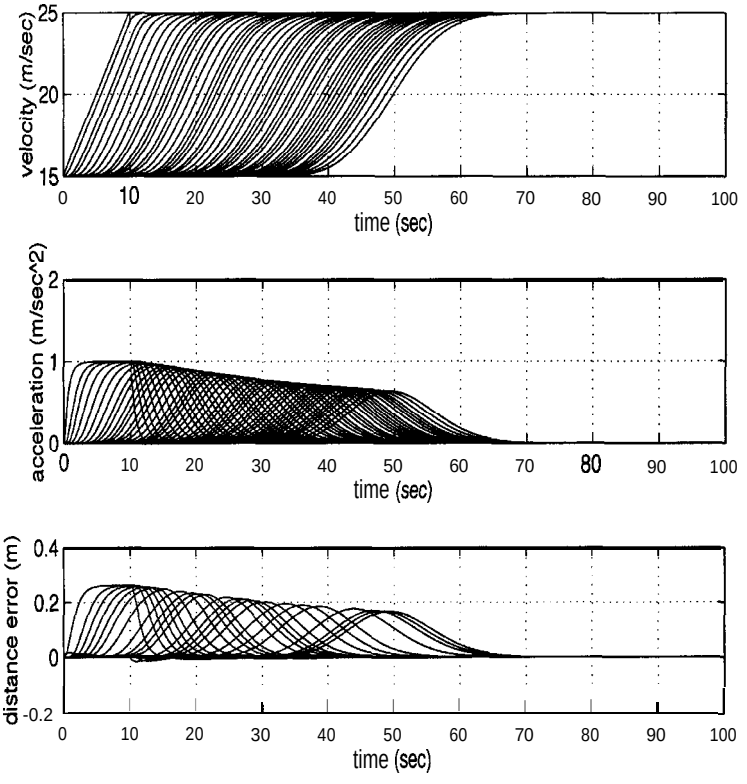

Figure 3.4.9: Transient Response in a Mixed Flow

3.5 Control of Traffic Flow Rate

There are two ways to control the flow rate of automated vehicles under headway control: change either cruising velocity or headway time. As figure 3.3.1 implies, however, decreasing headway time is more effective than increasing cruising velocity in order to increase the static flow rate in the headway control.

For example, suppose that the headway time is 0.7 seconds and the cruising velocity is 22.2 m/sec (50 mph). The resulting static flow rate is 37 11 vehicles /hour according to equ. 3.3.2. If, however, the headway time changes to 0.6 seconds and the velocity is held at 22.2 m/sec (50 mph), the flow rate is 4138 vehicles/hour, which means a 12% improvement. Similarly,

if the headway time is 0.7 seconds and the velocity increases to 31 m/sec (70 mph), the static flow rate is 4032 vehicles/hour, a 9% improvement. This means that in controlling the flow rate, even 20 mph increase in velocity is less effective than 0.1 second decrease in headway time. Moreover, in a mixed flow, since the manually operated vehicles do not always follow a given desired cruising velocity, the effects of changing it is complicated and unpredictable. From the standpoint of flow rate, controlling headway time is more effective and convenient.

The headway time, however, has dominant effects not only on the static flow rate but also on the transient response of traffic flow as shown in the previous sections. Since changing the headway time of preceding vehicles affects the transient responses of following ones, a change of headway time may result in a string instability, actuator saturation, or decreased riding comfort for drivers.

As a result, transient response due to a change in headway time should be evaluated. Although there are ways for vehicles on highways to get new headway times, one plausible assumption is that it be delivered to vehicles from outside, such as through an infrastructure-vehicle communication. There are two typical cases whereby the vehicles may receive new headway time information as illustrated in figure 3.5.1.

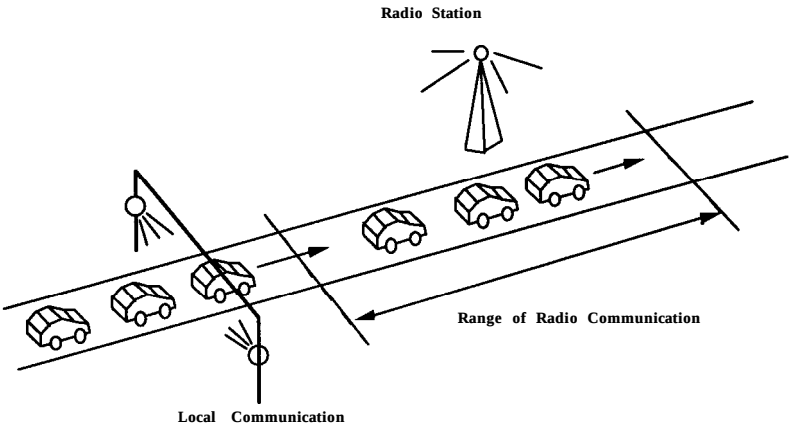

Figure 3.5.1: Typical Communication Methods

Case A: Many vehicles on a specific section of highway get headway time information simultaneously. This happens when a communication medium, like a radio wave or some other signal, covers a lengthy section of highway.

Case B: Each vehicle gets new headway time information after passing by a fixed point. This method is effective when communication is achieved using media, such as local communications with an infrared laser, a magnetic field, or a bar-code on roads and toll stations.

Both cases can't be fully realized in daily highway operations, and in general, an infrastructure-vehicle communication takes an intermediate form between the above two cases. For example, because a radio wave can't cover infinitely wide sections on highways, the communication at places near to the boundaries of the radio wave must be similar to Case B communication.

However, investigating the transient responses for these two cases is still crucial to evaluating the performance of an automated system . Therefore, some simulations will be done in order to verify transient responses for each case.

3.5.1 Change in Headway Time Triggered by Time

In Case A, all vehicles are supposed to get new headway time simultaneously, which the controllers begin to follow. To achieve good riding comfort, however, a transition period of T-second duration is supposed to exist. This headway time transition can be defined by

$$h_w(t) = h_{old} + (h_{new} - h_{old})\left\{\frac{t}{T} - \frac{1}{2\pi}\sin\left(\frac{2\pi}{T}t\right)\right\} \qquad \text{for } 0 \le t \le T \qquad (3.5.1)$$

where h_{old} and h_{new} are previous headway and newly given headway times, respectively. This equation assures continuity up to a second-order derivative and so should provide a smooth transition. Since equ. (2.6) assumes that the headway time is constant, the control input should be modified as follows:

$$u = \frac{1}{h_w}\left(\lambda(x_{j-1} - x_j - L_v - L_0) + (\dot{x}_{j-1} - \dot{x}_j) - (h_w\lambda + \dot{h}_w)\dot{x}_j\right) \qquad (3.5.2)$$

where $\dot{h}_w$ is the time derivative of headway time and can be calculated from equ. 3.5.1. Figure 3.5.2 shows simulation results of headway time that changes from 0.7 to 0.6 seconds with T = 10 seconds at 20 m/sec; the number of following vehicles is fifty.

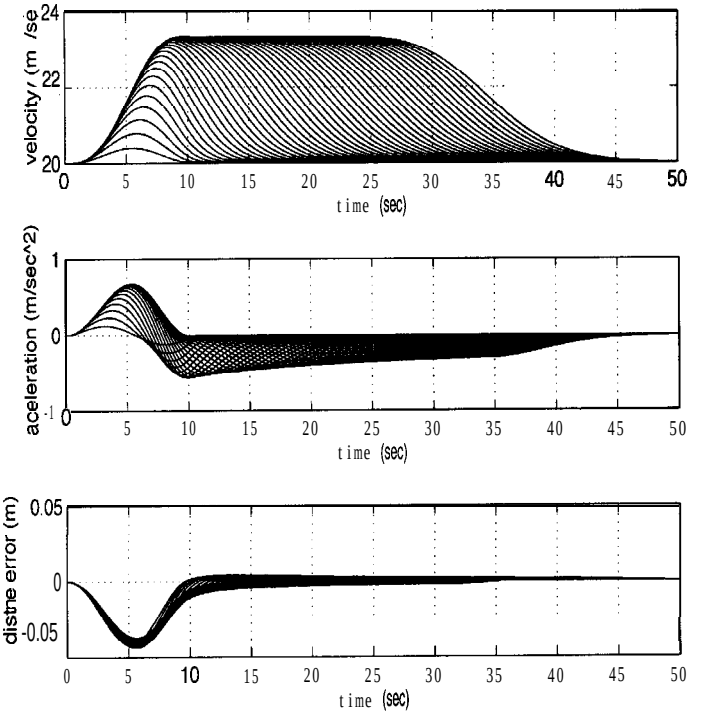

Figure 3.5.2: Headway Change Triggered by Time

Since the desired headway time decreases simultaneously, vehicles also begin to accelerate simultaneously. In the responses of the first several vehicles, the maximum velocity and acceleration increase as the vehicle index increases. The acceleration and the velocity, however, are saturated at certain values as the vehicle index increases, and the spacing-error deviation actually converges at zero. By supposing there is no delay time in actuator responses, the maximum velocity and acceleration during the transition are expressed through the traffic flow analysis as,

$$v_{max} = \frac{h_{old}}{h_{new}} v_0$$

$$a_{max} = \frac{2}{T} \frac{h_{old} - h_{new}}{h_{new}} v_0 \qquad (3.5.3)$$

where v_0 is the cruising velocity. The maximum acceleration is achieved in acceleration for the decrease in headway time. Note that maximum velocity does not depend on the duration of transition time. Equation 3.5.3 reveals that the system is always stable with any given new headway time and transition duration, but the new headway and duration of transition times should be chosen properly, so that both the maximum velocity and acceleration do not exceed allowable values. The transient flow rate in Case A is shown in figure 3.5.3; some overshoot exists, and the convergence time is about 45 seconds.

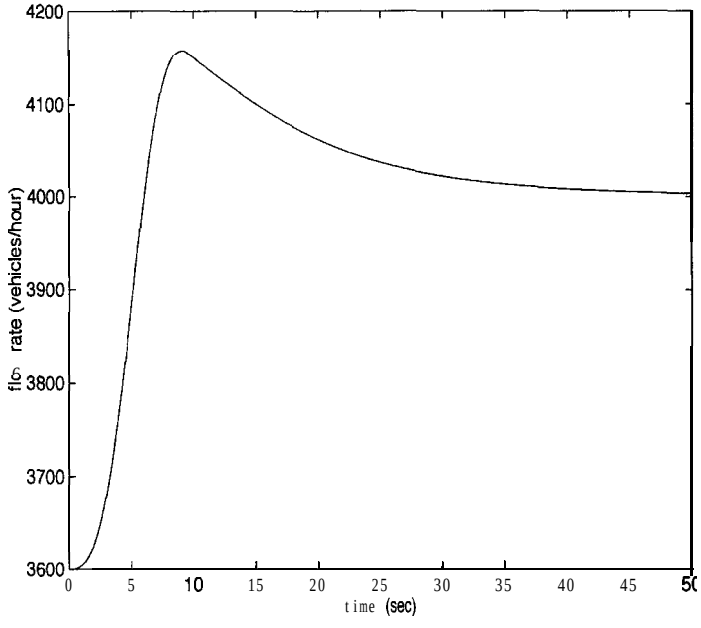

Figure 3.5.3: Transient Flow Rate due to Change in Headway Triggered by Time

3.52 Change in Headway Time Triggered by Position

In Case B, a vehicle that passes a fixed point on highways gets a new headway time, and its associated transition begins at a different moment in each vehicle. To avoid discontinuous

responses, it is assumed that equ. 3.5.1 will be again used for each vehicle's headway time transition, and equ. 3.5.2 will be applied for the acceleration input for each vehicle. The transient responses of a case where initial headway time is 0.7 seconds, final headway time is 0.6 seconds, transition duration is 10 seconds, and cruising velocity is 20 m/sec are presented in figure 3.5.4, and the corresponding transient flow rate is shown in figure 3.5.5.

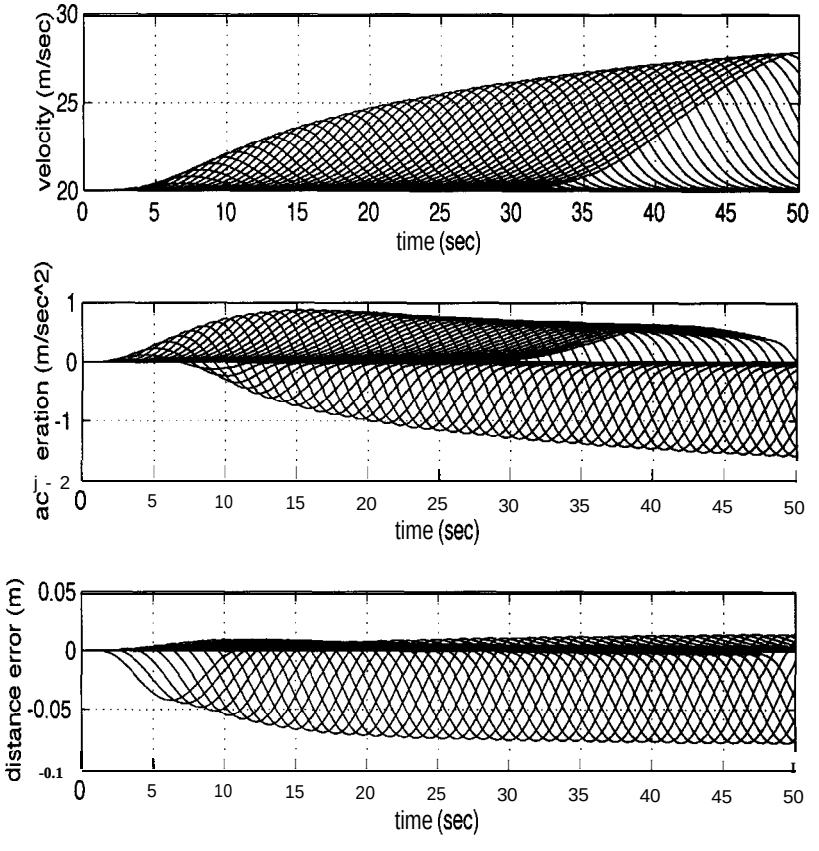

Figure 3.5.4: Headway Change Triggered by Position

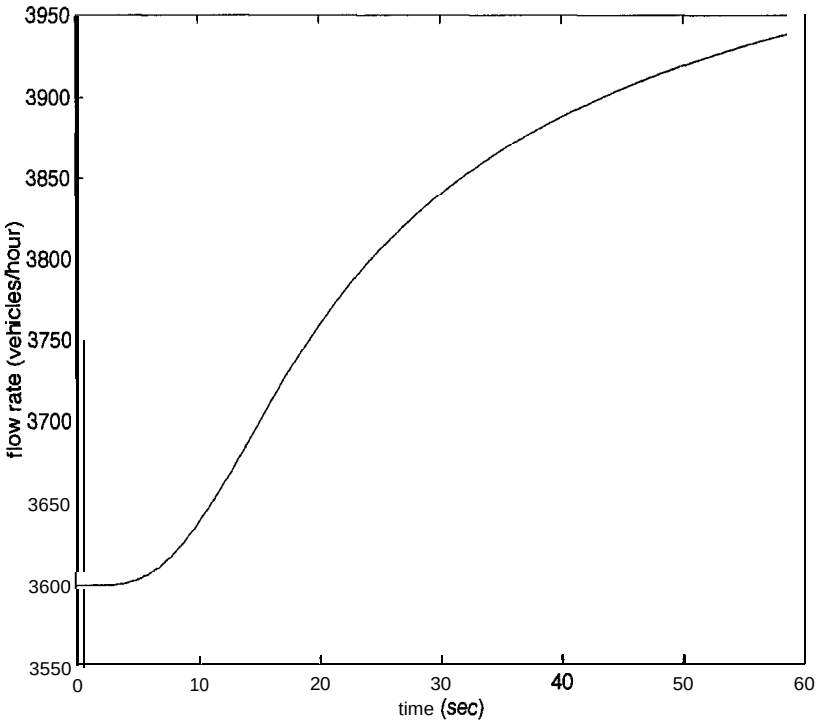

Figure 3.5.5: Transient Flow Rate due to Change in Headway Triggered by Position

The number of following vehicles is again fifty. Since following vehicles have to catch up with preceding ones, the maximum velocity of each vehicle increases according to the increase in vehicle index. Since the final velocity is the same as the original cruising velocity, each vehicle accelerates at the first stage of transition and then decelerates at the end. Although the change in headway time is the same as the simulation done in Case A, the maximum velocity fluctuation is much larger than that of the previous simulation (figure 3.5.4), and the flow-rate convergence also takes longer time (figure 3.5.5). Moreover, as far as the simulation shows, the maximum velocity might diverge to an infinitely large value. The string stability of the system, however, still can be proven based on a similar traffic flow analysis to that of Case A , and the maximum velocity and acceleration are shown to be saturated to the following values.

$$v_{max} = \frac{1}{1 - \frac{h_{old} - h_{new}}{L_v + L_0} v_0} v_0$$

$$a_{max} = \frac{2}{T} \frac{h_{old} - h_{new}}{L_v + L_0 - (h_{old} - h_{new}) v_0} v_0^2 \qquad (3.54)$$

Maximum acceleration is achieved in deceleration for the decrease in headway time. Equ. 3.5.4 shows that if the new headway time is too small in comparison with the old one, the system will be unstable because the denominator sign becomes negative. Thus, in order to keep the string-stability, the decrease in headway time must be smaller than

$$\Delta h_{decrease} \equiv \max \left| h_{new} - h_{old} \right| = \frac{L_v + L_0}{v_0} \qquad (3.5.5)$$

If equ. (3.5.5) is violated, the system becomes unstable as shown in figure 3.5.6.

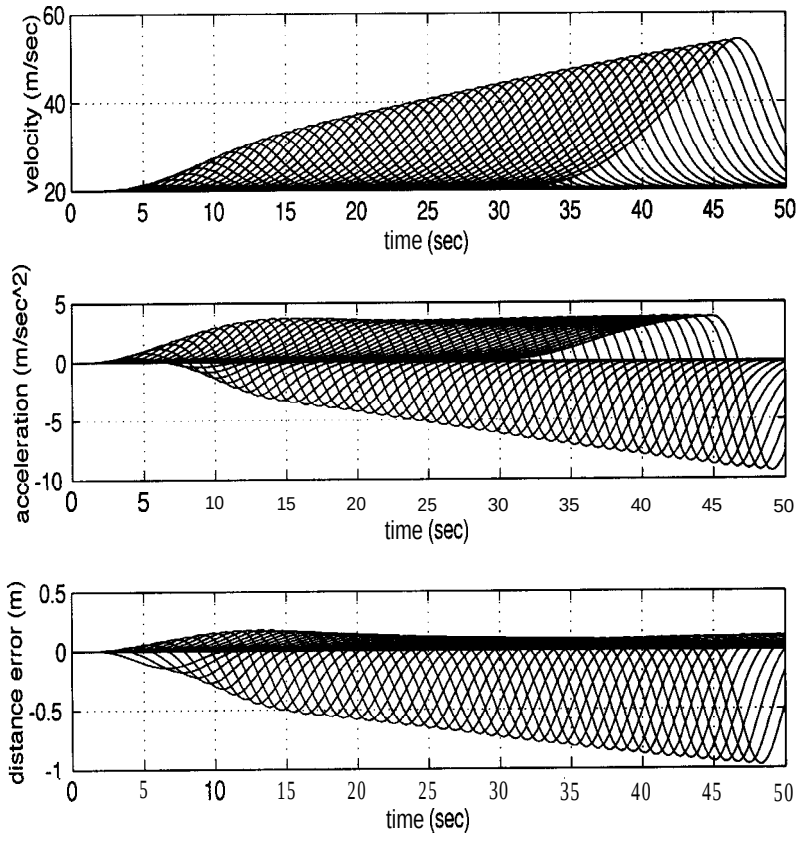

Figure 3.5.6: Headway Change by Position (Violating String Stability)

In this simulation, the new headway time is 0.4 seconds, and so a decrease in headway time is exactly the same as $A\, h_{decrease}$ with $L_v + L_0 = 6$ in equ. 3.5.5. As predicted, the maximum velocity of each vehicle keeps growing, and as the vehicle index increases, maximum acceleration diverges and maximum spacing error grows.

As for the change in headway time, a crucial problem is how to give this new information to the vehicles. Since equ. 3.5.5 implies that an allowable decrease in headway time for string stability is inversely proportional to vehicle velocity, communication methods such as those used in Case B should be avoided in highway operations. Even in the communication in Case A,

however, a radio wave can't cover infinitely wide ranges of highways, and the change in desired headway time may depend on fixed positions on highways. For example, the headway time should be controlled in some specific areas on highways where heavy congestion and traffic accidents are ahead, and this may trigger some transient responses similar to those in Case B. Thus, potential string instability due to Case B communication needs to be considered.

One way to prevent the system from losing string stability due to Case B communication is to let infrastructures give not only new headway time information but also the maximum velocity to vehicles. Figure 3.5.7 shows simulation results with the same conditions as those of figure 3.5.6 except an additional condition that the maximum velocity is 25 m/sec.

If a vehicle's velocity is larger than the maximum velocity and the acceleration command calculated from equ. 3.5.2 is positive, the acceleration input to the vehicle will be set to zero. As shown in the Figure, the magnitude of acceleration is not amplified as the vehicle index increases, and no slinky effect results. The spacing error, however, takes an extraordinarily large value, which is almost 8 meters, since the maximum velocity restriction degrades the tracking performance of the system. This spacing error does not mean that collisions will occur because the sign is positive; it means that the preceding vehicles are traveling "too far" ahead for a collision to occur.

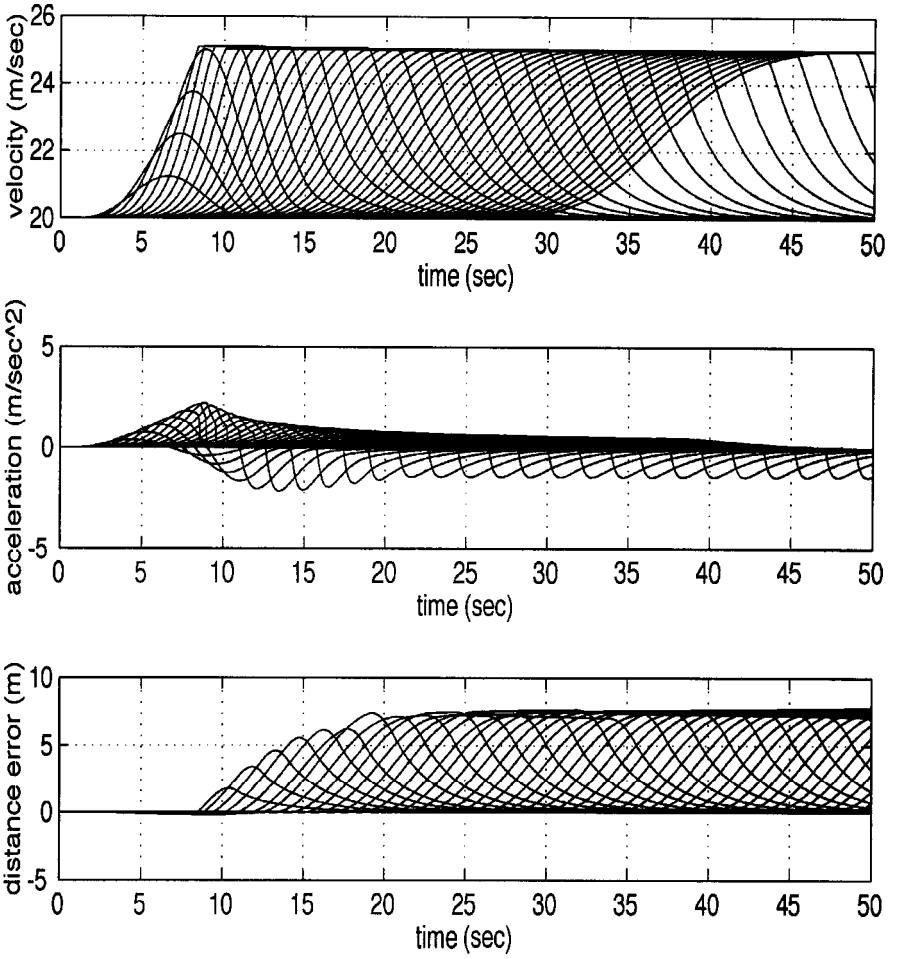

Figure 3.5.7: Headway Change by Position with Maximum Velocity Restriction

The effect of the spacing error appears in the transient flow rate, again as shown in figure 3.5.8.

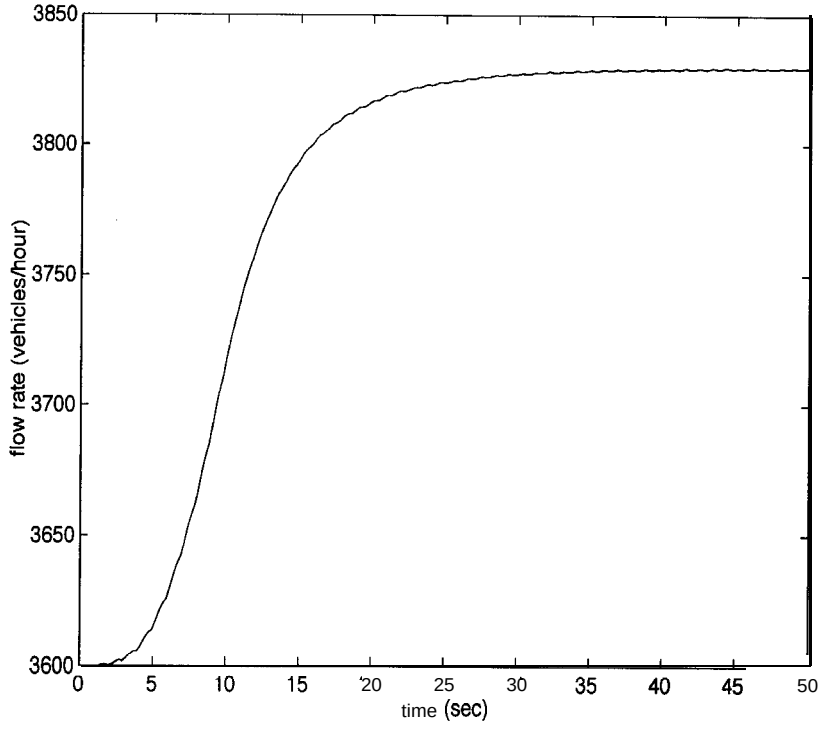

Figure 3.5.8: Transient Flow Rate with Maximum Velocity Restriction

Since the maximum velocity is restricted, the flow rate at the point of origin is not the desired value at the steady state. In this case, the flow rate should have increased from 3600 vehicles/hour (a static-flow rate of 0.7 seconds of headway time at 20 m/sec) to 4000 vehicles/hour (a static-flow rate of 0.6-seconds of headway time at 20 m/sec). But figure 3.5.8 shows that the maximum flow rate is only 3830 vehicles/hour, which is a static flow rate of 0.7 second headway time at 25 m/sec. This means that the maximum velocity restriction effectively improves the string stability of the system but also restricts its static rate of traffic flow.

3.6 Avoiding Rear End Collisions

Avoiding collisions, especially from behind, is also an important factor in automated control systems. Three typical cases of rear end collisions are ones with 1) stopping vehicles, 2) preceding vehicles that brake suddenly, and 3) cut-in vehicles. Since the performance of avoiding collisions depends on distancing control strategies, the performance of each control strategy should be evaluated.

In platooning, since highways should be fully automated and each vehicle has communication devices on it, vehicles should be able to transmit information about all the cases above, which means that collisions can be avoided effectively under platooning.

As for headway and human controls, however, since it is assumed that there is no communication among vehicles, they may collide with preceding ones in some cases. Thus, when headway controllers are designed, careful attention should be paid to avoid this.

Since the linear-optimal control model was developed to model how human drivers respond in vehicle-following, the model may not be adequate to use in solving for braking problems. In the following analysis, however, the model is sometimes used to grasp the general features and differences between headway control and the human model.

3.6.1 Collisions with Stopping Vehicles

In order to avoid collisions with stopping vehicles on highways, a vehicle has to start braking before a point beyond which it needs more than the maximum deceleration for a complete stop. The maximum deceleration, in turn, depends on many factors such as road temperature,

road surface condition, and brake capacity, all of which can be generally represented by a road-tire friction.

For headway control, an inter-vehicular distance where the brake begins to be applied is derived from equ. 3.2.6 by letting the acceleration command be zero and is described as

$$\Delta x = x_{j-1} - x_j - L_v = \left(\frac{1}{\lambda} + h_w - T_d\right) v_0 + L_0 \tag{3.6.1}$$

where T_d and v_0 are the delay time of the actuator and the vehicle's velocity. Applying the Laplace transform to equ. 3.6.1, the acceleration command of the headway controller can be expressed as

$$u(t) = \frac{\lambda}{1 - h_w \lambda}\left(e^{-\frac{t}{h_w}} - e^{-\lambda t}\right) v_0 \tag{3.6.2}$$

There is, however, some delay time due to the dynamics of the controller. By linearizing equ. 3.6.2, the time for the system to achieve maximum deceleration $\mu_{max}\, g$ can be approximately expressed as

$$T_e = \frac{\mu_{max}\, g}{v_0}\frac{h_w}{\lambda} \tag{3.6.3}$$

where μ_{max} and g are the maximum road-tire friction and the acceleration of gravity. To achieve a complete stop within the maximum acceleration limit, the distance defined by equ. 3.6.1 and the time defined by equ. 3.6.3 should satisfy

$$A x - T_e v_0 > \frac{v_0^2}{2\mu_{max} g} \tag{3.6.4}$$

By solving equs. 3.6.3 and 3.6.4 for λ, the control gain should not exceed the value defined by

$$\lambda_0 = \frac{1 - \frac{\mu_{max} g}{v_0} h_w}{\frac{1}{v_0}\left(\frac{v_0^2}{2\mu_{max} g} - L_0\right) - h_w + T_d} \tag{3.6.5}$$

To avoid collisions up to 30 m/sec^2 with 0.7 seconds of headway time, 0.6 g maximum deceleration, 0.1 seconds of actuator delay times and l-meter of distance offset, the control gain should not be larger than 0.45. Figure 3.6.1 and 3.6.2 show the simulation results of collision avoidance with a stopping vehicle.

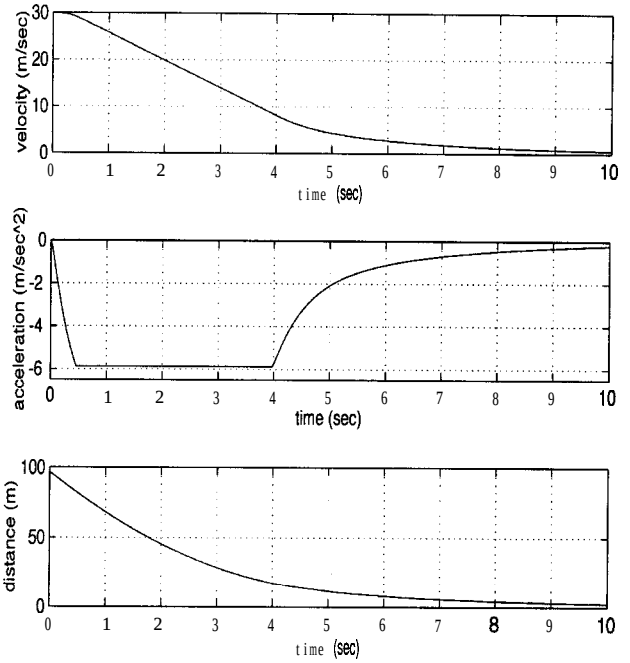

Figure 3.6.1: Headway Control with 0.4 Gain

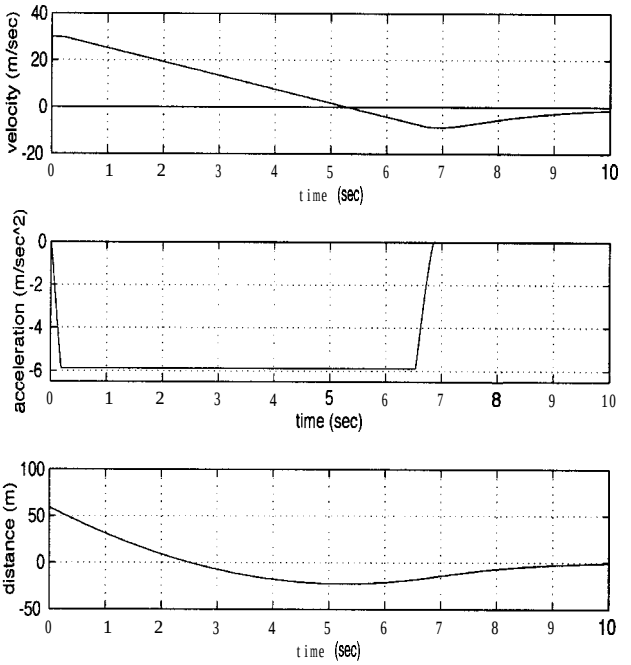

Figure 3.6.2: Headway Control with 0.8 Gain

In the simulation, the initial cruising velocity is 30 m/sec, the maximum deceleration is 0.6 g, and the control gain is 0.4 (figure 3.6.1 and 0.8 in Figure 3.6.2). A vehicle with 0.4-control gain begins to decelerate at about 90 meters in front of a stopping vehicle and will avoid colliding with it, while a vehicle with 0.8 control gain begins to decelerate at 60 meters in front of a stopping vehicle, colliding with it at about t = 2.5 sec.

To see the performance of avoiding collisions of human model, an inter-vehicular distance where the brake is first applied under the linear-optimal control model is derived. By letting the acceleration command be zero in equ. 3.2.12, the inter-vehicular distance can be described as

$$\Delta x = x_{j-1} - x_j - L_v = \left(C_c + \frac{C_v}{C_s}\right)v_0 + L_0 \tag{3.6.6}$$

Then, the maximum velocity at which the linear-optimal control model can avoid the collision with stopping vehicles is derived from equs. 3.6.4 and 3.6.5 as

$$v_{max} = \mu_{max}\, g\left(C_c + \frac{C_v}{C_s}\right) + \sqrt{\left\{\mu_{max}\, g\left(C_c + \frac{C_v}{C_s}\right)\right\}^2 + 2\mu_{max}\, g\, L_0} \tag{3.6.7}$$

$$= 17.7 \text{ m / sec}$$

This implies that if a vehicle's velocity is larger than 17.7 m/sec, the linear-optimal control model cannot help to avoid collisions.

3.6.2 Collisions with Vehicles that Brake Suddenly

The most important parameters for collisions with preceding vehicles that brake suddenly are the delay times of the controller and the actuator, as well as the difference in deceleration of preceding and following vehicles. If the maximum deceleration of preceding vehicles is the same as that of following ones, the inter-vehicular distance for safety can be very small [Ioannou and Chien, 1992]. In general cases, however, since the maximum deceleration that each vehicle can achieve depends on many circumstances and on a vehicle itself, there is the possibility that the maximum deceleration of following vehicles is smaller than that of preceding ones even if all of the vehicles are under the same automatic control. Moreover, since collisions with brick walls can happen in a mixed flow, an equivalent deceleration for following vehicles can be huge, and the dynamics of the controller also play an important role in avoiding such collisions. Thus, collision analyses are necessary for cases where a maximum difference in deceleration exists between preceding and following vehicles.

Figures 3.6.3, 3.6.4 and 3.6.5 show collision speeds under headway controls with times of 0.3 seconds, 0.7 seconds, and 1.14 seconds, respectively.

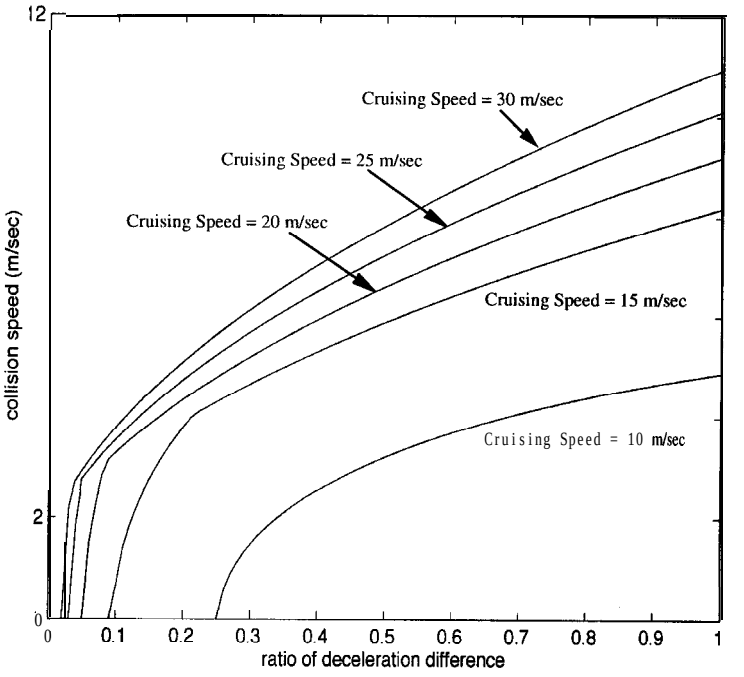

Figure 3.6.3: Collision Speed of 0.3 Sec. Headway Time

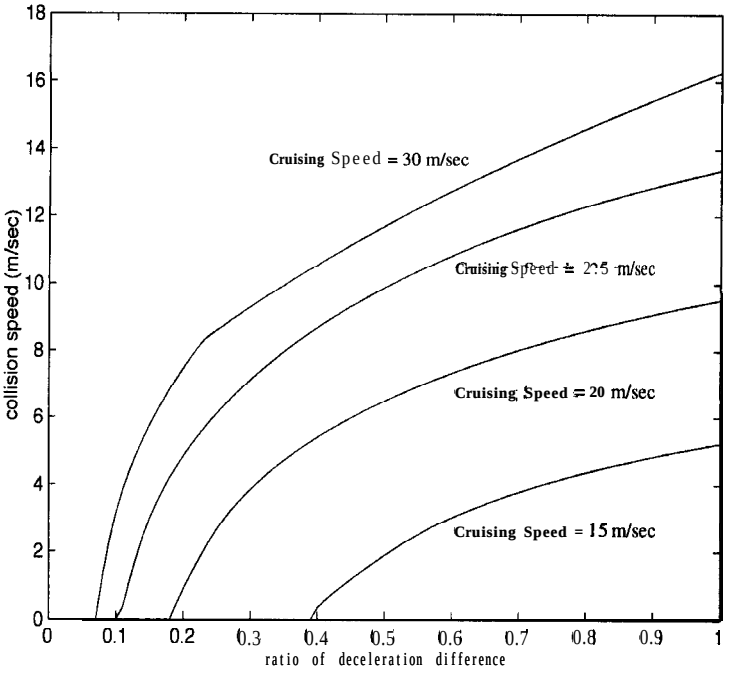

Figure 3.6.4: Collision Speed of 0.7 Sec. Headway Time

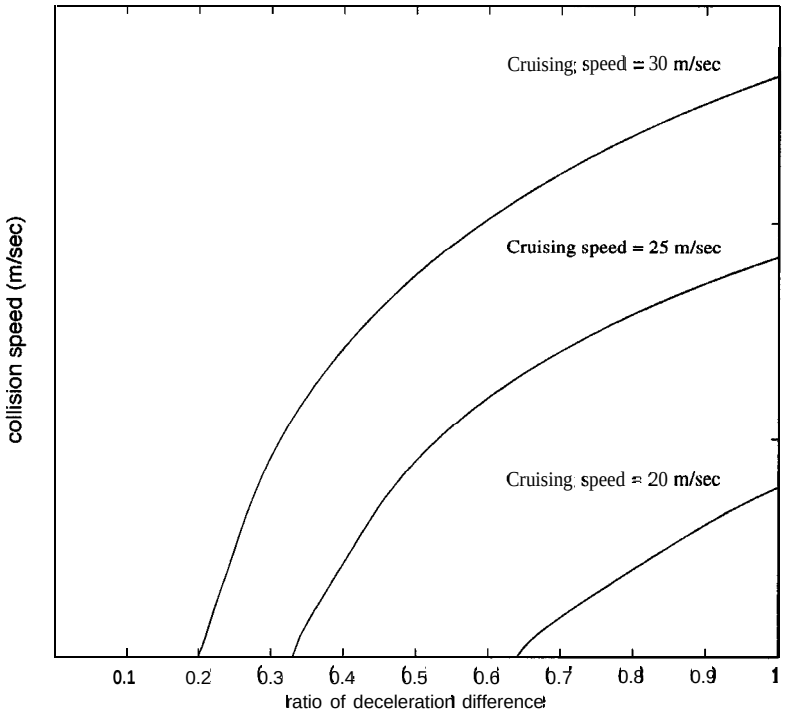

Figure 3.6.5: Collision Speed of 1.14 Sec. Headway Time

As previously mentioned, 1.14 seconds of headway control is equivalent to the linear optimal control model at the steady state. The conditions used in the simulations are as follows: 1) a preceding vehicle travels at a cruising velocity and one following it has an appropriate headway, and 2) the preceding vehicle begins to decelerate at a constant deceleration higher than the maximum deceleration of the following vehicle until it stops. The following vehicle is controlled by the headway control, and the actuator delay time is 0.1 seconds. The control gain λ for each headway time is defined by equ. 3.6.5 as 0.4 for 0.3 seconds of headway time, 0.45 for 0.7 seconds of headway time, and 0.5 for 1.14 seconds of headway time, respectively.

In each figure, collision speed is shown with respect to the ratio of differences in deceleration between a preceding vehicle and a following one at several cruising velocities. The ratio of differences in deceleration between a preceding vehicle and a following one are defined as

$$R = \frac{\alpha_p}{\mu_{max}\, g} - 1 \qquad (3.6.8)$$

where a_p is the deceleration of a preceding vehicle, and the maximum deceleration of a following vehicle is supposed to be 0.6 g for all simulations. The ratio is zero if the deceleration of a preceding vehicle is the same as the maximum deceleration of a following vehicles, and it is one if the deceleration of a preceding vehicle is twice as high as the maximum deceleration of a following vehicle. Simulation results are shown at every 5 m/sec cruising velocity.

As can be seen in figures 3.6.3 through 3.6.5, the capacity of avoidance systems to prevent collisions successfully depends on headway time and cruising velocity. In other words, as headway time increases, the margin of safety for the ratio of differences in deceleration increases: at 20 m/sec cruising velocity, 5% margin for 0.3-seconds of headway time, 18% margin for 0.7 seconds of headway time, and 65% margin for 1.14 seconds of headway time. Similarly, as cruising velocity decreases, the margin also increases: 7% margin for 30 m/sec cruising velocity, 25% for 20. m/sec, and 39% for 15 m/sec with 0.7 seconds of -headway time..

As for human model, simulation results of the linear-optimal control model are shown in figure 3.6.6.

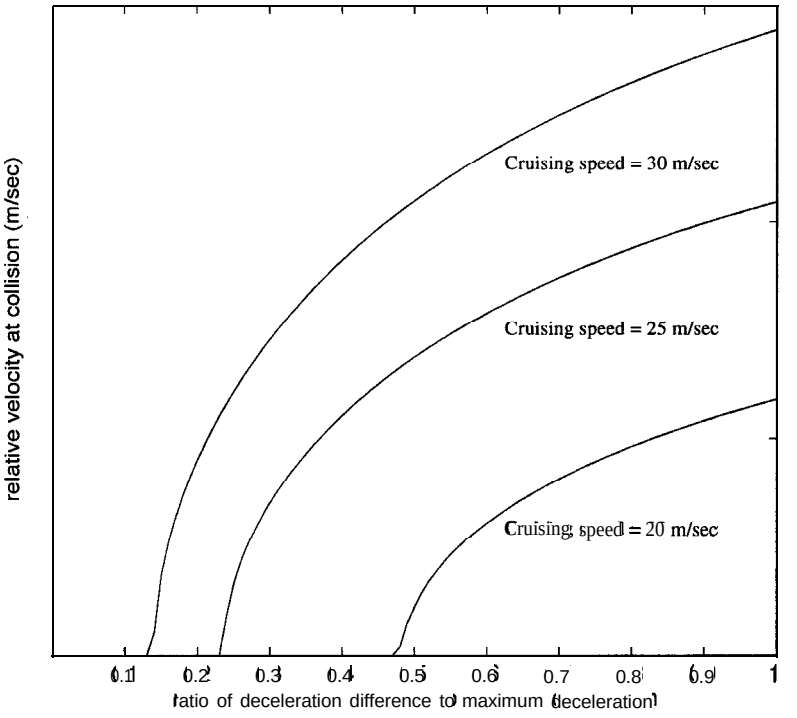

Figure 3.6.6: Collision Speed of Linear-optimal Control Model

Although the human model at the steady state is equivalent to 1.14 second headway control (results are shown in figure 3.6.5), the collision speed under the human model is substantially larger. The margin is 20% at 30 m/sec cruising velocity and 64% at 20 m/sec with 1.14 seconds of headway control while the margin of safety is 13% at 30 m/sec cruising velocity and 47% at 20 m/sec with the human model. The difference of the margin of safety between the linear-optimal control model and 1.14 seconds of headway control means that the headway control is faster than the linear-optimal control model in transient responses.

Then, it can be assumed that the faster controller will result in the better collision avoidance if the initial headway time is the same. As an extreme case, an example of a controller

will be cited that can set the maximum deceleration command as soon as the preceding vehicle begins to decelerate excessively. Figure 3.6.7 presents the collision speeds of this controller.

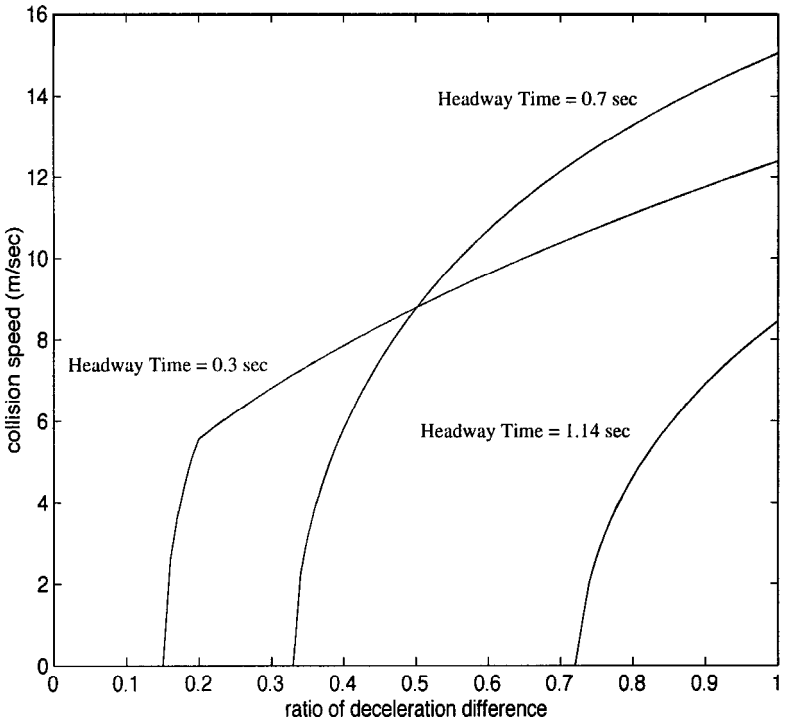

Figure 3.6.7: Collision Speed of Infinitely Fast Controller

In the simulation, the initial cruising velocity is 30 m/sec, and the actuator delay time is 0.1 second; its results correspond to the initial headway time of 0.3 seconds, 0.7 seconds, and 1.14 seconds, respectively. Since the controller instantaneously generates the maximum deceleration command, the margin of safety is much larger than that of the headway controller. The controller shows a 15% margin for 0.3 seconds of headway time, 33% for 0.7 seconds of headway time, and 73% for 1.14 seconds of headway time, while the headway controller shows 2% for 0.3 seconds of headway time, 7% for 0.7 seconds of headway time, and 20% for 1.14 seconds of headway

time. Since the headway time defines the dynamics for the headway controller shown in equ. 3.2.7, it cannot yield results as good as this controller. By utilizing the acceleration information of a preceding vehicle, however, there is a possibility that the headway controller can also improve transient responses.

3.6.3 Collisions with Cut-In Vehicles (R-Rdot Analysis)

Responses due to cut-in vehicles can be formulated as non-zero, initial condition problems. There are a variety of cases that illustrate cut-in vehicle maneuvers, and avoiding collisions both with stopping vehicles and with sudden braking ones are interpreted as special cases of collision avoidance with cut-in vehicles. Several cases are simulated by Ioannou and Chien, 1992, and the regions within which collision can occur are specified.

3.6.3.1 Region of Rear-End Collision

One way to observe what happens in cases of cut-in is to use R-Rdot analysis introduced by Fancher and Bareket, 1993. R-Rdot analysis describes vehicle trajectories on a diagram of a range (inter-vehicular distance) and a range rate (relative velocity). Collisions will occur when these trajectories come into a region of negative, inter-vehicular distance.

The R-Rdot analysis is advantageous because the responses of vehicles, including the controller; can be easily seen on the diagram. (An R-Rdot diagram is shown with the output of a headway controller in figure 3.6.8.)

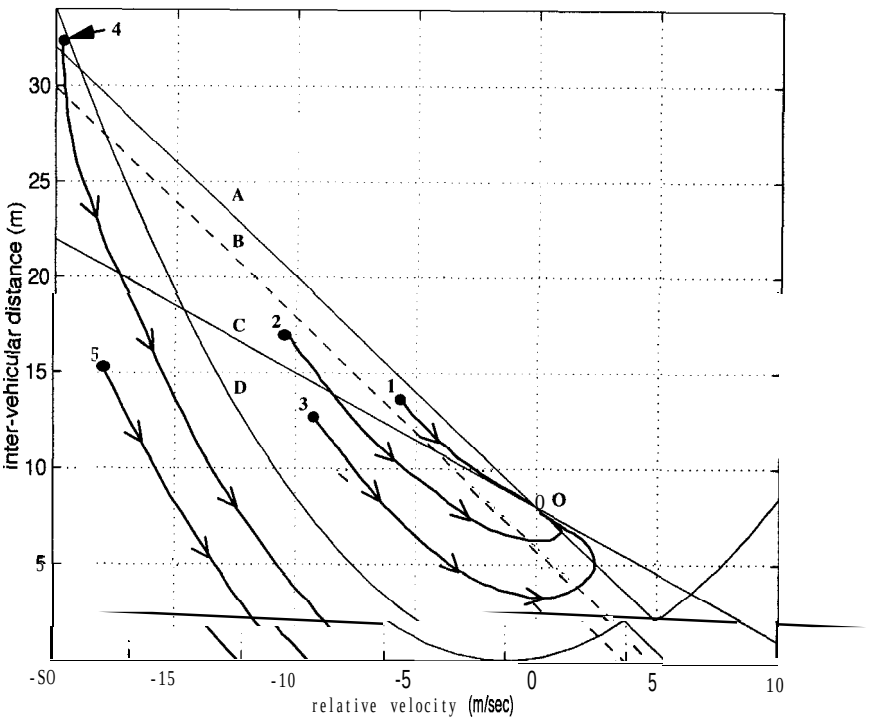

Figure 3.6.8: Example of R-Rdot Analysis

The diagram corresponds to a case where the velocity of a preceding vehicle is 10 m/sec, the maximum velocity of the following vehicle is 30 m/sec, the desired headway time is 0.7 seconds, and the control gain is 1.2. In the figure, each solid line is defined as

$$\text{Line A:} \quad \Delta x = \left(h_w + \frac{1}{\lambda} \right) v - \frac{1}{\lambda} v_p$$

$$\text{Line B:} \quad \Delta x = \left(h_w + \frac{1}{\lambda} \right) v - \frac{1}{\lambda} v_p - \frac{h_w}{\lambda} \mu_{max}\, g$$

$$\text{Line C:} \quad \Delta x = h_w\, v \qquad (3.6.9)$$

$$\text{Line D:} \quad \Delta x = \frac{(v_p - v)^2}{2 \mu_{max}\, g}$$

where v and v_p are the velocities of the following and preceding vehicles. **Line A** represents conditions in which the acceleration command is zero according to equ. 3.2.6. Similarly, Line B represents conditions in which the acceleration command is equal to the maximum deceleration. Line C corresponds to the steady state of headway control where the inter-vehicular distance is identical to the desired headway distance. Line D shows braking distance with maximum deceleration.

By supposing that the velocity of a preceding vehicle is constant, trajectories that originated from several initial states are observed as follows. If the initial state is at Point 1, a vehicle begins to decelerate at once and converges to the steady state at Point 0. If the initial state is at Points 2 or 3, a vehicle decelerates at the maximum deceleration at first and then accelerates to reach Point 0. If the initial state is at Point 4, a vehicle does not decelerate at first because Point 4 is above Line A. As soon as the state falls below Line B, however, the vehicle begins to decelerate at the maximum deceleration, but it will collide with a preceding vehicle since its state is below Line D. The trajectory from Point 5 shows a similar result; since the initial state is located below Line D, a following vehicle collides with a preceding one. Thus, the initial state must be above Line D, and the initial relative velocity must be larger than a value at the intersection of Line A and Line D to avoid collisions with a preceding vehicle with a constant velocity.

If a preceding vehicle is under a constant deceleration, the inter-vehicular distance for collision avoidance will increase, since relative deceleration decreases. This new safety boundary is defined as

$$\text{Line E: } Ax = \frac{(v_p - v)^2}{2(\mu_{max}\, g - \alpha_p)} \tag{3.6.10}$$

where α_p is the deceleration of a preceding vehicle. Equ. 3.6.10, however, is too pessimistic to estimate the region of collisions because it does not take into account that a preceding vehicle stops prior to colliding with a following vehicle. Since the acceleration of a preceding vehicle becomes zero as soon as it stops, relative deceleration increases to the original maximum deceleration of a following vehicle. Suppose that a preceding vehicle stops at $t = t_1$, and a following one collides with it at $t = t_2$ with the constant, relative deceleration of $\mu_{max}\, g - a_p$. Then, based on inter-vehicular distance, relative velocity and vehicle's velocity, t, and t_2 are expressed as

$$t_1 = \frac{v_p}{\alpha_p}$$

$$t_2 = \frac{\Delta v_0}{\mu_{max}\, g - \alpha_p} + \sqrt{\frac{2\Delta x_0}{\mu_{max}\, g - \alpha_p}} \tag{3.6.11}$$

where ${}_A x_0$ and ${}_A v_0$ are the initial, inter-vehicular distance and the initial relative velocity. If $t1$ is larger than $t2$, the following vehicle collides with the preceding one while the latter decelerates, and if $t1$ is smaller than $t2$, the preceding vehicle stops before the following one collides with it. From equ. 3.6.11, a state trajectory with the condition of $t1 = t2$ is expressed as

$$\text{Line } E' : Ax = \frac{1}{2(\mu_{max} g - \alpha_p)} \left((v_p - v) + \frac{\mu_{max} g - \alpha_p}{\alpha_p} v_p \right)^2 \qquad (3.6.12)$$

If the initial state is above the boundary defined by equ. 3.6.12, a following vehicle can avoid a collision even if a preceding one decelerates at a_p. For a given maximum deceleration of a following vehicle and deceleration of a preceding one, the region where the rear-end collision takes place can be illustrated in figure 3.6.9.

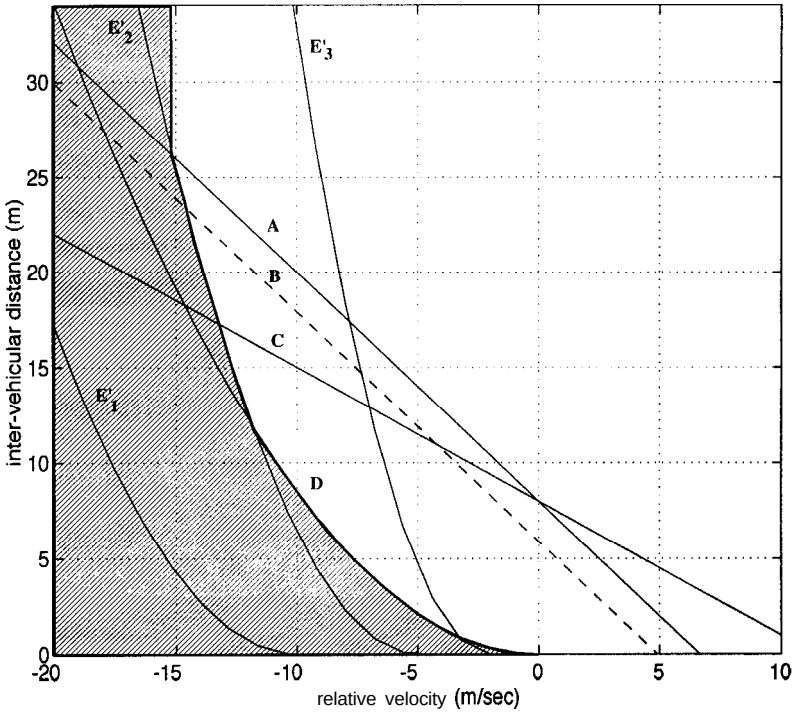

Figure 3.6.9: R-Rdot Analysis with Constant Deceleration of Preceding Vehicle

Three additional lines, E' 1, E'2, and E'3, correspond to the preceding vehicle's deceleration of 0.3 g, 0.4 g, and 0.5 g, respectively. If a preceding vehicle decelerates at 0.4 g, the rear-end collision occurs when the initial condition is in the "hatched" area. By following the above procedure, the region of collision can be identified.

3.6.3.2 Transient Response in the Case of a Cut-In

The R-Rdot analysis implies that it is impossible for the headway control to avoid collisions under all initial conditions, but by properly choosing a desired headway and a control gain, a headway-controlled vehicle can avoid collisions in certain regions on the R-Rdot diagram.

The R-Rdot analysis also offers information on riding comfort during maneuvers. In figure 3.6.8, for example, a following vehicle begins to decelerate at 0.3 g when a preceding one suddenly appears at Point 1. This is because Point 1 is located approximately in the middle line of Lines A and B. If a preceding vehicle appears at Points 2, 3, or 5, the deceleration will have its maximum value since the initial states are below Line B.

The maximum deceleration is defined by the initial condition, or the position and the velocity of a preceding vehicle at the instance when it appears in front of a following one. A few transient responses of headway-controlled vehicles due to cut-in are presented in figures 3.6.10(a) and 3.6.10(b).

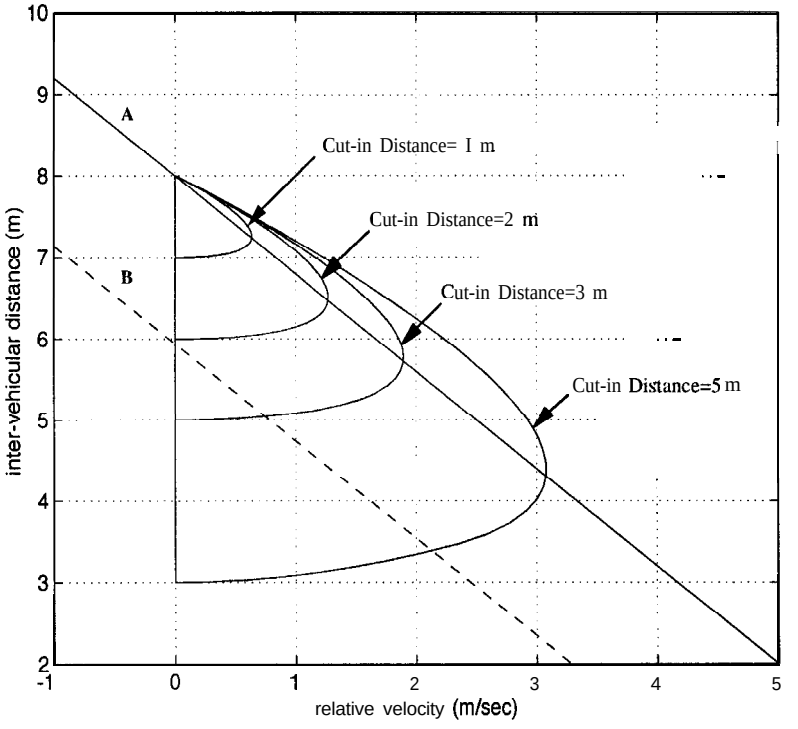

Figure 3.6.10(a): R-Rdot Diagram of Cut-in Vehicle

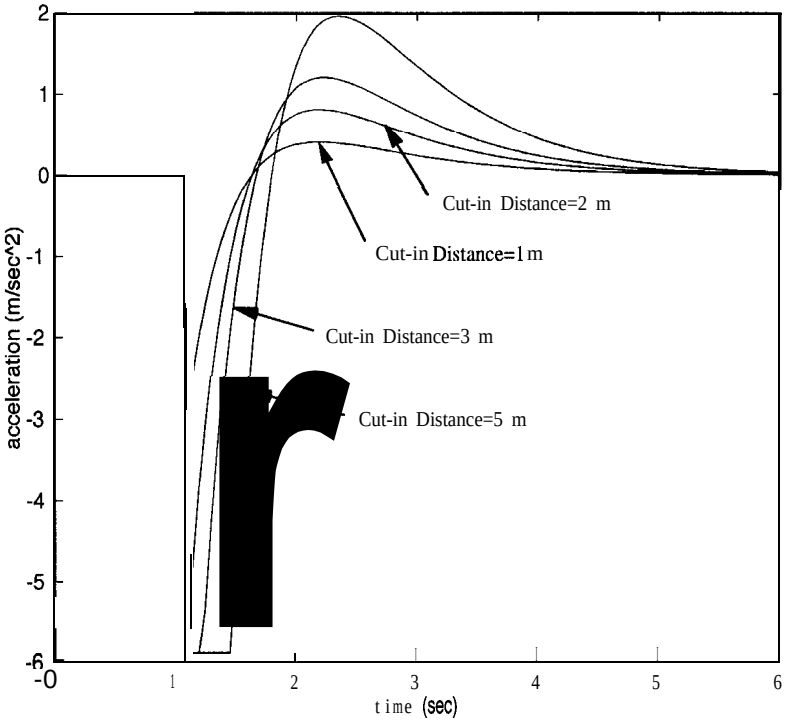

Figure 3.6.10(b): Acceleration Due to Cut-in

In the simulations, the velocities of vehicles are 10 m/sec at first. Then one vehicle suddenly cuts in front of another traveling at the same velocity at distances of 1, 2, 3, or 5 meters less than the desired headway distance. (In figures 3.6.10 (a) and (b), when another vehicle cuts in at a distance of x meters less than the desired headway time, "cut-in distance" is called as x meters.) The headway time is 0.7 seconds, and the control gain is 2.0.

Figure 3.6.10 (a) describes the R-Rdot trajectory for each case; Lines A and B are the same as those in figures 3.6.8 and 3.6.9. Since Line B intersects the inter-vehicular distance at 2 meters less than the desired headway distance at zero relative velocity, it is observed that if cut-in distance is larger than 2 m, deceleration will be the maximum.

Figure 3.6.10 (b) shows acceleration responses. Since a preceding vehicle suddenly cuts in at t = 1 sec, deceleration also suddenly takes its maximum value at that moment. Moreover, when cut-in distance is larger than 2 m, deceleration at t = 1 sec is the maximum deceleration. This abrupt change in deceleration, however, results in an extremely large jerk or the time derivative of acceleration, and it considerably degrades riding comfort for passengers in vehicles. This comfort is crucial for human drivers, especially because they are supposed to steer in headway controlled vehicles. Thus, the sudden change in deceleration shown above should be avoided unless vehicle is in the dangerous region based on R-Rdot diagram.

3.7 Conclusion and CICC System

Intelligent cruise control systems have become an important area of research and development, largely because the aim of these systems is to achieve greater highway capacity, while at the same time increasing the safety and comfort of drivers. To determine how CICC should be organized, some analytical results for intelligent cruise control systems were conducted in this report.

In section 3.2, general features of spacing control, headway control and the linear-optimal control model (human model) were summarized. Since headway control does not require the information of preceding vehicle's acceleration and lead car's velocity and acceleration to satisfy the string stability, headway control is more adequate to be used for vehicle-following control in a mixed flow. However, if delay times exist in sensors, actuators, or the plant itself, the string stability may be violated. The maximum delay times depend on both control gain and headway time; they decrease as control gain increases and as headway time decreases. Moreover, in CICC,

since human drivers are required to steer and they need a prediction time greater than 0.3 seconds, the headway time cannot be very small.

In section 3.3, the effects of several factors on static flow rate were evaluated. It was verified that the percentage of automated vehicles on highways influences the total highway capacity. Although inter-vehicular communication and lanes for only automated vehicles could improve the capacity of highways with a large percentage of automated vehicles, they were not effective if the percentage of automated vehicles is less than 30%. Thus, neither inter-vehicular communication nor lanes for only automated vehicles will be used in CICC.

In section 3.4, the transient responses due to changes in the lead car's velocity were evaluated. Headway control yielded delay time in tracking, while spacing control did not show any delay. In comparison with the human model, headway control is still better from the standpoint of distance error. The transient responses of a mixed flow showed intermediate responses between headway controlled vehicles and manually operated ones, and it was verified that headway control can be applied to a mixed flow.

In section 3.5, two methods of infrastructure-vehicle communication were compared in transient responses due to the changes in headway time. To achieve a stable transition, using a wide-range communication, such as radio communication, is more effective than using a local communication, such as beacons. To prevent vehicle velocities from diverging, it was effective to introduce a maximum velocity suppression, while it resulted in an insufficient increase of flow rate.

In section 3.6, the capacity of avoiding collisions was evaluated in several cases. To confirm the region where collisions can be avoided, it was shown to be very convenient to use **R-**

Rdot analysis. In cases where a preceding vehicle decelerates at a deceleration larger than the maximum one that can be achieved by a following vehicle, headway control again shows better performance than the human model. This result implied that a controller which is capable of responding to the preceding vehicle's deceleration quickly, can improve the capacity of avoiding rear-end collisions. Moreover, through R-Rdot analysis, even smaller deceleration of a preceding vehicle could degrade the collision avoidance. Thus, although the information of preceding vehicle's acceleration is not necessary for headway control, estimating it is still very helpful to avoid collisions.

Based on the above observations, CICC will use headway control for vehicle-following. As for infrastructure-vehicle communication, CICC will be given the information of a desired headway time, maximum velocity and road-tire friction by infrastructures through wide-range communication. CICC should also contain a module which estimates the acceleration of a preceding vehicle, and the estimated acceleration will be used to improve the capacity of avoiding collisions. The detailed processes of designing CICC will be described in another PATH report.

4. Effect of Communication Delays on Performance of Vehicle Platoons

Yu-Han Chen

4.1 Introduction

In controlling the spacing between vehicles in a large platoon, it is useful to have information from the other vehicles in the platoon. In the control law considered in this section, the preceding vehicle information, lead vehicle information, and total spacing error relative to the lead vehicle are all needed. In the ideal case, this control law will guarantee that the spacing errors will decrease as they progress backwards through the platoon. However, the behavior of the communications system will result in delayed information being given to the control law. The duration and "placement" of these delays can affect the performance of the control law in maintaining constant spacing between vehicles in the platoon. The purpose of this project is to analyze the effect of an imperfect communications system on the performance of the control law, and to come up with some requirements on the communications system in order to ensure the preservation of a "nice" behavior with respect to the spacing error and ride quality of the vehicles in the platoon.

4.1 .1 Hardware Description

The communications system under consideration for this project is the radio communications within a platoon of vehicles. The radio hardware currently used for the intraplatoon communications system consists of a spread-spectrum radio transceiver mounted in

each vehicle, and its associated computer interface boards. The Proxim RXA-1000 radio transceiver operates in half-duplex mode, and uses the 902-928 MHz frequency band. Since the transceiver can only transmit or receive, the switching is controlled by an ATcomm interface board, which also controls the flow of data between the vehicle's communication software and the Proxim transceiver.

In order to conserve bandwidth (the usage of available radio frequencies), all the radios within a platoon will operate on a single frequency. It is possible for each vehicle in the platoon to be addressed by a different receiving frequency, but this would require a very large available bandwidth for platoons which are expected grow up to twenty vehicles in length. This also does not leave much available bandwidth for other platoons which might be nearby. As a result of operating on a single frequency, the vehicles in the platoon are restricted to one transmission at a time. The protocol for determining which vehicle can transmit at any given time is the token bus protocol, which is explained in detail later in this paper.

For any transmitter/receiver pairs, before any data can be sent through the radio, there must be a "handshaking" routine which establishes that the receivers are ready to receive. This time interval is sometimes called the turnaround time of the radio. Since the current radio is spread-spectrum, whenever a transmission is made the receiving and transmitting radios must synchronize their spreading codes. This is done through a preamble in front of each transmission, and is currently the most time consuming part of transmitting data through the radios. There are other types of radios which do not require such a long turnaround time. It is this time which will be examined as one of the specifications for the communications system.

An additional facet that will be added to the communications system in the future is an infrared transceiver that will be able to transfer information from two adjacent vehicles in a platoon. The advantage to this is that since this communications link deals with only two vehicles, there is no need to reestablish a communication link every time a transmission must be made. The procedure of establishing a communications link need only be performed once, and then checked occasionally. This method of transmitting information is much faster than the radio system. However, since infrared can be blocked or hampered by dust and rain, the radio system must remain as a backup system.

In general, for any given transmitter/receiver be it radio or infrared, its affect on the data used by the control law can be simplified to appropriate time delays corresponding to its functions. Transmissions between every vehicle and the rest of the platoon involve three types of time delays, as shown in figure 4.1.1.

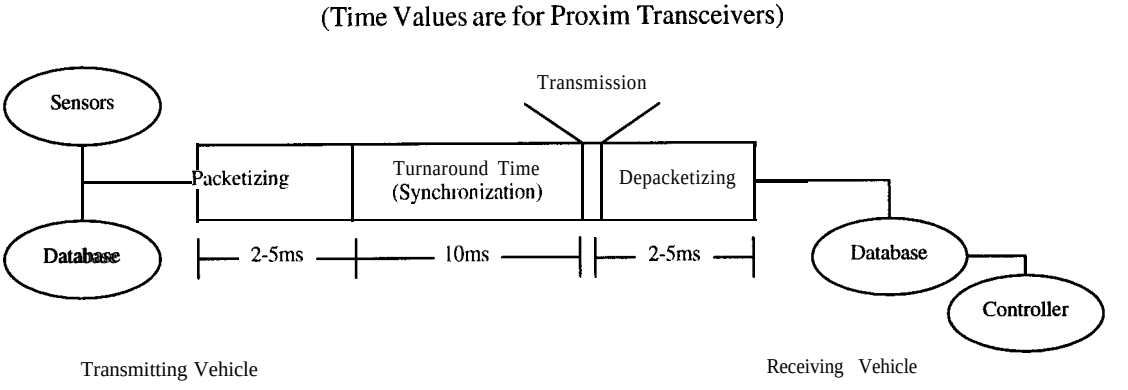

Figure 4.1.1: Breakdown of Time Delays

The first is the time that the software needs to process a data packet. This involves either assembling the raw data from the sensors and/or a database into a packet for transmission; or decoding a received packet and processing the data within. This delay is a function of the processing speed of the CPU installed in the vehicle, and the processing load placed on that CPU. The second delay is the time needed for the transceivers on the receiving vehicles to synchronize with the signal on the transmitting vehicle. The average synchronization time for one pair of the Proxim transceivers is approximately 7.5ms; however, a software implemented time window of 10ms is used to allow the entire platoon sufficient time to synchronize with the transmitting signal. The remaining delay comes from the time required to broadcast the packet, which is a function of the bit transfer rate of the transceiver, and the size of the packet being transmitted. With the Proxim transceivers, this delay is insignificant compared to the synchronization (or turnaround) time, so it can be ignored for this particular radio.

4.1.2 Token Bus Architecture

The way in which the communication delays accumulate can be best understood by examining how the communication structure operates. The radios in a platoon operate on a token bus architecture. Within a single platoon, only one radio frequency is used, and is therefore analogous to a computer bus. The entire platoon can "hear" what is being broadcast on the frequency "bus". A "right-to-transmit token" is simply a data bit incorporated into a transmission packet that informs the platoon which vehicle is permitted to broadcast. The protocol (and the associated time delays) operates roughly as follows:

1. If vehicle i has the right-to-transmit token, it assembles a data packet (2-5ms processing delay), and broadcasts it to the rest of the platoon (10ms turnaround time).
2. Every vehicle in the platoon receives this broadcast and begins to process the data packet (2-5ms delay). Using the transmitting vehicle ID number, these vehicles can determine what information (if any) to keep in their individual databases.
3. After decoding its packet, the $(i+1)$th vehicle will determine that it possesses the token and begin the process again.
4. The token is thus "passed' from the front of the platoon to the rear of the platoon, then the cycle repeats itself.
5. If a transmission error occurs, the token gets "dropped" from the platoon. If the lead vehicle does not detect a "last vehicle" transmission within a specified time, it restarts the token cycle by broadcasting again.

4.1.3 Control Law and Modelled Vehicle Dynamics

The sliding control law considered in this project uses a simplified two-state model of each vehicle [Swaroop, 1994] where the vehicle is taken to be a lumped mass, and the external forces which are included are the aerodynamic drag force, the rolling friction force, and the control force,

$$\ddot{x}_i = \frac{u_i - c_v \dot{x}_i^2 - F_r}{M_i} \qquad (4.1.1)$$

where c_v is the drag coefficient of the vehicle, M_i is the mass of the vehicle, and F_r is the rolling friction. The subscript i denotes the i-th vehicle in the platoon. Defining a control force which has the form,

$$u_i \equiv c_v \dot{x}_i^2 + F_r + M_i u_{i.sl} \tag{4.1.2}$$

where $u_{i,sl}$ is the "synthetic sliding input", the vehicle dynamics are further simplified to,

$$\ddot{x}_i = u_{i.sl} \tag{4.1.3}$$

This assumes that it is possible to compute a desired throttle input such that the engine can provide the necessary control force u_i. The sliding control law considered in this section is as follows [Swaroop, 1994],

$$\begin{aligned} u_{i,sl} &= \frac{1}{1+q_3}\left[\ddot{x}_{i-1} + q_3\ddot{x}_1 - q_1(v_i - v_{i-1}) - q_4(v_i - v_1) - \lambda_1 s_i\right] \\ s_i &= (v_i - v_{i-1}) + q_1(x_i - x_{i-1} + S + L) + q_3(v_i - v_1) + q_4\sum_{k=1}^{i}(x_k - x_{k-1} + S + L) \end{aligned} \tag{4.1.4}$$

Where S is the desired spacing between vehicles, and L is the length of each vehicle. For the computer simulations, it is assumed that the desired spacings, vehicles lengths, and vehicle masses are the same throughout the platoon. This control law uses previous and lead vehicle information to guarantee string stability (in the absence of communication delays), as long as the gains,

$$q_1 q_3 > q_4 \tag{4.1.5}$$

This control law requires that the lead vehicle velocity and acceleration be broadcast to the entire platoon, and that each vehicle (excluding the lead vehicle) broadcasts velocity and acceleration to the vehicle immediately behind it.

It also requires that each vehicle has access to the spacing errors of all the vehicles that precede it in the platoon. There are two ways that this information can be passed backwards to

the appropriate vehicle. One method is to have each vehicle sum the spacing error from the vehicle preceding it with its own spacing error, and passing that sum back through the platoon. This would be ideal if this information were to be passed through a line-of-sight communications link such as the infrared transmitters. The second method is to have every vehicle listen in on every broadcast within the platoon, and to "download" the spacing errors of all the vehicles preceding it and sum these errors when the control law requires a total spacing error. This method would be more optimal for the radio system. The delay associated with this second method is slightly more difficult to model, but it produces more recent information on the average for the control law, given the use of radios.

4.2 Software Structure

The software which controls the computing functions of each vehicle in the actual platoon consists of several "modules" (Figure 4.2.1). All modules operate fairly independently of each other and interact mostly through a shared database. The "segment" of the software that concerns the communications module is shown below. The communications software module takes care of the communications architecture, interaction with the transceivers, and packet processing. Data gathered through the communication module is placed into the database, and data to be sent through the transceivers is taken from the database. The control module in turn gets this information from the database whenever it is needed. The control module can also poll the database to determine when a new piece of information has arrived.

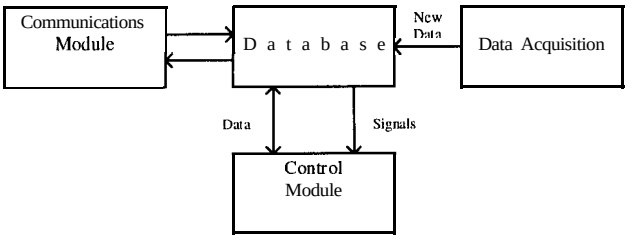

Fig. 4.2.1: Software Module Interaction

4.3 Computer Simulation Description

The basic computer simulation used for this project is the "long_sim" longitudinal control program used in the Vehicle Dynamics Laboratory at U.C. Berkeley. It uses a simplified seven state model for the vehicle dynamics,

- mass of air in intake manifold
- engine speed
- vehicle velocity
- vehicle position
- brake torque
- throttle angle

with three control inputs, of commanded brake torque, commanded throttle angle and gear reduction ratio. However, for simplicity, the gear reduction ratio is kept constant for this series of simulations. The engine is modeled using a simple two-state model, and is computed using a series of lookup tables. The throttle and brake are similarly modeled using lookup tables.

The original program did not take into account any time delays that occur in the communications system. To simulate the effect of the "delayed knowledge" caused by

transmission delays, an additional program module, radio.c, was created (see appendix A). This module essentially creates a memory buffer for each vehicle in the platoon, which represents what information the vehicles have about the rest of the platoon at any given time. This memory buffer is updated according to the characteristics of the radio token bus protocol. The main program, when computing the control inputs and resulting motion of each vehicle, calls on the module radio.c to provide previous and lead vehicle information instead of using the "real-time" data. In simulating the effect of the communications delays on the platoon, sensor noise is neglected, since any performance degradation will likely take on the form of low amplitude, high frequency oscillations about the "normal" responses, and might be indistinguishable from the effects of noise. There is no "noise" associated with the transmission of information packets. The way the transceivers operate, the packet is either received without errors, or it is lost ("dropped"). This packet error rate occurs at around 0.1% of total transmissions, and is incorporated into the simulation. However, unless a significant number of errors occur in a continuous sequence, they are unlikely to affect the platoon to any perceptible degree.

The effect of the communications delays is to prevent the control law from using the most recent information. The previous vehicle velocity and acceleration information is updated every:

$$t_{d,cycle} = N\left(t_{d,sync.} + t_{d,process} + t_{d,process}\right) \qquad (4.3.1)$$

for each vehicle; where N is the number of vehicles in the platoon. The time delay $t_{d,sync.}$ is a fixed quantity, while $t_{d,process}$ is a stochastic quantity with a logarithmic probability distribution of approximated by the equation shown in figure 4.3.1.

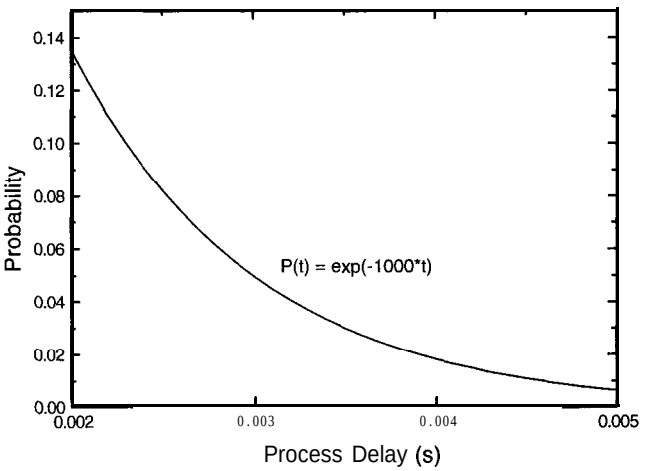

Fig. 4.3.1: Probability Distribution of Processing Delay

A small software module was added to the simulation to provide a randomly generated processing time delay with the above probability distribution. This probability distribution is correct for the current 486 machines operating in the test vehicles. Since the processing delay is a randomly varying quantity, it is useful to define a mean process delay time whose corresponding probability density is,

$$\begin{aligned} P_{proc,m} &= \frac{1}{0.005-0.002}\int_{\tau=0.002}^{\tau=0.005} e^{-1000\tau}d\tau \\ &= \frac{1}{0.003}\left[\frac{-1}{1000}e^{-1000\tau}\right]_{0.002}^{0.005} \\ &= 0.0429 \end{aligned} \tag{4.3.2}$$

which corresponds to the time value,

$$\begin{aligned} 0.0429 &= e^{-1000t} \\ t_{proc,m} &= \frac{-1}{1000}\ln(0.0429) \\ &= 0.003\,1\ \text{s} \end{aligned} \tag{4.3.3}$$

Using this mean processing delay, we can define a mean token cycle delay which will be useful as a parameter in the quantitative analysis of the communications system.

As a result of the time delays, the previous vehicle velocity/acceleration information that the controller must use looks like a sample and hold function with a "hold time" of $t_{d,cycle}$. The control law also uses an "absolute" spacing error term, which is the difference between the desired position of the i-th vehicle relative to the lead vehicle, and the actual position of the i-th vehicle relative to the lead vehicle. This absolute error term can be computed by summing the spacing errors of each of the (N-i) vehicles preceding the i-th vehicle. This absolute error information is also discontinuous, since the spacing error of any given vehicle is only broadcast when that vehicle has the transmission token. However, it is more difficult to describe in mathematical terms the discontinuity of the spacing error information, since only one part in the sum is updated every $t_{d,cycle}/N$ seconds.

It should also be noted that this control law has been constructed using continuous-time techniques [Swaroop, 1994], but is implemented in a discrete fashion. Currently the "implementation-rate" of the control law is every 20 ms. The effect of the communications delays on the performance of the control law will be related to this discrete implementation rate.

4.4 Qualitative Analysis

Two different lead vehicle velocity/acceleration profiles were used to analyze different characteristics of the platoon performance. An acceleration, deceleration profile, shown in figure 4.4.1,

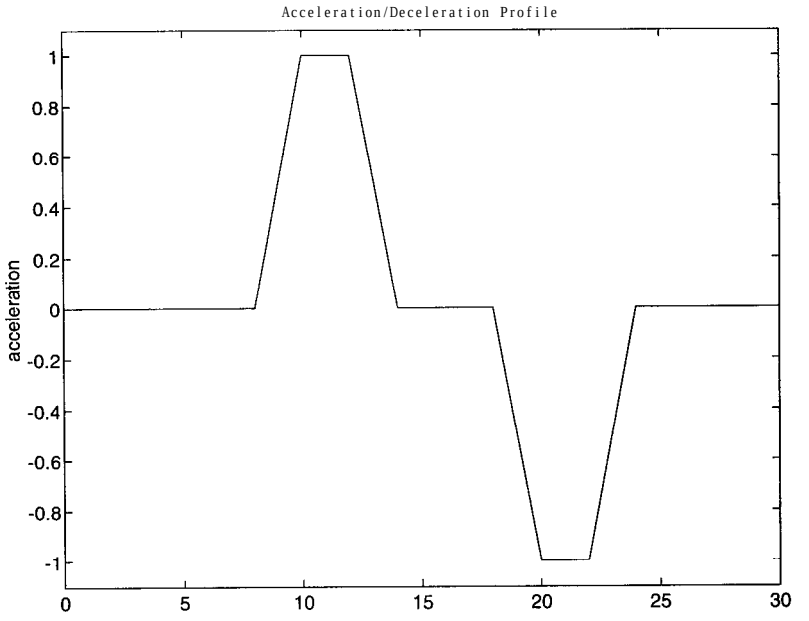

Fig. 4.4.1: Acceleration Profile for Lead Vehicle

was used to observe the tracking error performance of the platoon under acceleration and braking conditions. However, since the acceleration profile is discontinuous, it is difficult to observe the jerk characteristics. Also, during a hard acceleration maneuver, jerk becomes less important than error tracking. Passenger comfort is more important when the platoon is performing low acceleration maneuvers. A slow sinusoidal velocity profile, shown in figure 4.4.2, was therefore created to observe the effect of delayed information on jerk.

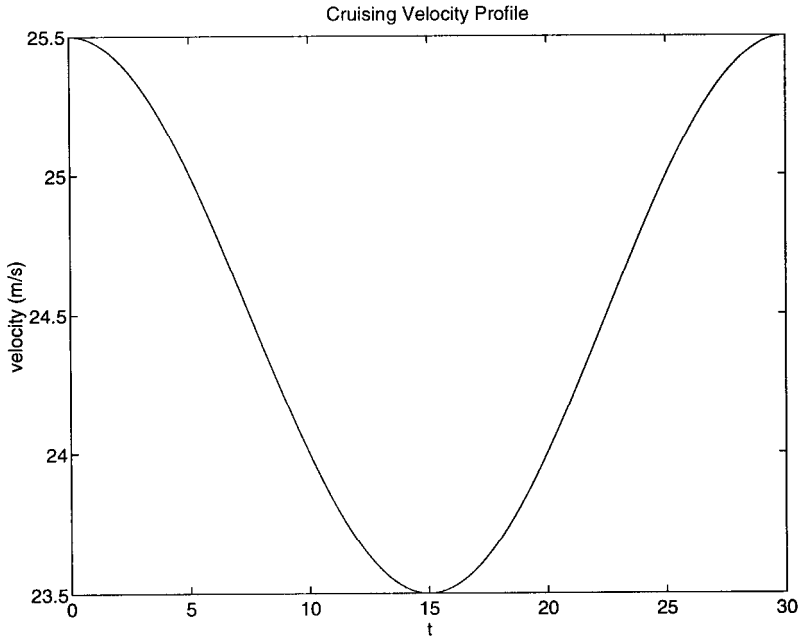

Fig. 4.4.2: Sinusoidal Velocity Profile for Lead Vehicle

The frequency of the sinusoid is approximately 0.5 Hertz, which was chosen to roughly approximate the velocity oscillations a "normal" human driver might experience on an uncongested freeway due to fluctuations in traffic flow.

Platoons of ten and twenty vehicles were simulated using delays starting from the current 10ms turnaround time. The length of the turnaround time was then decreased until an "acceptable" level of performance was obtained. The criterion of acceptability is somewhat subjective, especially where jerk is concerned. It is nominally based on the performance of a four vehicle platoon with a 10ms turnaround time. This is the platoon size and communications system that is currently being field tested, and has been observed to perform "reasonably" well.

4.4.1 String Stability of Spacing Errors

Looking at the results of the four vehicle platoon with 10ms turnaround time, it can be observed that the tracking error decreases, as expected, as we progress down the platoon. The lead vehicle does not have a "spacing error" and thus only the second to fourth vehicle errors are plotted in figure 4.4.3.

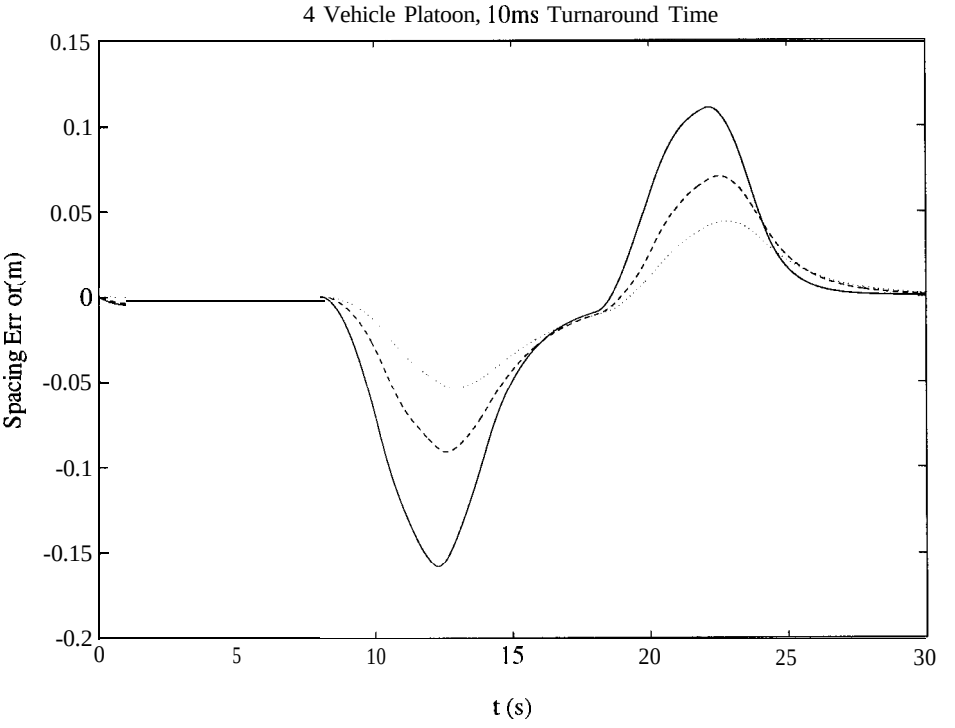

Fig. 4.4.3: Spacing Error for a Four Vehicle Platoon

The largest spacing error occurs with the second vehicle in the platoon, and decreases further back in the platoon. For the ten (figure 4.4.4) and twenty (figure 4.4.5) vehicle platoons, as the communication cycle delay is increased (either by increasing the length of the platoon or by increasing the turnaround time of the radios), the spacing errors also increased, but remained

string stable in a general sense. The following plots show that although the magnitude of the error grows as the communication cycle delay grows, they do not grow uncontrollably as we progress down the platoon.

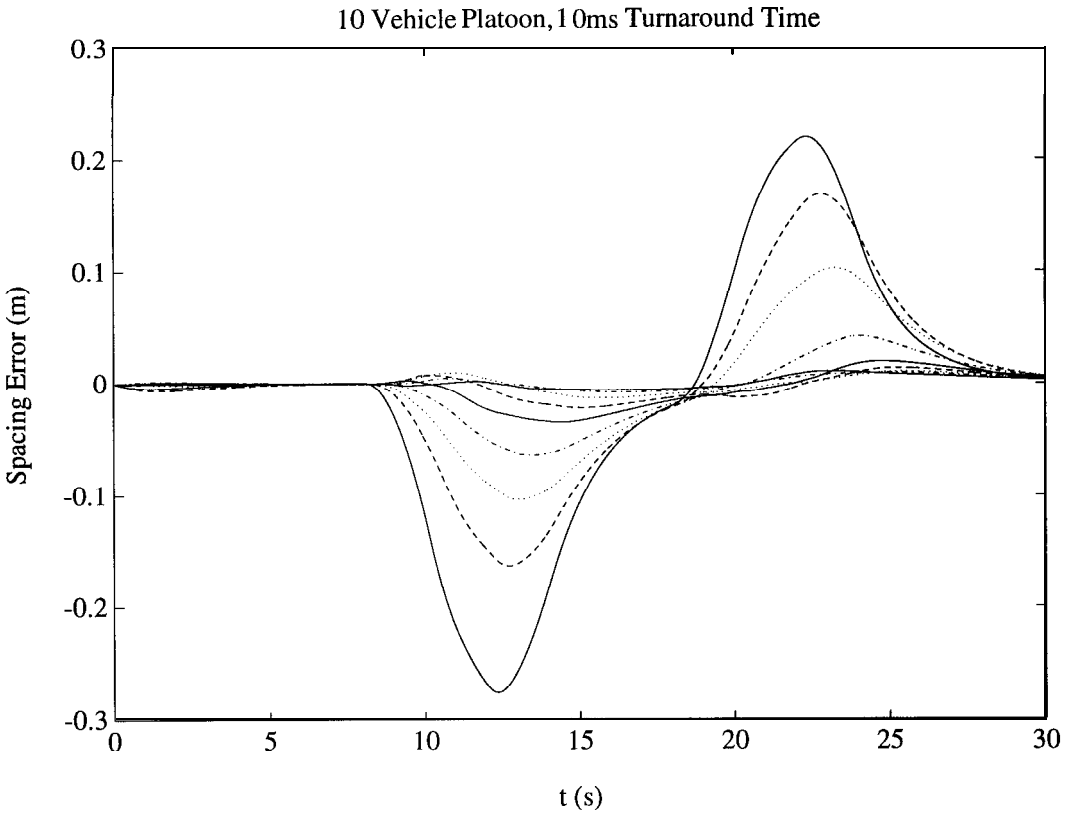

Fig. 4.4.4: Spacing Error For a Ten Vehicle Platoon

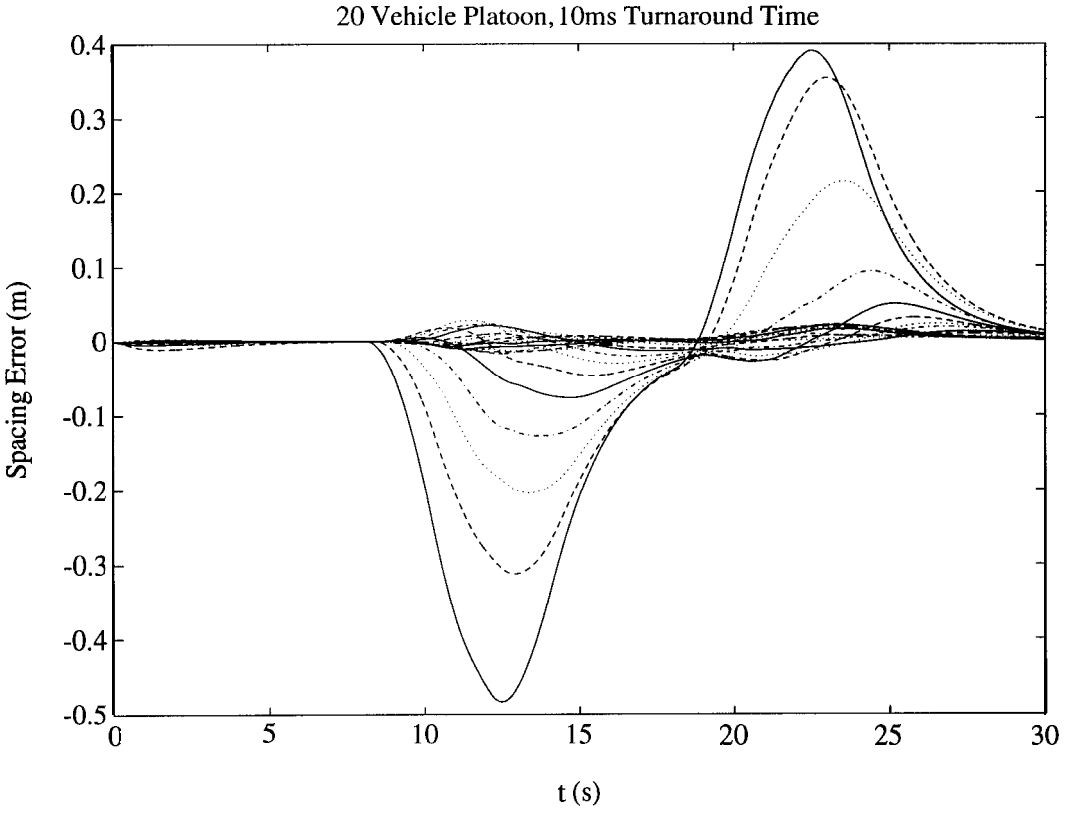

Fig. 4.4.5: Spacing Error For a Twenty Vehicle Platoon

What is meant by "string stable in a general sense" is that although the maximum amplitude of the spacing errors along the platoon do not grow as we progress down the line of vehicles, it is no longer true that at any given time that the errors follow the weak string stability criterion $\varepsilon_{i+1} < \varepsilon_i$ (a larger 'i' indicates a vehicle further back in the platoon). For example, the third vehicle spacing error is slightly greater than the second vehicle error after 20 seconds. The reason that the errors in the tail end of the platoon simply oscillate around the zero axis is that the control law,

$$u_{i,sl} = \frac{1}{1+q_3}\left[\ddot{x}_{i-1} + q_3\ddot{x}_1 - q_1(v_i - v_{i-1}) - q_4(v_i - v_1) - \lambda_1 s_i\right]$$
$$s_i = (v_i - v_{i-1}) + q_1(x_i - x_{i-1} + S + L) + q_3(v_i - v_1) + q_4\sum_{k=1}^{\cdot}(x_k - x_{k-1} + S + L) \qquad (4.4.1)$$

has terms which are influenced by the position and velocity error with respect to the lead vehicle as well as terms which are influenced by the "local" position and velocity error. The large adjustments occur towards the front of any platoon and by the time the maneuver filters back to the trailing vehicles, the entire platoon has had a chance to adjust to the new velocity and acceleration so that the individual spacing errors are smaller.

It is necessary to place a bound on how large the errors can grow due to the communication delays. Eventually, it is hoped to have an inter-vehicle spacing of three meters. The spacing error can be nominally required to be less than 10% of the desired spacing (0.33 meters, or approximately one foot). This desired behavior can be seen in the previous plot for a ten vehicle platoon with a 10 millisecond turnaround time. Using the mean processing time delay, a mean communication cycle time of,

$$\begin{aligned} t_{cycle,m} &= 10(0.010 + 2 \cdot 0.003\,1) \\ &= 0.162\ \text{s} \end{aligned} \tag{4.4.2}$$

is computed. To verify this, for a 20 vehicle platoon, this mean communication cycle time corresponds to a turnaround time of two milliseconds, which result in the error plot shown in figure 4.4.6.

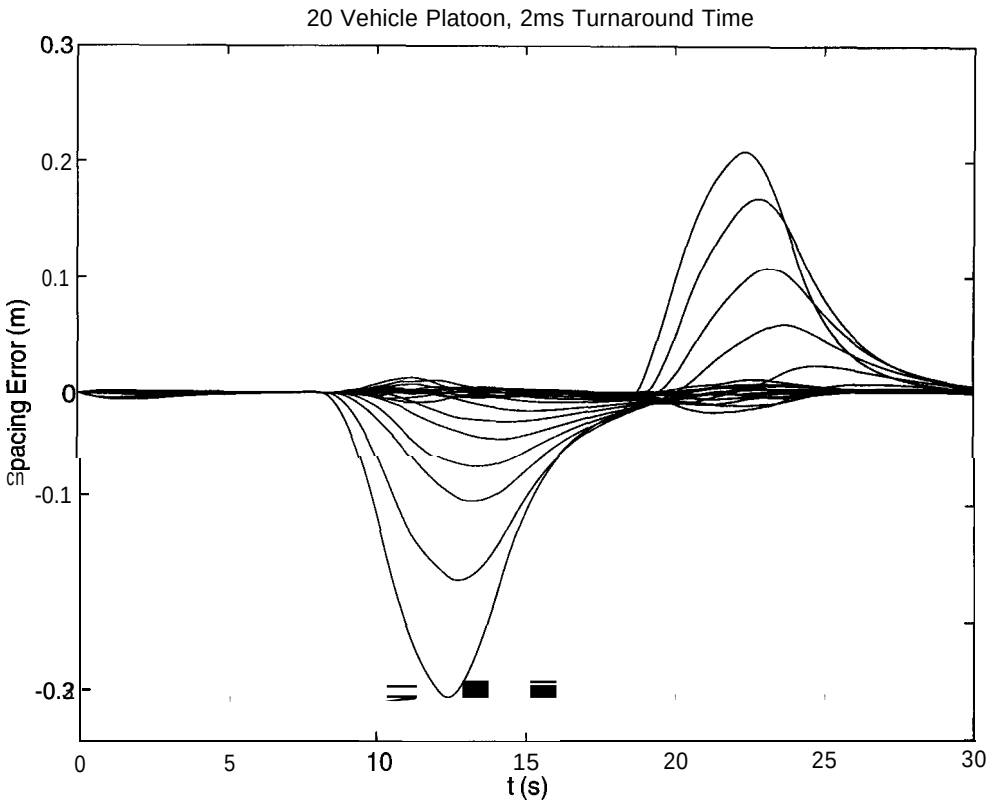

Fig. 4.4.6: Spacing Error Using a 2 ms Turnaround Time

From the plot it can be seen that maximum error remains within the desired bound. It must be noted that although the mean communication cycle time for this 20 vehicle platoon is,

$$\begin{aligned} t_{cycle,m} &= 20(0.002 + 2 \cdot 0.003\,1) \\ &= 0.164 \text{ s} \end{aligned} \tag{4.4.3}$$

the range of possible communication cycle times, due to the variation in $t_{process}$, has increased to $t = [0.120, 0.240]$ from the range of $t = [0.140, 0.200]$ for the case of a ten vehicle platoon and a ten millisecond turnaround time. The magnitude of the error is slightly better than the expected

0.3 m for the 20 vehicle platoon because the shorter processing delay values have a slightly higher chance of occurring than the longer delay values, due to the logarithmic probability density.

4.4.2 Ride Quality (Jerk)

The more restrictive performance characteristic turns out to be the jerk. Since the communication cycle delay is on the order of milliseconds, the control law is trying to follow discontinuous information that takes the form of very fast staircase functions. A maximum acceptable magnitude for jerk has been determined to be approximately 2 m/s^3. However, a more comfortable value for jerk is approximately 1 m/s^3. Using the sinusoidal velocity profile, the jerk of each vehicle can be seen to have a sinusoidal shape on the average, with a high frequency chatter superimposed on it. The larger the token cycle delay, the larger the amplitude of this chatter. For the four vehicle platoon (10ms turnaround time), the "chatter" has an amplitude of around 0.05 m/s^3 (or a peak to peak amplitude of 0.1 m/s^3).

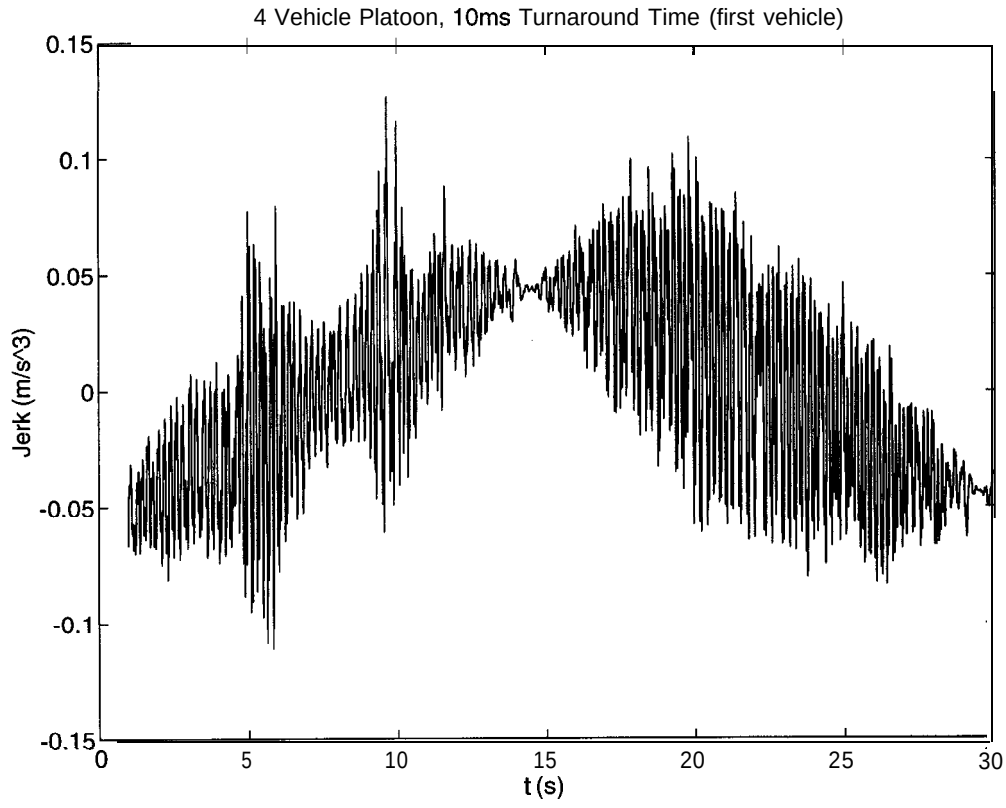

Fig. 4.4.7: Jerk Plot for the First Follower of a Four Vehicle Platoon

The four vehicle platoon with a 10 millisecond turnaround time has a mean token cycle time of 0.065 seconds. A four vehicle platoon has been field tested with a communications system that has these parameters, and the passengers felt that the ride quality was acceptable. Since ride quality is a somewhat subjective quantity, this will be the nominal baseline for comparison purposes. To approximate this jerk value, the turnaround time for a 10 vehicle platoon must be around 2ms; and for a 20 vehicle platoon, it must be under 0. lms.

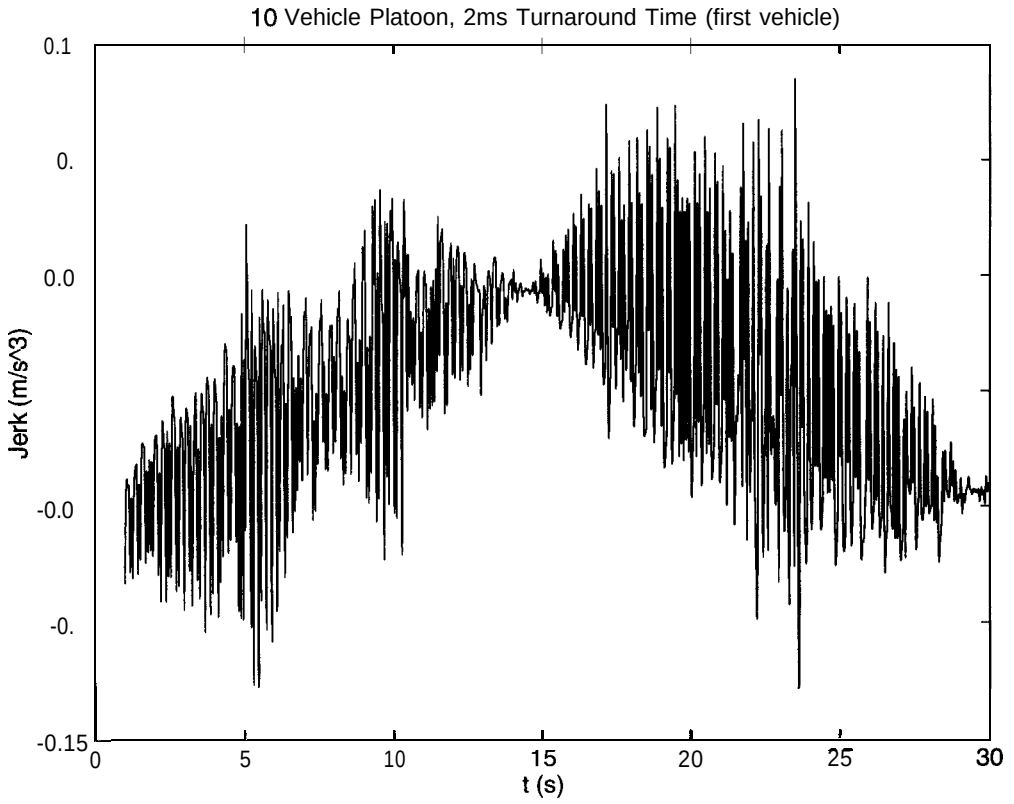

Fig. 4.4.8: Jerk Plot for the First Follower of a Ten Vehicle Platoon

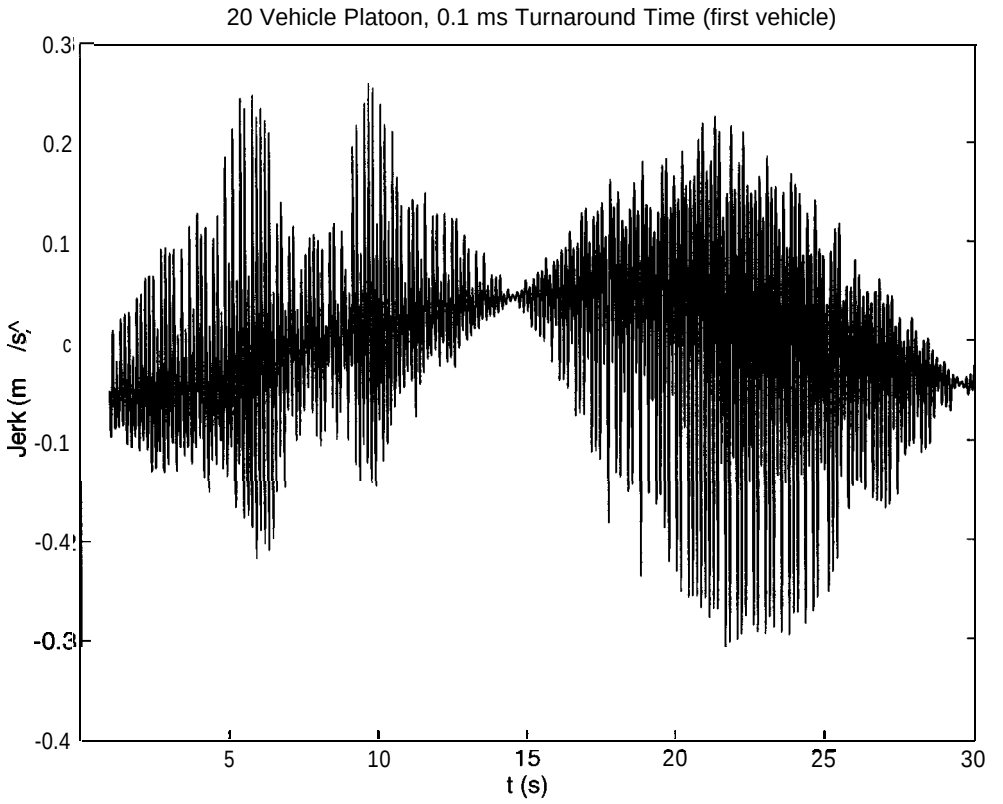

Fig. 4.4.9: Jerk Plot for the First Follower of a Twenty Vehicle Platoon

These requirements follow the relation that the jerk grows somewhat proportionally to the mean token cycle time. Therefore, to maintain a certain level of jerk, the mean token cycle delay should be roughly the same for different sized platoons. For a 20 vehicle platoon, it becomes impossible to meet this time requirement by reducing the radio turnaround time, because the processing delays become the limiting factor in the communication cycle time delay. The jerk, which appears as chatter, is most likely caused by the "overreaction" of the control forces when old and "out-of-date" information gets updated through the communications system. The performance characteristic that makes this likely is that the throttle angle of each vehicle looks like a first order response to a series of step functions. The plot shown in figure 4.4.10 is of a simulation where it

is assumed that all data except the lead vehicle data is known instantaneously by every vehicle in the platoon, and shows the throttle angle of the second (solid line), fifth (dashed line), and tenth (dotted line) vehicles in a ten vehicle platoon:

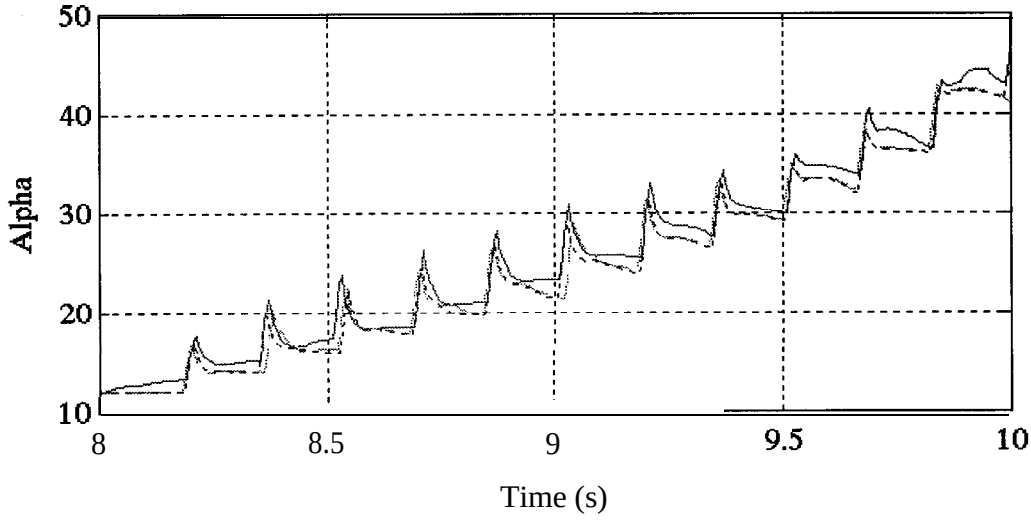

Fig. 4.4.10: Throttle Angle for Second, Fifth, and Tenth Vehicles in a Ten Vehicle Platoon

The rest of the vehicles in the platoon show similar spikes in the throttle angle responses. The brake torque response has similar spikes in the response. The longer the communication cycle delay, the larger these spikes become. It can also be seen that some spikes tend to be larger than others.

4.5 Conclusions and Recommendations

In terms of a communications protocol for the radio, the token bus is best suited for control purposes. The reason being that for a token type protocol, the delays due to the radio can be bounded and are deterministic. Other protocols, such as Ethernet, have delays and wait times

that are stochastic. Even though on average they may deliver information from one point in the system to another more efficiently, we cannot determine a maximum bound for the delays in these types of protocols. For control purposes, we rely on the ability to bound the time delays in order to guarantee a certain level of performance.

Of the two types of delays in the communications system, the processing delays are a property of the CPU speed of the computers installed in the vehicles. This delay can only be improved by more efficient software, a faster computer, or a dedicated CPU, and not by improving the properties of the radio. Therefore, in order to decrease the communication cycle delay, it is preferable to reduce the length of the switching/synchronization time. If this turnaround time is reduced enough, the transmission time may become a significant fraction of the total communications delay. In this case, it would also be necessary to consider the bit rate of the radio, as well as the number of bits of information any given transmission would have. In any case, the larger the platoon is, the quicker the turnaround time must be in order to maintain the same level of performance.

For the $\pm 1 \mathrm{m/s^2}$ acceleration/deceleration profile, in order to maintain an acceptable spacing error of less than 10% of the desired 3 meter vehicle spacing, a mean token cycle time of approximately 0.160 seconds is required. This corresponds to a length of eight control implementation time intervals, and a radio turnaround time of 0.002 seconds for a 20 vehicle platoon. For larger platoons, the mean communication cycle time can be slightly larger, since the range of possible communication cycle times grows with the size of the platoon. This is because the probability distribution for the communication cycle time is not Gaussian, but logarithmic,

with the probability distribution favoring the occurrence of shorter communication cycle time values.

In terms of maintaining a comfortable ride quality, the recommended specifications for the radios are more stringent. The goal is to maintain the same magnitude of jerk as observed for the four vehicle platoon with a 10 millisecond turnaround time. For a ten vehicle platoon, this requires a two millisecond turnaround time. For a twenty vehicle platoon, the desired magnitude of jerk cannot be achieved unless the packet processing time can be reduced. However, the magnitude of the jerk in this case is still well under the "comfortable" level of 1 m/s^3 for a radio turnaround time of one millisecond. Since the comfort level for jerk is a very subjective quantity, the requirement for the radio set by this quantity is not very rigid.

For the twenty vehicle platoon, the bottleneck in reducing the communication delays is often the packet processing time. To reduce this type of delay , one can either use a faster CPU, or reduce the computational load on the available one. A reduction in the time needed for the CPU to process communications information can be achieved by adding an additional CPU that specifically handles communications processes. This reduces the load on the dedicated "communications" CPU since it does not need to process any control or data acquisition routines at the same time. Determining a maximum "comfortable" level of jerk is a rather subjective process, however it would be preferable not to increase the magnitude of jerk as observed for the four vehicle platoon with a 10 millisecond radio turnaround time.

Because of the very small synchronization times that are demanded of the radios, an infrared communications system may be more suited to transferring at least the preceding vehicle information from vehicle to vehicle. This would significantly decrease the delays in at least some

of the variable which are needed by the control law. Since the error dynamics for the two-state vehicle model are,

$$\ddot{\varepsilon}_i = \ddot{x}_{i-1}\frac{q_3}{1+q_3} - \frac{q_3}{1+q_3}\ddot{x}_{i-1} + \frac{q_4 + \lambda_1 q_3}{1+q_3}\dot{x}_{i-1} + \frac{q_4 + \lambda_1}{1+q_3}\dot{x}_{i-1} - \frac{q_1 + q_4 + \lambda_1 + \lambda_1 q_3}{1+q_3}\dot{x}_i - \frac{\lambda_1(q_1+q_4)}{1+q_3}\varepsilon_i - \frac{\lambda_1 q_4}{1+q_3}\sum_{k=1}^{i-1}\varepsilon_k \tag{4.5.1}$$

some of the gains can be adjusted to “soften” the effect of some variables being delayed. The infrared link could handle the previous vehicle information, while the radio would conduct the lead vehicle data and any broadcast messages that may be necessary.

5. Transition Maneuvers

Tom Connolly

5.1 Introduction

There are three basic transition maneuvers required in an Automated Highway System. The first two maneuvers, join and split, are required for the formation of platoons and allowing individual vehicles to exit a platoon. In a join maneuver, a single vehicle or mini-platoon accelerates to join a platoon as shown in figure 5.1.1. In a split, a platoon splits up into two smaller platoons as shown in figure 5.1.2. A split is basically the reverse process of a join maneuver. A vehicle decelerates or accelerates in order to split from a platoon. The third transition maneuver is a lane change. A lane change consists of an individual vehicle moving into the adjacent lane, which is necessary for vehicles to enter and exit automated lanes.

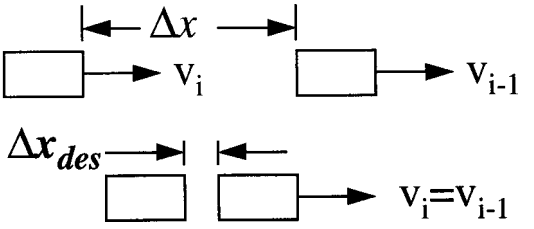

Figure 5.1.1: Join maneuver

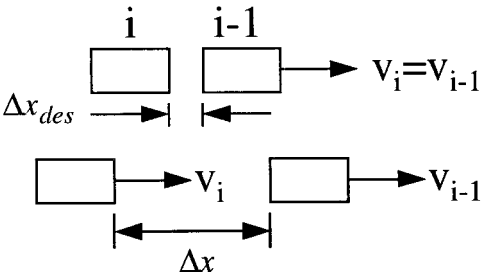

Figure 5.1.2: Split Maneuver

The focus of this work has been the longitudinal aspect of the transition maneuvers. In order for a vehicle to join with a platoon it must follow an acceleration/deceleration profile that allows it to safely join the preceding platoon. Control laws must be developed to ensure that the vehicle properly follows the desired profile. The controller must be robust enough to account for velocity changes of the preceding platoon.

Previous work in the area of transition maneuvers has resulted in the development of two trajectory designs for joining, an open loop design by Narendran, 1994, and a design based on maintaining a safe relative velocity between the merging vehicle and platoon developed by Frankel et. al., 1994. Although there currently exists a standard simulation program within the longitudinal control group, both of these designs were tested on different simulation programs. Previously there has not been a join or join module in the standard simulation program. It was desired to include a join module in a standard simulation so that different designs could be tested and compared, in order to determine an optimum design. Section 5.2 gives a brief description of the standard simulation model. Section 5.3 describes the join module added to the simulation as well as gives a brief description of the two previously developed trajectory design methods for joining. Section 5.4 discusses some future work in the area of transition maneuvers.

5.2 Simulation

In the longitudinal control group there had been a tendency for each researcher to develop their own simulation program to verify and validate the developed control laws. A standard simulation model was developed by Patrick Yip based on the vehicle models developed by Peng, 1992, and the Vehicle Dynamics Lab. This section gives a brief description of the standard simulation model. For a more detailed description of the simulation, refer to the actual program.

The simulation allows for the design and testing of vehicle follower control laws within a platoon. There are two models in the simulation, one for purely longitudinal control and one that is a combined model for longitudinal and lateral control. The longitudinal model contains two engine states (manifold air mass and engine speed), three car states (driven wheel angular velocity, velocity and position) and two actuator states (throttle angle and brake torque). The combined

model is based on a 6 degree of freedom model ($x,y,z,\varphi,\theta,\psi$) and includes an additional state for steering angle and lateral position. The dynamic equations include the inertial coupling between the lateral and longitudinal motion. A controller module in the simulation allows for the implementation of various follower control laws which determine the throttle angle/brake torque and steering angle. Because the simulation is structured to deal with only one platoon, a separate module had not previously been included to account for transition maneuvers.

The main routine for the longitudinal model is contained in long-sim. This is the main shell of the program which increments time and performs initialization tasks for the longitudinal simulation. An integration routine is called from long-sim to update the state variables every time step. This module takes the current states and controls and using the longitudinal dynamics model determines the derivative of the state variables. A fourth order Runga-Kutta routine is then used to determine the updated state variables. A controller module is also called every sampling instant from long-sim that uses the given control laws to perform follower control for succeeding cars in the platoon. This controller module determines the desired throttle angle or brake torque.

The main routine for the combined model is contained in comb-sim. Like long-sim, this is the main shell of the program which increments time and performs initialization tasks for the combined lateral and longitudinal simulation. An integration routine, analogous to the one used in the longitudinal model, is called from comb-sim to update state variables. A tire model by Bakker, Pacejka and Lidner, 1989, has been included to provide the longitudinal and lateral tire forces, thereby giving the coupling of the longitudinal and lateral motion. A controller module is also called which determines the desired throttle angle, brake torque and steering angle of each vehicle in the platoon.

5.3 Merge Control

As previously mentioned, it was desired to add a module to the simulation program that would allow for transition maneuvers. At this point, a transition module has been added to the longitudinal simulation. A transition maneuver module will be added to the combined simulation as well in the future. The module added to the longitudinal simulation allows for a vehicle or mini-platoon to join with another platoon. Since the program was developed for simulating one

platoon, the vehicles are actually part of the same platoon, only the vehicle that is to join is given a large initial spacing error. Because of this large spacing error, the vehicle will be controlled by a join module instead of the follower control module which controls the other vehicles within the platoon. This module designs a trajectory, based on the initial conditions, that will reduce the spacing error from the initial error to the desired intra-platoon spacing. The module also includes feedback control laws to ensure the vehicle follows the desired trajectory and to compensate for any changes in the lead vehicle velocity. Different trajectory designs and control laws can be introduced into the module so that the different designs can be tested and compared. Two trajectory designs have currently been included in the simulation. A brief description of these designs will be given in this section.

An open loop trajectory design has been described by Narendran, 1994. This design is based on the initial spacing and velocities of the merging vehicle and the platoon. A sinusoidal or trapezoidal acceleration profile is designed for the merging vehicle. Appropriate parameters for the acceleration profile can be chosen to ensure that the vehicle is within safety and comfort limits. A sliding surface control approach is used to ensure the vehicle follows the desired trajectory. The error term is defined as

$$e = sp_{act} - sp_{des}$$

where sp_{act} is the actual spacing between the joining vehicle and the platoon and sp_{des} is the desired spacing. The sliding surface is defined as

$$s = \dot{e} + c_1 e + c_2 \int e$$

The control input, which is the joining vehicle's throttle angle/brake torque, is calculated by requiring the sliding condition, $\dot{s} = -ks$, be satisfied. A detailed derivation of the control law is given by Narendran.

A second trajectory design is described by Frankel et. al., 1994. This design is based on the objective to ensure that a high speed collision does not occur if the lead vehicle suddenly decelerates. For any spacing and lead platoon velocity, a maximum safe velocity for the joining vehicle can be determined such that if a collision would occur it would be at a low relative velocity. The desired trajectory is such that the joining vehicle velocity never exceeds this maximum safe velocity. Figure 5.3.1 shows the relative velocity as a function of spacing such that

if the lead vehicle suddenly decelerated, the collision would occur with a relative velocity below 3 m/s. The safe velocity curve is continuously calculated so that any change in the lead vehicle's velocity will affect the safe relative velocity. Several feedback control laws are used to keep the joining vehicle's velocity on the desired velocity curve.

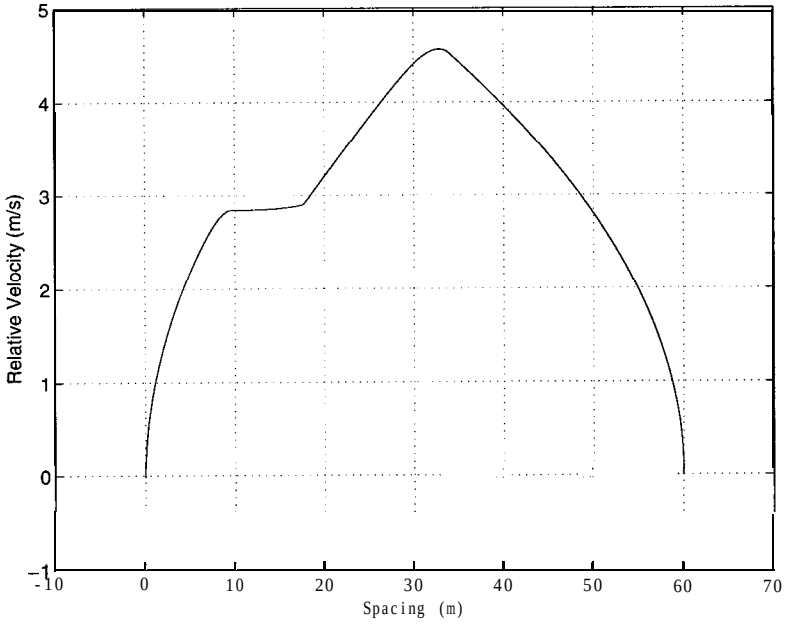

Figure 5.3.1: Desired Relative Velocity vs. Spacing for Join Maneuver

5.4 Future Work

There are several areas of future work concerning transition maneuvers within the Automated Highway System. A transition maneuver module needs to be added to the combined simulation model. This module should be capable of determining initial errors, design trajectories and contain the necessary control laws to ensure the vehicle follows the desired trajectory. There is also work to be done with the system level commands and tasks to ensure that safe transition maneuvers occur when there are multiple platoons involved.

There is also the need for simulation analysis of different trajectory designs for transition maneuvers to compare them in terms of safety, comfort and time optimization. Using the

simulations, optimum trajectory designs and controls need to be developed and then tested on actual vehicles.

6. Conclusion

In the past few years the basic approaches of longitudinal and lateral control have been realized both theoretically and experimentally. In the subsequent years there has been more emphasis on intermediate maneuvers, and analysis and control of the system under degraded modes of operation. Also there is also a move towards examining alternate methods of sensing, actuation, and vehicle control approaches.

Transition maneuvers include join, merge, split, and lane change operations. Lane change operations require vehicle lateral spacing with respect to some reference. Current experimental work relies on imbedding magnets in the center of the lane and using a magnetometer for obtaining vehicle lateral deviation from the center of the lane. Lane changes performed under this system will be complicated for two main reasons. The magnetometer must have a large range of operation, and as the vehicle moves into the adjoining lane, there will be interference from the magnets imbedded in the adjoining lane. The autonomous lateral control technique presented in Chapter 2, introduces an alternate lateral sensing technique. Lateral deviation is calculated using line-of-sight sensor information. Also the method does not require knowledge of road curvature for control. Lateral control of a string of vehicles under this methodology has been investigated. An analytic expression was derived to approximate the steady state lateral error as a function of vehicle longitudinal and lateral velocity, longitudinal spacing, and road curvature. A controller was developed and applied to the vehicle lane change maneuver. Lane changes will require a large view angle for the sensor. The Qualimatrix sensor was tested for potential use for such a sensing system.

Chapter 3 examined a Cooperative Intelligent Cruise Control approach. The method is aimed at alleviating some of the infrastructural needs for vehicle control in the current framework for an Automated Highway System. This chapter investigates the CICC method and examines the flow characteristics and string stability requirements under this method. The method requires an automatic throttle and brake control, and simple infrastructure-vehicle communication. The method is designed to let a vehicle operate as a conventional cruise control system in the absence of traffic around the controlled vehicle, but will work as a distancing control system when other vehicles are within the range of its sensors. It is shown that intervehicle communication and lanes restricted to automated vehicles increases highway capacity only when there is a large percentage of automated vehicles on the highway. Also it was seen that headway control can be applied to a mixed traffic flow. The R-Rdot analysis was introduced to examine the regions for avoiding collisions.

Prior studies in longitudinal platooning have indicated the need for intervehicle communication of acceleration and velocity information of the preceding vehicle as well as the lead vehicle of the platoon to ensure the string stability of the system. In Chapter 4, the effects of communications lag on the performance of platoons of vehicles was studied. A token ring architecture was adopted and performance of the control law under a variety of communications system lag times was studied. An effort has been made to come up with requirements on the communications system in order to ensure the preservation of a “nice” behavior with respect to the spacing error and ride quality of the vehicles in the platoon.

In an effort to standardize the development of control laws for vehicle platooning and lateral control in IVHS, a standardized "C" program was developed which captures all the

relevant vehicle dynamics. The last part of the report deals with the extension of this program to include modules that will allow researchers to perform a variety of transition maneuvers. This lets one compare various maneuvering strategies in an effort to develop optimal transition maneuver strategies.

The focus of this project in the future is to examine the robustness of the control laws developed thus far for platooning as well as transition maneuvers. The studies will also investigate alternate methodologies to effect longitudinal and lateral control of vehicles in an IVHS framework. The control laws developed must be tested for a variety of non-ideal conditions and efforts will be made to optimize system tasks.

7. References

Bakker, E., Pacejka, H. B., Lidner, L. 1989. "A New Tire Model with an Application in Vehicle Dynamics Studies," SAE Transactions, J. of Passenger Cars, Vol. 98, SAE Technical Paper No. *890087*.

Burnham, G. O., Seo, J. and G. A. Bekey. December, 1974. "Identification of Human Driver Models in Car Following," IEEE Transactions on Automatic Control, Vol. AC-19, No. 6.

Cho, D., Hedrick, J. K. December 1989. "Automotive Powertrain Modeling for Control," Transactions ASME Journal of Dynamics Systems, Measurement and Control, Vol 111, No. 4.

D. V. A. H. G. Swaroop; 1994. "String Stability of Interconnected Systems: An Application to Platooning in Automated Highway Systems"; Ph.D. Thesis; University of California at Berkeley.

Francher, P. and Z. Bareket. 1993. "Evaluation Headway Control Using Range Versus Range-Rate Relationships," The University of Michigan Transportation Research Institute.

Frankel, J. , Alvarez, L. , Horowitz, R. , Li, P. September, 1994. "Robust Platoon Maneuvers for AVHS." Department of Mechanical Engineering, University of California at Berkeley. PATH Technical Note 94-9.

Green, J., Hedrick, J. K. 1990. "Nonlinear Torque Control for Gasoline Engines," *Proceedings of the I990 American Control Conference,* San Diego, CA.

Hedrick, J. K., McMahon, D., Naranedran, V., Swaroop, D. 1991 "Longitudinal Vehicle Controller Design for IVHS Systems," *Proceedings of the 1990 American Control Conference,* pp 3107-3112.

Hedrick, J. K., McMahon, D. H. and D. Swaroop. 1993. "Vehicle Modeling and Control for Automated Highway Systems," PATH Technical Report, UCB-ITS-PRR-93-24.

Ioannou, P. and C. C. Chien, 1992. "Autonomous Intelligent Cruise Control," IVHS America.

Isaac R. Porche; 1992 "Communication Protocols to Implement Coordinated Maneuvers of Automatically Controlled Vehicles"; Research Project; University of California at Berkeley.

Mitschke, M. 1990. "Control Loop 'Driver-Vehicle' under the Influence of Cross Wind," Transportation Systems.

Narendran, V. K. May, 1994. "Transition Maneuvers In Intelligent Vehicle Highway Systems", Ph.D. Dissertation, University of California at Berkeley.

Narendran, V. K., and Hedrick, J. K., July, 1993. "Autonomous Lateral Control" Submitted to Vehicle System Dynamics.

Peng, Huei. May, 1992. "Vehicle Lateral Control for Highway Automation," Ph.D. Dissertation, University of California at Berkeley.

Pham, H., December, 1993. "Combined Lateral and Longitudinal Controller of Vehicles for IVHS,", M.S. Thesis, University of California at Berkeley.

Pipes, L. A. 1953. "An Operational Analysis of Traffic Dynamics," Journal of Applied Physics, Vol. 24.

Qualimatrix, 1993. "PATH Optical Ranging System Development," PATH Research Report draft no. 93-32.

Salman, M. 1990. "Coordinated Control of Braking and Steering," Transportation Systems.

Shladover, S. E., Desoer, C. A., Hedrick, J. K., Tomizuka, M., Walrand, W. B., Zhang, W. B., McMahon, D., Peng, H., Sheikholeslan, S. and N. McKeown. 1991. "Automatic Control Development in the PATH Program," IEEE Transaction on Vehicular Technology, vol 40.

Slotine, J-J., E. and Li, W., 1991. "Applied Nonlinear Control", Prentice Hall.

Streisand, S.L. and J. Walrand; February, 1992. "A Communication Architecture for IVHS"; Research Project; University of California, Berkeley.

Walrand; J. c 1991. "Communication Networks: A First Course"; Aksen Associates; Irwin.